REVISTA INTERNACIONAL

DESASTRES NATURALES, ACCIDENTES E INFRAESTRUCTURA CIVIL

ISSN 1535-0088

Volumen 22 ● Número 1 ● Mayo 2022

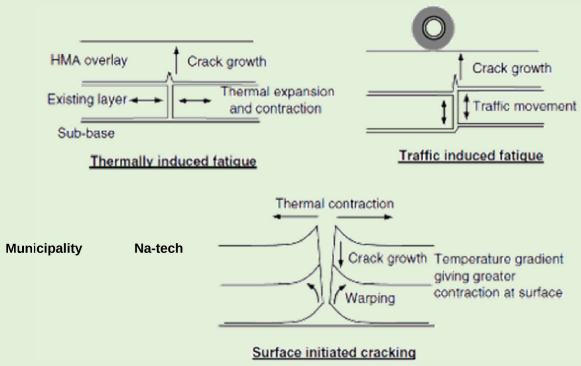

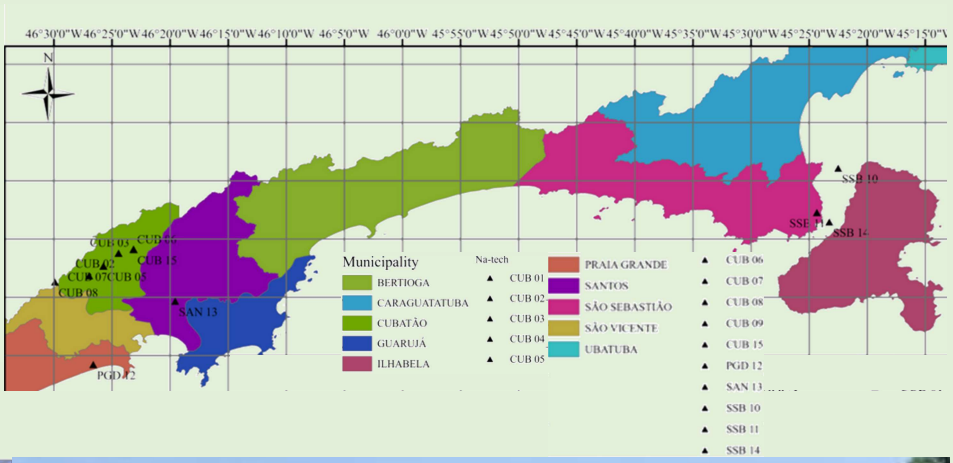

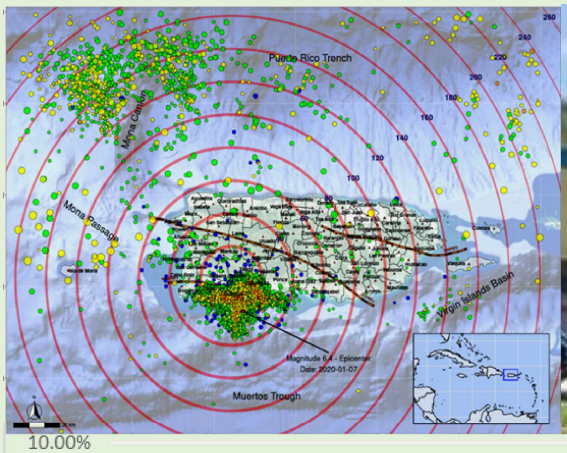

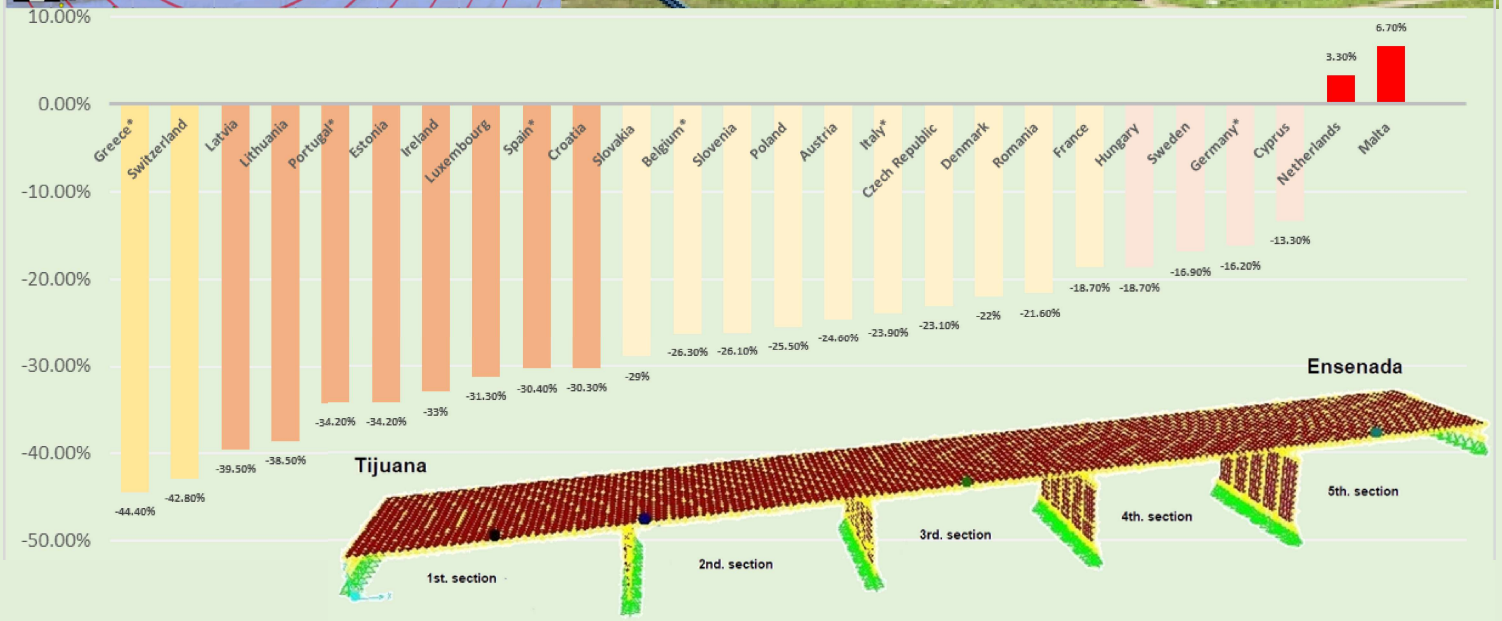

UNIVERSIDAD DE PUERTO RICO, RECINTO UNIVERSITARIO DE MAYAGÜEZ

REVISTA INTERNACIONAL DE DESASTRES NATURALES, ACCIDENTES E INFRAESTRUCTURA CIVIL

REVISTA INTERNACIONAL DE DESASTRES NATURALES, ACCIDENTES E INFRAESTRUCTURA CIVIL

ISSN 1535-0088

REVISTA INTERNACIONAL DE DESASTRES NATURALES, ACCIDENTES E INFRAESTRUCTURA CIVIL

Volumen 22, Número 1, Mayo 2022

ISSN 1535-0088

CONTENIDO **Págs.**

MENSAJE DEL PRESIDENTE COMISIÓN EDITORIAL RIDNAIC


Benjamín Colucci Ríos

¡Saludos! Esta edición de la Revista Internacional de Desastres Naturales, Accidentes e Infraestructura Civil (RIDNAIC) consiste en seis artículos técnicos de estudios científicos en cinco países Iberoamericanos que colaboraron veinte autores. Los trabajos de investigación están relacionados a la actividad sísmica como objetivo de estudio y sus efectos sobre las estructuras, desastres debido a la pérdida de materiales peligrosos, vulnerabilidad de las escuelas localizadas en zonas costeras, mantenimiento y rehabilitación de carreteras, y las variables que aumentan las lesiones por choques de tránsito.

En el primer artículo, *Exploración Estadística de Datos Sísmicos en Puerto Rico en el Periodo de Diciembre 2019 hasta Enero 2021*, Dr. Cabrera-Ríos y demás investigadores ofrecen resúmenes estadísticos de los eventos sísmicos reportados en la zona sur y suroeste de Puerto Rico durante dicho periodo. El estudio se basó en 69,570 datos recopilados del USGS y 41,742 estadísticas calculadas. De dicho análisis estadístico los municipios de Guánica y Guayanilla registraron el mayor número de sismos significativos con 1,284 y 1,203 respectivamente (67.5% del total), seguidos por los municipios de Yauco, Lajas, Peñuelas y Cabo Rojo.

En el segundo artículo, *Dynamic Seismic Response of La Mission Bridge in Baja California, México,* los investigadores Hoon, Huerta-López y García-Gastélum presentan la respuesta dinámica pronosticada por el programa SAP 2000 que experimenta la estructura de un puente y la caracterización del terreno alrededor de dicha estructura. Los resultados muestran cambios en la rigidez a través del suelo y como éstos afectan su comportamiento esperado y la respuesta del terreno a amplificar sus movimientos a diferentes frecuencias alrededor del puente.

En el tercer artículo, *Na- tech Events in the Coastal Region of São Paulo, Brazil: Data and Frequency*, los Dres. De Moura y De Sousa exponen como los eventos que involucran la pérdida de contención de materiales peligrosos debido a un evento natural ("na-tech") afectan los cuerpos de agua. Los investigadores culminan proponiendo un método para estimar las frecuencias de estos eventos radicales correlacionándolos al número de empresas que son propicias a generarlos.

En el cuarto artículo, *Vulnerability of Schools in Puerto Rico to Tsunami Events*, los investigadores buscan evaluar la vulnerabilidad de las escuelas ante peligros de tsunamis reconociendo que éstas son de vital importancia las cuales comprenden de una alta población y son instalaciones esenciales. Los hallazgos exhiben que las escuelas más vulnerables presentan tiempos de evacuación excesivos cuyas rutas son inseguras e inadecuadas.

En el quinto artículo*, Lessons Learned from the Virginia Reflective Cracking Study under Accelerated Pavement Testing*, los Dres. Salado y Flintsch estudian el desempeño, rendimiento y la viabilidad de diferentes materiales y estructuras de pavimentos bajo cargas aceleradas a través de un simulador de vehículos pesados. Las lecciones aprendidas, cambios experimentales y los resultados de estudio en términos de rendimiento de agrietamiento y ahuellamiento también se presentan en esta investigación.

El sexto y último artículo, *Traffic Crash Injuries Occurrence Varieties Across Barcelona Districts in Spain*, busca identificar el distrito que tiene mayor número de lesiones por choques de tránsito en comparación con otras áreas en la ciudad de Barcelona, España. Los investigadores Robusté y Aiash demostraron que el distrito Eixample con mayor densidad poblacional tiene mayor riesgo y para los demás distritos variaron según el nivel de lesión.

Agradezco a los Miembros de la Comisión Editorial de RIDNAIC y a los autores que sometieron sus artículos para hacer una realidad esta edición. Un agradecimiento muy especial a Ciara Toro-Rosario Asistente Administrativo del Centro de Transferencia de Tecnología en Transportación por su titánico apoyo en el montaje de esta edición y a Sra. Irmalí Franco-Ramírez Oficial Administrativo del Centro de Transferencia en el diseño del arte de la portada. Agradezco además a Katherine Muñiz-Rodríguez, por su apoyo en la edición final de la revista.

Espero que esta Edición de la Revista Internacional de Desastres Naturales, Accidentes e Infraestructura Civil (RIDNAIC) cumpla con las expectativas de la comunidad científica en contribuir a reducir la vulnerabilidad de la infraestructura ante los fenómenos naturales extremos para el bienestar de la humanidad.

Con mi mayor aprecio y admiración,

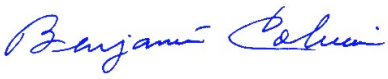

Benjamín Colucci, PhD, PE, PTOE, F. ASCE, F.ITE, API, JD
Presidente, Comisión Editorial Internacional RIDNAIC
Catedrático, Universidad de Puerto Rico-Mayagüez

MESSAGE FROM THE PRESIDENT OF THE RIDNAIC EDITORIAL COMMISSION


Benjamín Colucci-Ríos

Greetings! This edition of the International Journal of Natural Disasters, Accidents and Civil Infrastructure (RIDNAIC) consists of six technical articles of scientific studies in five Ibero-American countries with the collaboration of twenty authors. The research works are related to seismic activity as an objective of study and its effects on structures, disasters due to the loss of hazardous materials, vulnerability of schools located in coastal areas, maintenance and rehabilitation of highways, and the variables that increase traffic crash injuries.

In the first article, *Statistical Exploration of Seismic Data in Puerto Rico in the Period from December 2019 to January 2021*, Dr. Cabrera-Ríos and other researchers offer statistical summaries of the seismic events reported in the south and southwest of Puerto Rico during that period. The study was based on 69,570 data collected from the USGS and 41,742 calculated statistics. Based on the statistical analysis, the municipalities of Guánica and Guayanilla registered the highest number of significant earthquakes with 1,284 and 1,203 respectively (67.5% of the total), followed by the municipalities of Yauco, Lajas, Peñuelas and Cabo Rojo.

In the second article, *Dynamic Seismic Response of La Mission Bridge, Baja California, Mexico*, researchers Hoon, Huerta-López and García-Gastélum present the dynamic response predicted by the SAP 2000 program experienced by the structure of a bridge and the characterization of the terrain around said structure. The results show changes in the stiffness through the ground and how these affect its expected behavior and the response of the ground to amplifying its movements at different frequencies around the bridge.

In the third article, *Na-tech Events in the Coastal Region of Sao Paulo, Brazil: Data and Frequency*, Drs. De Moura and De Sousa expose how the events that involve the loss of containment of hazardous materials due to a natural event (na-tech) affect water bodies. The researchers conclude by proposing a method to estimate the frequencies of these radical events by correlating them to the number of companies that are likely to generate them.

In the fourth article, *Vulnerability of Schools in Puerto Rico to Tsunami Events*, the researchers seek to assess the vulnerability of schools to tsunami hazards, recognizing that schools are of vital importance, comprise high populations, and are essential facilities. The findings show that the most vulnerable schools have excessive evacuation times whose routes are unsafe and inadequate.

In the fifth article, *Lessons Learned from the Virginia Reflective Cracking Study under Accelerated Pavement Testing*, Drs. Salado and Flintsch study the performance, performance, and feasibility of different pavement materials and structures under accelerated loads through a heavy-duty vehicle simulator. Lessons learned, experimental changes and study results in terms of cracking and rutting performance are also presented in this research.

The sixth and last article, *Traffic Crash Injuries Occurrence Varieties Across Barcelona Districts in Spain*, seeks to identify the district that has the highest number of traffic crash injuries compared to other areas in the city of Barcelona, Spain. The researchers Robusté and Aiash demonstrated that the Eixample district with the highest population density has the highest risk and for the other districts they varied according to the level of injury.

I am grateful to the Members of the RIDNAIC Editorial Commission and the authors who submitted their articles to make this edition a reality. A very special thanks to Ciara Toro-Rosario, Administrative Assistant of the Transportation Technology Transfer Center for her titanic support in the preparation of this edition and to Irmalí Franco-Ramírez, Administrative Official of the Center for the assistance in the design of the art of the cover page. I also thank Katherine Muñiz-Rodríguez for her support in the final edition of the RIDNAIC Journal.

I hope that this International Journal of Natural Disasters, Accidents and Civil Infrastructure RIDNAIC Edition meets the expectations of the scientific community in helping to reduce the vulnerability of infrastructure to extreme natural phenomena for the well-being of humanity.

With my greatest appreciation and admiration,

Benjamín Colucci, PhD, PE, PTOE, F. ASCE, F.ITE, API, JD
President, RIDNAIC International Editorial Commission
Professor, University of Puerto Rico-Mayagüez

MENSAJE DEL DIRECTOR DE DEPARTAMENTO DE INGENIERÍA CIVIL Y AGRIMENSURA-UPRM

Ismael Pagán-Trinidad

En representación de la facultad, los estudiantes y todo el personal del departamento de Ingeniería Civil y Agrimensura del Recinto Universitario de Mayagüez de la Universidad de Puerto Rico, reciban un cordial saludo y mejores deseos de que este volumen de la Revista Internacional de Desastres Naturales, Accidentes e Infraestructura Civil (RIDNAIC) sea de su entero agrado. Este mensaje enfoca el tema sísmico incluido en este volumen y es extensivo al resto de los artículos técnicos.

El archipiélago de Puerto Rico vivió experiencias extremadamente aterradoras y únicas que marcaron nuestra historia antes y después de la secuencia de terremotos que vivimos al comienzo del 2020 y que dejó una secuela de eventos que permitieron registrar nuestra huella sísmica de la Isla gracias a las experiencias vividas. El efecto emocional de inseguridad, sentido de incertidumbre y vulnerabilidad en la comunidad es digno de empatía, identificación y estudio por las disciplinas del comportamiento humano. Sin embargo, los efectos en nuestra infraestructura civil y el récord recopilado nos sirven de base para caracterizar el comportamiento sísmico de la Isla, gestionar nuevos conocimientos y definir normas que puedan permitir el diseño y la construcción resiliente de nuestra infraestructura crítica para el futuro.

Reconocemos que el estado de nuestra infraestructura en la Isla es incierto, y por otro lado, es vulnerable debido al historial del tipo de construcción, limitaciones en las mejores prácticas de diseño y construcción sismorresistente del pasado, y el envejecimiento. Existen retos inherentes en el comportamiento de la infraestructura por la falta de un programa de inspección y mantenimiento riguroso que pueda detectar, prevenir y remediar cualquier debilidad en una estructura existente. Es inherente de las mejores prácticas de ingeniería que prospectivamente se consideren alternativas viables para hacer nuestra infraestructura menos vulnerable y más resiliente a eventos de terremotos extremos. Investigadores involucrados en análisis de riesgos proponen que la práctica de la ingeniería debe moverse de una de diseño prescriptivo a uno que sea basado en análisis de riesgos. Nos parece que estas son avenidas de conocimientos y mejores prácticas que pueden fortalecer la resiliencia de la construcción de nuestra infraestructura en el futuro.

El estudio y la investigación de los terremotos ha sido parte de las áreas focales de educación e investigación en nuestra institución. Sin embargo, estos eventos históricos en Puerto Rico han revivido excelentes oportunidades y compromisos para la academia en múltiples disciplinas, tanto en la fase curricular como la de investigación, para ampliar los conocimientos en la ingeniería y otras disciplinas relacionadas a la sismicidad y sus impactos en la sociedad.

La revista RIDNAIC es un tributo a aquellos que sienten ese compromiso y que se involucran adelantando el conocimiento para aspirar a lograr un mundo más seguro, menos vulnerable y más resiliente a los riesgos naturales, tecnológicos y por accidentes. Invitamos a nuestra audiencia a continuar comprometidos y activos con contribuciones relevantes y pertinentes como las que nuestros investigadores de este volumen han presentado.

Nuestra historia narrada en este mensaje puede ser replicada en cualquier otro lugar que tenga riesgos y vulnerabilidad sísmica o de cualquier otro evento natural, tecnológico o por accidentes como lo demuestra la totalidad estos artículos. Por ello nos parece relevante compartirla con nuestra audiencia y motivarles a continuar la misión de crear una sociedad menos vulnerable y más segura ante los riesgos y peligros naturales y tecnológicos a los cuales podamos estar expuestos.

MESSAGE FROM THE DIRECTOR
CIVIL ENGINEERING AND SURVEYING DEPARTMENT AT UPRM

Ismael Pagán-Trinidad

On behalf of the faculty, students, and staff of the Civil Engineering and Surveying Department of the University of Puerto Rico at Mayagüez, receive cordial greetings and best wishes that this volume of the International Journal of Natural Disasters, Accidents and Civil Infrastructure (RIDNAIC) satisfies your research interests. This message focuses on the seismic topic included in this volume and is extensive to the rest of the technical articles.

The archipelago of Puerto Rico experienced extremely terrifying and unique events that marked our history before and after the sequence of earthquakes at the beginning of 2020 that left a sequel of events that allowed us to record our seismic footprint on the Island thanks to the experiences lived. The emotional effect of insecurity, sense of uncertainty and vulnerability in the community is worthy of empathy, identification, and study by the disciplines of human behavior. However, the effects on our civil infrastructure and the record compiled serve as the basis for characterizing the seismic behavior of the Island, managing new knowledge, and defining standards that may allow the design and resilient construction of our critical infrastructure for the future.

The status of our infrastructure on the Island is uncertain, and on the other hand, it is vulnerable due to the history of the type of construction, limitations in the best practices of design and seismic resistant construction of the past, and aging. There are inherent challenges in the behavior of the infrastructure due to the lack of a rigorous inspection and maintenance program that can detect, prevent, and remedy any weakness in an existing structure. It is inherent to best engineering practices that prospective alternatives are considered to make our infrastructure less vulnerable and more resilient to extreme earthquake events. Researchers involved in risk analysis propose that engineering practice should move from one of prescriptive design to one that is based on risk analysis. It seems to us that these are avenues of knowledge and best practices that can strengthen the resilience of our infrastructure construction in the future.

The study and research of earthquakes has been part of the focal areas of education and research in our institution. However, these historical events in Puerto Rico have revived excellent opportunities and commitments for the academy in multiple disciplines, both in the curricular and in the research phase, to expand knowledge in engineering and other disciplines related to seismicity and its impacts on the society.

The RIDNAIC journal is a tribute to those who feel that commitment and who are involved in advancing knowledge to aspire to achieve a safer world, less vulnerable and more resilient to natural, technological and accident risks. I invite our audience to continue to be engaged and active with relevant and pertinent contributions such as those presented by our researchers in this volume.

The story that I have narrated in this message can be replicated in any other place that has seismic risks and vulnerability or any other natural, technological or accident event as evidenced by all these articles. For this reason, it seems relevant to us to share it with our audience and motivate them to continue the mission of creating a less vulnerable and safer society in the face of natural and technological risks and dangers to which our society may be exposed.

EXPLORACIÓN ESTADÍSTICA DE DATOS SÍSMICOS EN PUERTO RICO EN EL PERIODO DE DICIEMBRE 2019 HASTA ENERO 2021[1]

Shirley Huanca[2], Roberto Trespalacios[3], Zulma Acevedo[4], Dalia Alizo[5], Angelie Nieves[6], Clara Isaza[7], Mauricio Cabrera-Ríos[8]

RESUMEN: En diciembre de 2019, Puerto Rico experimentó un incremento notorio de actividad sísmica principalmente en las regiones sur y suroeste de la isla. Los cientos de edificios y hogares dañados o destruidos propiciaron la instalación emergente y temporal de múltiples refugios para damnificados y demostraron lo poco preparado que estaban los municipios para emergencias de esta índole y magnitud. En particular, Guánica y Guayanilla reportaron los mayores impactos tanto en la cantidad como en la magnitud de sismos, sin embargo, varios pueblos cercanos también fueron afectados significativamente. A pesar de que en febrero de 2020 hubo una disminución de estos fenómenos, las fluctuaciones en ocurrencia y magnitud persistieron. La pandemia de COVID-19, al ser una emergencia de alcance global, eclipsó aquella de los sismos, dentro de muchas otras emergencias. En este trabajo se ofrecen datos y resúmenes estadísticos sobre tales eventos en un período comprendido desde la primera semana de diciembre de 2019 hasta la segunda semana de 2021 que pueden ser de utilidad para futuros investigadores en el área de ingeniería sísmica y ramas afines.

Palabras claves: actividad sísmica, infraestructura, refugios, Suroeste de Puerto Rico, terremotos

STATISTICAL EXPLORATION OF SEISMIC DATA IN PUERTO RICO FROM DECEMBER 2019 TO JANUARY 2021

ABSTRACT: In December 2019, Puerto Rico experienced an increment in seismic activity, especially in the South and Southwestern regions of the island. The hundreds of buildings and homes damaged or destroyed prompted the hasty installation of multiple shelters and showed the little preparedness of the municipalities of the island to face emergencies of this kind and magnitude. The municipalities of Guánica and Guayanilla reported the largest impacts in terms of number and magnitudes of earthquakes. Surrounding municipalities, however, were also importantly affected. Despite a decrease in seismic activity in February 2020, event occurrences and magnitudes continued to fluctuate. The COVID-19 pandemic, due to its global reach, eclipsed many other emergencies including that of the seismic activity in the island. This study provides data and statistical summaries on this activity from the first week of December 2019 until the second week of 2021 that may be useful for future researchers in the area of seismic engineering and related fields.

Keywords: seismic activities, infrastructure, refugees, southwest area of Puerto Rico, earthquakes

[1] Artículo recibido el 6 de febrero de 2022 y aceptado para publicación el 30 de abril de 2022.
[2] Miembro, *The Applied Optimization Group*, Universidad de Puerto Rico, Recinto Universitario de Mayagüez (UPRM), Mayagüez, Puerto Rico 00681-9041. Email: Shirley.huanca@upr.edu
[3]Miembro, *The Applied Optimization Group* & Profesor e Investigador, Departamento de Ciencias Básicas, Universidad Tecnológica de Bolívar, Calle del Bouquet Carr. 21 #25-92, Cartagena de Indias, Colombia. Email: Roberto.trespalacio@upr.edu
[4] Estudiante, Departamento de Ingeniería Industrial & Miembro, *The Applied Optimization Group*, Universidad de Puerto Rico, Recinto Universitario de Mayagüez. Email: Zulma.acevedo3@upr.edu
[5] Miembro, *The Applied Optimization Group*, Universidad de Puerto Rico, Recinto Universitario de Mayagüez. Email: Dalia.alizo@upr.edu
[6] Estudiante Graduada, *Colorado State University* & Pasado Miembro, The Applied Optimization Group, Universidad de Puerto Rico, Recinto Universitario de Mayagüez. Email: Angelie.nieves1@upr.edu
[7] Catedrática Auxiliar, Departamento de Biología & Co-directora, *The Applied Optimization Group*, Universidad de Puerto Rico, Recinto Universitario de Mayagüez. Email: Clara.Isaza@upr.edu
[8] Catedrático, Departamento de Ingeniería Industrial; Programa Graduado de Bioingeniería & Co-director, The Applied Optimization Group, Universidad de Puerto Rico, Recinto Universitario de Mayagüez. Email: Mauricio.cabrera1@upr.edu

INTRODUCCIÓN

Puerto Rico, la menor de las Antillas Mayores del Caribe, experimentó un aumento en actividad sísmica en diciembre del año 2019. Desde esa fecha, los sismos de mayor impacto a la población ocurrieron en el área sur y suroeste del país. Un terremoto es un temblor rápido y repentino de la tierra provocado por el rompimiento y desplazamiento de roca en las placas tectónicas. Los terremotos ocurren a lo largo de grietas en la superficie de la tierra llamadas líneas de falla, y se pueden sentir en grandes áreas a pesar de que, por lo general, duran menos de un minuto (Bommer y Martínez-Pereira, 1999). Las ubicaciones directamente debajo y encima de la superficie de la tierra donde comienza el terremoto se denominan hipocentro y epicentro, respectivamente. Dos de las principales medidas que caracterizan a un sismo son la magnitud y la profundidad; la magnitud mide la cantidad aproximada de energía liberada por la tierra durante el sismo; y actualmente, la escala de magnitud de momento (denotada por Mw) es la escala estándar utilizada para dar información sobre terremotos. Ésta es una escala logarítmica y en ella el aumento de 1 unidad en la magnitud del terremoto representa un incremento de 10 veces en la amplitud medida, lo cual equivale a una liberación de energía 32 veces mayor (USGS, 2020).

Los terremotos han ocasionado un gran impacto negativo en la economía, desarrollo y demografía de los pueblos del sur de Puerto Rico. Muchas familias tuvieron que abandonar sus hogares para poder protegerse ya que gran parte de las viviendas fueron catalogadas como inestables o inseguras. El gobierno central en conjunto con los representantes locales adecuó una serie de refugios temporales con los cuales se dio albergue a aquellas familias cuyo riesgo del colapso de sus viviendas fuera muy probable.

En este trabajo, se hace una exploración estadística de los fenómenos sísmicos desde finales del 2019 a los inicios del 2021, buscando renovar la atención a su estudio. Es importante seguir enfatizando la prevención de pérdida de vidas humanas y, en ese aspecto, conocer más sobre el período descrito puede ser una herramienta útil para dar soporte a la creación de planes de emergencia efectivos y eficientes como lo señalan varias fuentes (DW, 2020). En efecto, durante los sismos se perdieron vidas, hogares, iglesias, colegios, bancos y el efecto psicológico en la población es todo menos desdeñable.

ANTECEDENTES

Este trabajo se centra en el análisis de los sismos ocurridos en Puerto Rico durante el periodo del 01-12-2019 a las 00:00:00 hasta el 15-01-2021 a las 23:59:59. Después de mediados del año 2019, más precisamente durante la última semana del mes de septiembre (23-09-2019 a las 11:23 p.m.), se presentó una secuencia sísmica que inició con un evento principal de magnitud 6.0 Mw en el Cañón de la Mona, y que produjo posteriormente una serie de sismos (RSPR, 2019; López et al., 2020). Una segunda secuencia sísmica se presentó a partir del 28-12-2019 a las 6:35 p.m. con un sismo de magnitud 4.7 Mw con epicentro a 11 km al sureste de Guánica el cual fue registrado sobre la falla Punto Montalva (NBBPMfz) y fue seguido de cuatro sismos ocurridos también en Guánica dentro de las 3 horas siguientes. Las magnitudes, horas y ubicaciones de cada uno de estos cuatro sismos son respectivamente: uno de 3.7 Mw a las 7:35 p.m. a 11 km al sur de Indios, uno de 3.5 Mw a las 8:34 p.m. a 14 km del sureste de Guánica, uno de 5.0 Mw a las 9:06 p.m. a 9 km al sur de Indios y uno de 4.70 Mw a las 9:21 p.m. a 11 km al sureste de María Antonia (Voces del Sur, 2019).

A diferencia de la secuencia sísmica que inició el 23-09-2019 en el Cañón de la Mona, esta última secuencia iniciada el 28-12-2019 sobre la falla Punto Montalva (NBBPMfz) se sintió fuertemente en todo Puerto Rico y afectó principalmente de manera importante a los pueblos de las zonas sur y suroeste de la isla con sismos recurrentes a partir de ese día. Se presentaron dos terremotos, uno de 5.80 Mw el 6 de enero de 2020 a las 6:32 a.m. a 9 km del sureste de Indios seguido por el evento más importante de la secuencia

sísmica que tuvo una magnitud de 6.4 Mw ocurrido en menos de 24 horas, exactamente a las 4:24 a.m. del 7 de enero de 2020; ambos se dieron sobre la falla Punto Montalva (NBBPMfz) y sorprendieron a gran parte de la población en sus hogares, el del día 7 de enero por la hora en que ocurrió y el del día 6 por ser uno de los días feriados más importantes de la isla, el Día de Reyes.

Debido a la recurrencia de los sismos, pero sobre todo a la magnitud de estos dos terremotos, se decidió analizar desde la secuencia sísmica del 28 de diciembre de 2019 hasta el 15 de enero de 2021. Es importante mencionar que en el año 2019 ocurrieron en total 6509 sismos, equivalente a 1.8 veces el promedio anual de sismos (3,542) registrados en Puerto Rico desde el 2014; sin embargo, esa cifra representa aproximadamente la mitad de los sismos ocurridos en el 2020 que cerró con una cifra de 3.5 veces ese promedio (12,489 sismos).

EXPLORACIÓN ESTADÍSTICA

El estudio de actividad sísmica en el periodo de estudio se basó en 69,570 datos recopilados (USGS, 2020) y 41,742 cantidades estadísticas calculadas a partir de ellos. Se presentan entonces tablas y gráficas que comprenden 13,914 sismos (3,687 ocurridos en tierra y 10,227 en el océano).

La Figura 1 muestra los pueblos de Puerto Rico donde se evidenció la mayor cantidad de sismos. El área que se analizó es de un radio de 60 km a partir del centroide de los eventos, un área que cubre al menos el 99% de los sismos alrededor de Puerto Rico y que ocurrieron en el periodo de estudio. Además, en la Figura 1 se observa la gran proporción de sismos en los dos grupos de magnitud mayor o igual que 2.08 Mw y menor que 4.24 Mw (identificados con color verde y amarillo respectivamente) frente a los otros rangos, como los 71 sismos con magnitud mayor o igual que 4.24 Mw (colores naranja y rojo) que representan el 0.51% del total, los más significativos a pesar de su porcentaje pequeño. En el mapa también se puede observar que el 100% de los sismos con magnitud mayor a 5.32 Mw (color rojo) ocurrió en el área suroeste de Puerto Rico, ya sea en tierra o en el mar, y todos ocurrieron en un radio aproximadamente de 25 km del centro de masa. Más adelante veremos que la Tabla 1 retoma información de la Figura 1 y añade un análisis de magnitudes.

Entre los resultados que se obtuvieron al analizar la base de datos “Earthquake” de USGS, a partir de la información de latitud y longitud se rescató información sobre las localizaciones de los epicentros de cada sismo en el período de estudio, encontrando así un total de 144 localizaciones. La cantidad de incidencias según la localización fue muy variada y más adelante se muestran detalles de las 37 localizaciones más destacadas según ese número; sin embargo, a partir de la Figura 2, es importante mencionar que las primeras 9 localizaciones que lideran esta jerarquía de epicentros en tierra (3, 687) fueron: Montalva (Guánica), Boca (Guayanilla), Barinas (Yauco), Carenero (Guánica), Costa (Lajas), Tallaboa Poniente (Peñuelas), Indios, Cedro y Magas (en Guayanilla los tres). Estas 9 localizaciones muestran frecuencias superiores a 125 sismos y en conjunto con las del océano acumulan 13,140 sismos (aprox. 94.44% del total).

Por otro lado, a partir de la localización es importante reconocer y presentar resúmenes de datos y gráficos según el pueblo al que pertenecían; el diagrama de barras de frecuencia de sismos por pueblo y localización de la Figura 2 es uno de ellos. Esta Figura nos permite detectar también entre todas las localizaciones epicentro aquellos pueblos que sobresalen tanto por la cantidad de sismos como por su magnitud. En este sentido, se destacan 6 pueblos con el mayor número de sismos significativos, siendo Guánica y Guayanilla los pueblos con mayor cantidad de sismos ocurridos en tierra con: 1,284 y 1,203 respectivamente (67.5% del total), seguidos por Yauco, Lajas, Peñuelas y finalmente Cabo Rojo (ver Figura 2). Es importante resaltar que del total de pueblos no considerados en la Figura 2 destacó Ponce,

cuya cantidad de sismos es similar a la de Cabo Rojo; y que a su vez fue el epicentro de un sismo de 4.4 Mw, una magnitud resaltante. Ponce muestra también un promedio de magnitud de sismos superior a 2.5 Mw durante el periodo considerado. El valor de la magnitud para los 13,914 registros de sismos muestra un comportamiento relativamente variable y sesgado a la derecha, con una mediana de 2.54 Mw y muchos valores fuera de rango.

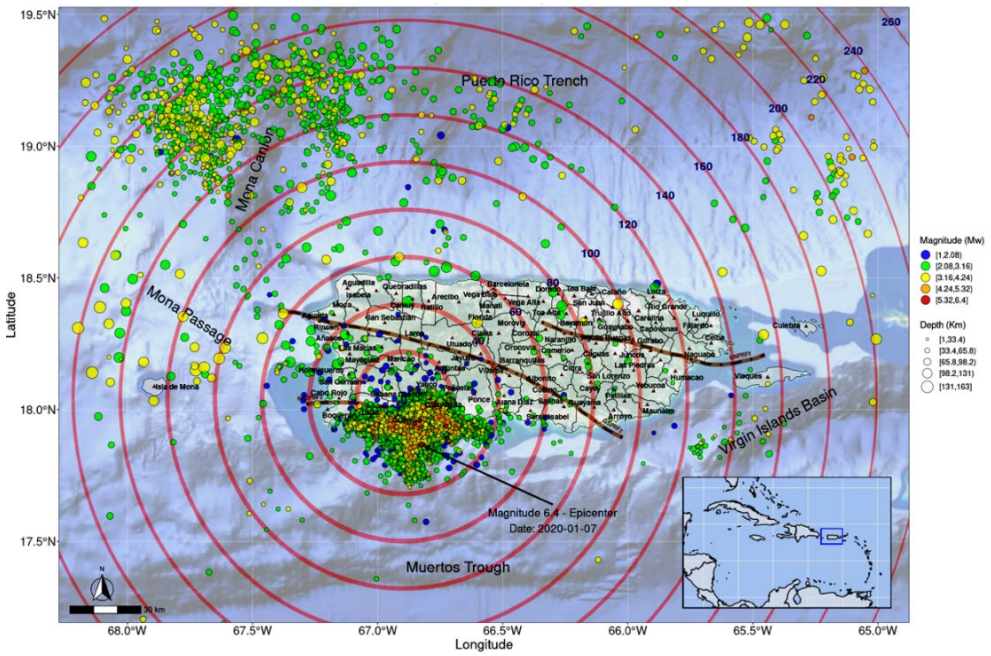

Figura 1: Actividad sísmica en Puerto Rico (01-12-2019 a 15-01-2021) por magnitud y profundidad. Cada sismo está representado por un círculo; el color define la magnitud en escala ascendente: azul, verde, amarillo, naranja y rojo. El tamaño del círculo, define la profundidad del sismo, también en escala ascendente, es decir; a mayor profundidad, mayor tamaño.

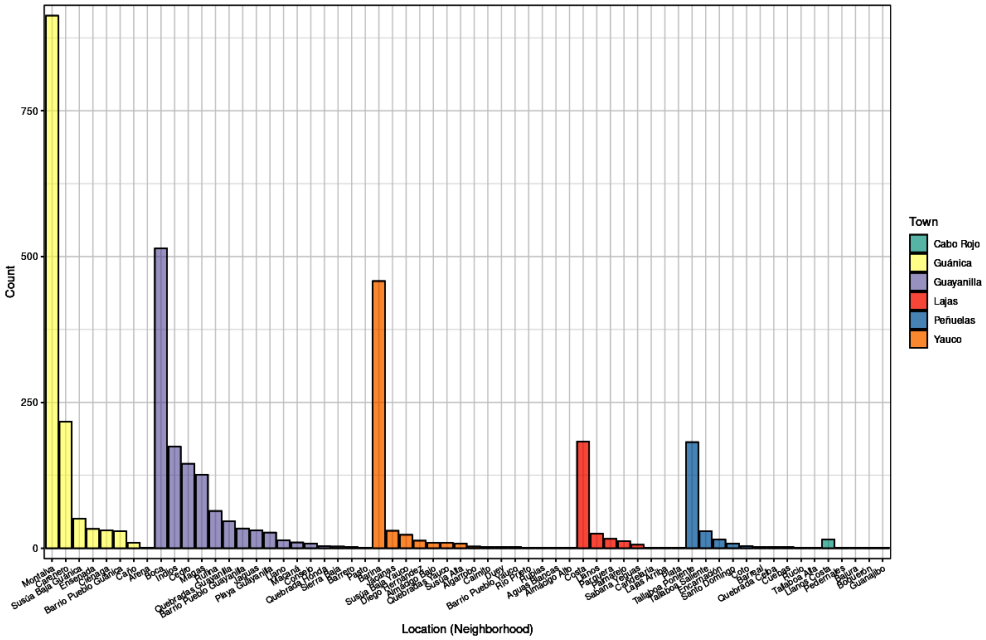

Figura 2: Localización de la mayor frecuencia de sismos por pueblo.

Tabla 1: Número de sismos de magnitud mayor a 4 Mw por lugar o pueblo y localización.

LUGAR O PUEBLO	LOCALIZACIÓN	MAGNITUD (MW)			TOTAL
		4.0 - 4.42	4.5 - 4.9	5.0 - 6.4	
Océano; 78%	Océano	66	25	13	104
Guayanilla; 7.5%	Magas	0	0	1	1
	Indios	1	0	1	2
	Boca	3	2	0	5
	Cedro	1	0	0	1
	Playa Guayanilla	1	0	0	1
Guánica; 10%	Carenero	0	1	0	1
	Montalva	8	4	0	12
	Ensenada	1	0	0	1
Ponce; 1%	Canas	1	0	0	1
Peñuelas; 1.5%	Tallaboa Saliente	1	0	0	1
	Tallaboa Poniente	1	0	0	1
Yauco; 2%	Barinas	3	0	0	3
TOTAL		87	32	15	134

Del número total de sismos, se observó que 134 tuvieron una magnitud igual o mayor a 4.0 Mw, 87 de los cuales presentaron magnitudes entre 4.0 y 4.4 Mw, 32 entre 4.5 Mw y 4.9 Mw; y 15 mayores o iguales a 5.0 Mw (Tabla 1).

La Tabla 1 muestra el resumen del número de sismos con magnitud mayor o igual a 4Mw por lugar o pueblo y localización, en ella podemos observar que 104 de los 134 sismos (78%) de gran magnitud tuvieron como epicentro el mar, 13 de los cuales tuvieron una magnitud mayor que 5.00 Mw. Analizando los epicentros de los sismos ocurridos en tierra, Guánica y Guayanilla fueron pueblos epicentro del 17.5% del total de sismos (ver Tabla 1). De ellos dos, se resume que Guánica fue el pueblo de Puerto Rico con mayor cantidad de sismos en tierra (10%), 12 de los cuales tuvieron como epicentro al sector Montalva; luego sigue el pueblo de Guayanilla con 7.5% del total de sismos fuertes, 2 de los cuales fueron de magnitud mayor o igual que 5.00 Mw con epicentros en Indios y Magas. Les siguen en ese orden: Yauco, Peñuelas y Ponce que representan juntos casi el 4.5% restante. Estos cinco pueblos coinciden con el mayor número de sismos registrados en todo Puerto Rico de la Figura 2; sin embargo, Guayanilla destaca más entre ellos por los dos sismos de magnitud mayor o igual a 5.0 Mw.

Por otro lado, respecto a las localizaciones es importante mencionar que Montalva, Boca y Barinas prevalecen como las localizaciones del número de sismos de magnitud mayor que 4.0 Mw (20 de los 134); Indios y Magas por su parte se destacan por haber sido epicentros cada uno de un sismo de magnitud

superior a 5.0 Mw y un máximo de 6.4 Mw (Tabla 1). Al analizar la profundidad global del total de los sismos estudiados, se obtiene que aproximadamente 3,479 (el 25% del total) tuvieron una profundidad de 7 km o más; el 50% de los sismos tuvieron una profundidad igual o mayor a 11.52 km.

La magnitud y profundidad para los sismos dentro de los 6 pueblos (y sus respectivas localizaciones) con mayor incidencia, y relevantes entre todos los sismos registrados en el periodo analizado se muestran en las Figuras 3 y 4. Ambas figuras muestran valores descriptivos de la distribución de los datos por sector que son comparativos y permiten identificar gráficamente valores fuera de rango de magnitud y profundidad por epicentro (la Figura 3 por pueblos mientras que la Figura 4 lo hace para las principales localizaciones dentro de cada pueblo). En este entender, respecto a las variables magnitud y profundidad comparadas entre los 6 pueblos con mayor incidencia de sismos (ver Figura 3), se observó que con excepción de Cabo Rojo, todos presentan sismos con mediana de magnitud entre 2.38 Mw y 2.54 Mw; Guayanilla y Guánica tienen muchos valores fuera de rango (sismos de magnitud igual o mayor que 3.5 Mw), Peñuelas tuvo una mediana de magnitud de sismos mayor que las demás, y Cabo Rojo fue el de menor de entre los 6 (tal como se observó en la Figura 2), seguido por Yauco que fue epicentro de tres sismos de mayor magnitud (uno de 4.17 Mw y dos de 4.20 Mw). La Figura 3 resalta también la proporción de sismos con magnitudes mayores que 4.00 Mw de los tres pueblos más destacados (Tabla 1).

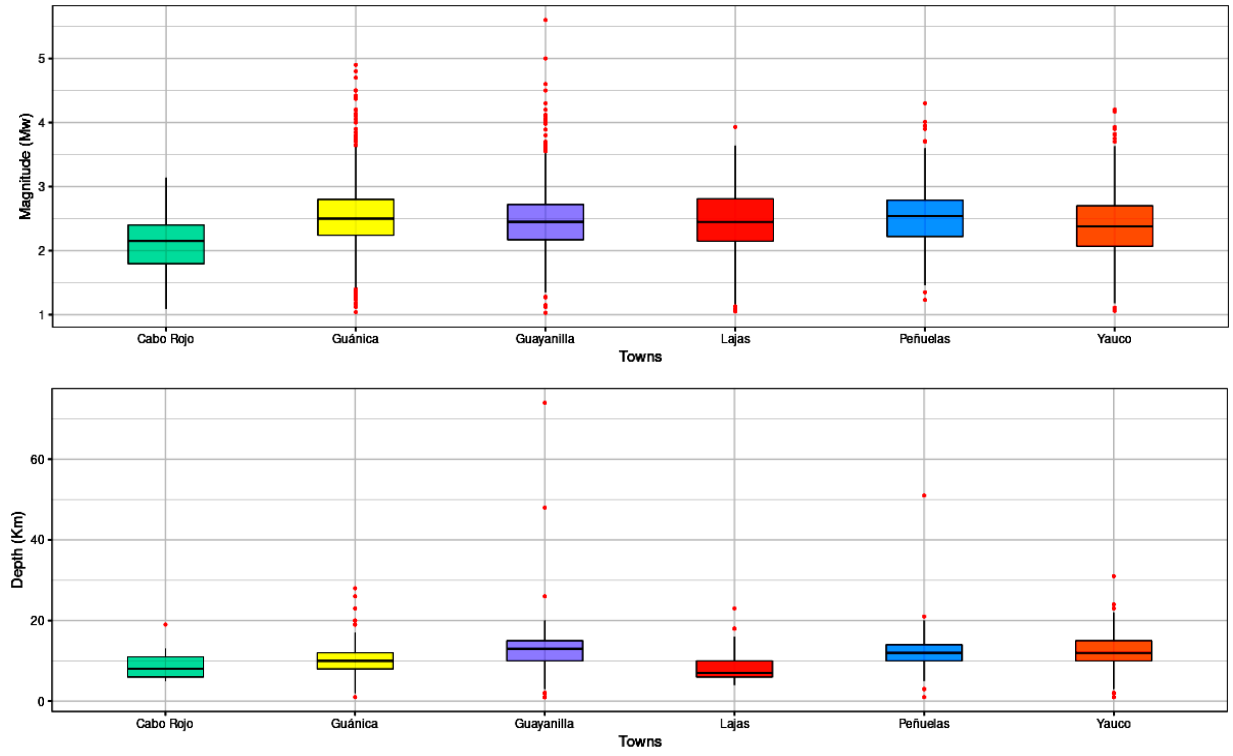

Figura 3: Diagrama de cajas de magnitud (parte superior) y profundidad (parte inferior) para los 6 pueblos con mayor incidencia de sismos.

En la distribución de profundidad de los sismos ocurridos comparados por pueblos se observa que los valores en los 6 pueblos oscilan entre 7 km y 13 km, de ellos tanto Cabo Rojo como Lajas describen los valores menores; a su vez, Lajas también se destaca por ser la de mayor variabilidad en profundidad, y los otros 5 restantes quedan en un término medio compartiendo una profundidad mediana próxima a 10 km (parte inferior de la Figura 3).

Al ser analizadas estas dos variables respecto a la localización epicentro de los sismos mostrados en la Figura 4, las diferencias son más marcadas entre las localizaciones pertenecientes a los 6 pueblos. Se observa menos similitud en su distribución y mayor variabilidad en los valores tanto de magnitud como de profundidad; un ejemplo de esto es que el sector epicentro predominante del pueblo de Guánica fue Montalva; sin embargo, la magnitud mediana de esta localización fue Me=2.52Mw, menor frente a otro sector como Barrio Pueblo Guánica cuya mediana fue de Me=2.6Mw.

Una situación similar ocurre en la magnitud del sector de Quebrada Honda y Playa Guayanilla con medianas Me=2.77Mw y Me=2.64Mw respectivamente, ambas superiores a la mediana de magnitud de Boca (Me=2.47Mw) la cual es una de las dos localizaciones epicentro con mayor número de sismos.

Por otro lado, en lo que respecta a la profundidad por localización (parte inferior de la Figura 4), se ve que Coto en Peñuelas, Caño en Guánica, Macano en Guayanilla y Susua Alta en Yauco presentan mayor variabilidad en cuanto a la profundidad de los sismos ocurridos.

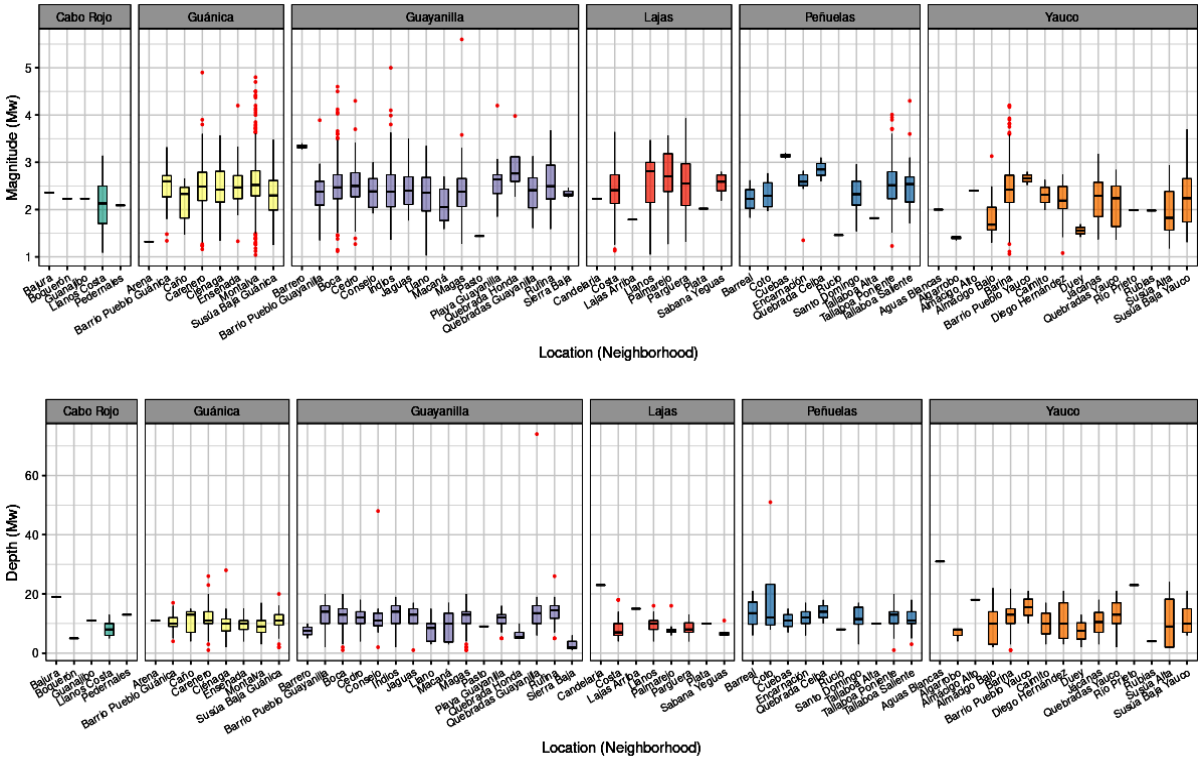

Figura 4: Diagramas de cajas de magnitud (parte superior) y profundidad (parte inferior) para las principales localizaciones dentro de los 6 pueblos con mayor incidencia de sismos.

En este estudio, se agregó también la información de las regiones sísmicas epicentro a las cuales pertenecían todos los sismos registrados en el periodo; la Tabla 2 y Figura 5 resumen esta información. Como resultado de esta subdivisión se pudieron clasificar ocho regiones sísmicas, las cuales en orden de importancia son: Falla Punto Montalva (NBBPMfz) que destaca por sobre todas al ser epicentro de aproximadamente el 91% de los sismos, seguida del Cañón de la Mona, la gran Trinchera del Norte de Puerto Rico, Gran Falla del Sur de Puerto Rico (GSPRFz), depresiones de Islas Vírgenes y Anegada, Pasaje de la Mona, Trinchera de Los Muertos y Gran Falla del Norte de Puerto Rico (GNPRFz).

Del número de sismos más fuertes y por tanto más relevantes del estudio clasificados por región sísmica (Tabla 2), se observa que el 88% del total tuvo como epicentro a la Falla Punto Montalva (NBBPMfz) y 7.5% al Cañón de la Mona con 10 sismos de magnitud de entre 4.0 Mw y 4.9 Mw.

Las otras dos regiones sísmicas que forman parte del conjunto de sismos significativos son: la Gran Trinchera del Norte y la Gran Falla del Sur de Puerto Rico (GSPRFz).

Tabla 2: Número de sismos de magnitud mayor a 4Mw por región sísmica y epicentro.

FALLA SÍSMICA	LUGAR	MAGNITUD (MW)			TOTAL
		4.0 - 4.42	4.5 - 4.9	5.0 - 6.4	
Punto Montalva (NBBPMfz); 88%	Océano 77%	57	21	13	91
	Tierra 23%	18	7	2	27
Cañón de la Mona; 7.5%	Océano 100%	9	1	0	10
	Tierra 0%	0	0	0	0
Gran Trinchera del Norte; 3.7%	Océano 100%	2	3	0	5
	Tierra 0%	0	0	0	0
Gran Falla del Sur de Puerto Rico (GSPRFz); 0.75%	Océano 100%	1	0	0	1
	Tierra 0%	0	0	0	0
TOTAL		87	32	15	134

Al analizar la Figura 5 que incluye los diagramas de caja comparativos de magnitud y profundidad para las Fallas: Punto Montalva (NBBPMFz), región sísmica del 91% de los sismos estudiados y Cañón de la Mona. Aunque esta última sólo representa cerca al 4% del total de sismos, supera tanto en la mediana de magnitud como de profundidad a la primera; además de ser la región sísmica principal epicentro de los pueblos de Aguadilla y Rincón, ambos con sismos de magnitud promedio de 2.87 Mw y valores máximos de magnitud de 4.10 Mw (Aguadilla) y 3.10 Mw (Rincón).

En general, evaluando estas dos regiones se puede ver una distribución similar respecto a la simetría y dispersión de los valores de magnitud para ambas fallas; sin embargo, la magnitud de los sismos debidos a la falla Cañón de la Mona muestra valores más altos con una mediana de Me=3.05 Mw. Mientras que en la falla Punto Montalva (NBBPMfz) la mediana es de Me=2.49 Mw; esto lo que significa es que aproximadamente el 50% de los sismos de la Falla Cañón de la Mona fueron mayores o iguales que 3.05 Mw mientras que en la falla Punto Montalva (NBBPMfz) aproximadamente el 25% de los sismos fueron mayores o iguales que 2.8 Mw (tercer cuartil de Q3=2.8 Mw aprox.); esto hace también determinante a la Falla Cañón de la Mona en la distribución de magnitud de los sismos analizados.

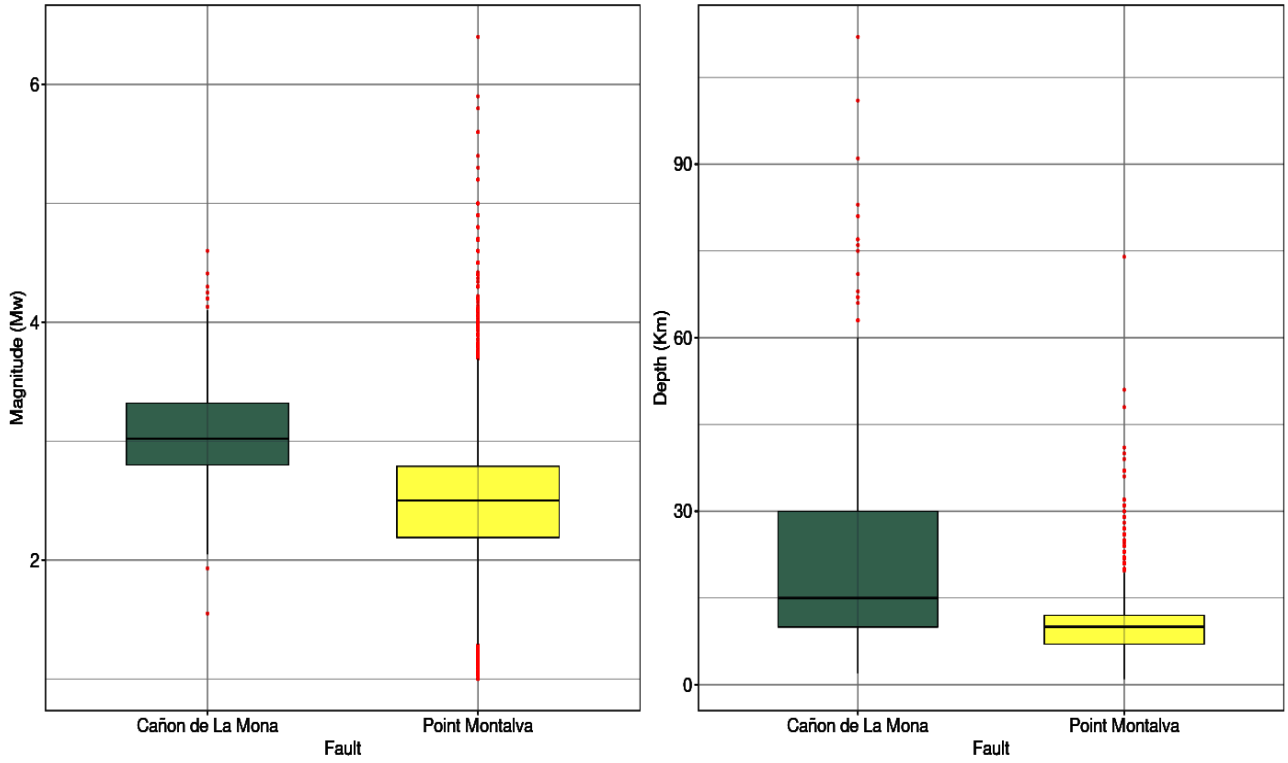

Figura 5: Actividad sísmica comparativa en magnitud (izquierda) y profundidad (derecha) para la Fallas: Punto Montalva (NBBPMFz) y Cañón de la Mona.

Por otro lado, se puede observar que, pese a que sólo el 4% del total de sismos se presentó en el Cañón de la Mona, esta falla fue epicentro de seis sismos de magnitudes mayores o iguales que 4.2 Mw y el 75% de los sismos de los cuales fue epicentro, tuvieron magnitudes mayores o iguales que 2.8 Mw. Respecto a la Falla Punto Montalva (NBBPMfz), es la región epicentro de 118 de los 134 sismos más fuertes, con magnitudes mayores o iguales que 4.0 Mw (aprox. 88%).

Según el estudio de la profundidad para estas principales Fallas (parte derecha de la Figura 5), se observó que los sismos de la Falla Punto Montalva (NBBPMfz) tuvieron una profundidad media de poco menos de 10 km, mientras que los sismos ocurridos en el Cañón de la Mona son sesgados a la derecha y con mayor dispersión $Media = 21.97\ km$).

En la Figura 6, se muestra la distribución mensual de la cantidad de sismos ocurridos durante el periodo de estudio y podemos resaltar la gran diferencia observada de la cantidad de sismos ocurridos en enero de 2020 respecto a los demás meses de ese año y la primera quincena del 2021; esos más de 4500 sismos del mes de enero de 2020, se redujeron en tres cuartas partes durante el mes de febrero y fueron disminuyendo paulatinamente hasta antes de julio de ese año en que volvieron a aumentar para luego continuar decreciendo con excepción de los meses de noviembre y diciembre en que aumentaron ligeramente, para finalmente disminuir drásticamente en enero de 2021.

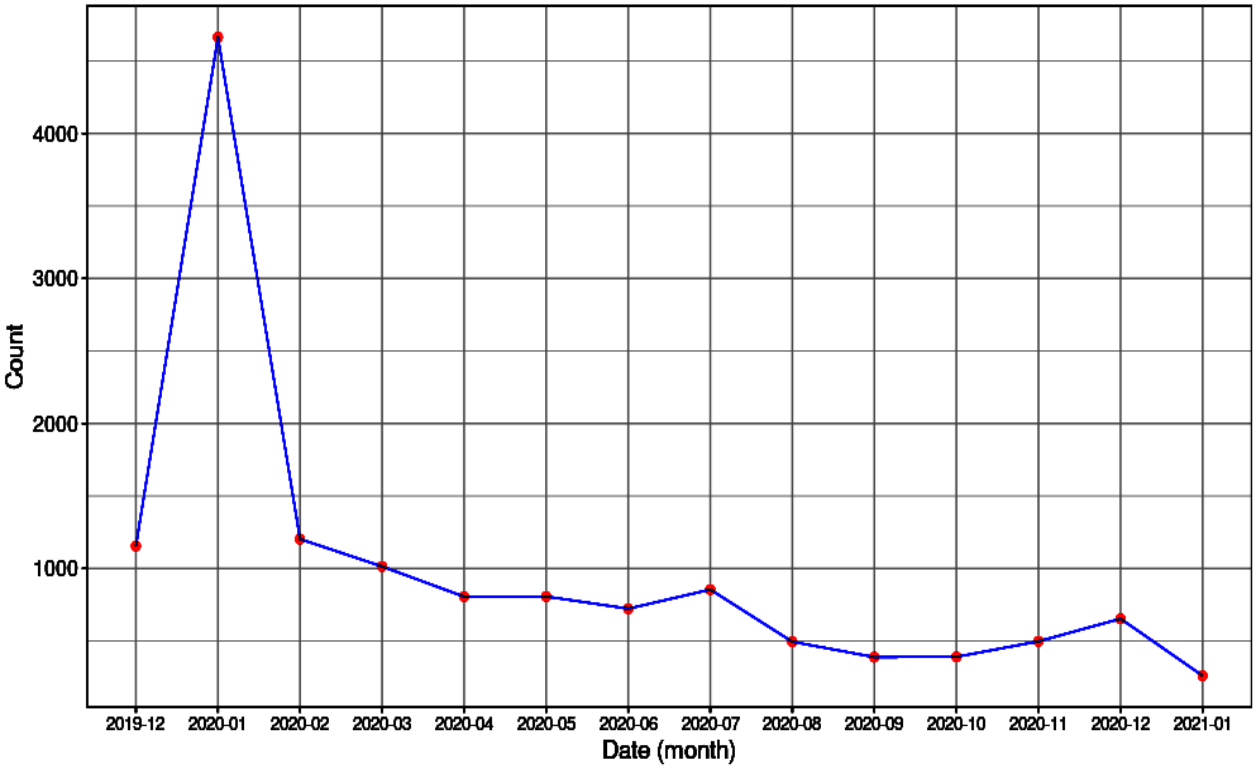

Figura 6: Serie de tiempo del número de sismos en Puerto Rico (01-12-2019 a 15-01-2021.

La distribución del conteo de sismos por área se muestra en la Figura 7, en ella podemos notar que aproximadamente el 91% de los sismos se presentan en una región circular cuyo centro es el centro de masa de todos los sismos que ocurrieron durante el periodo de estudio; a esta región la denominamos *región I*. El área de la *región I* es de 5 026 km^2. Por otro lado, el área completa que abarca nuestro análisis es la región rectangular cuyas coordenadas son: latitud 17.2º S, 19.5º N y longitud 68.2º W, 65º E; esta región tiene un área de 76 748.9 km^2 (ver Figura 1). A la región que está fuera de la *región I* pero dentro de la región completa de estudio, se le llamó *región II*. Cabe recalcar que las regiones *I* y *II* son muy diferentes no sólo en tamaño, sino que presentan algunas características importantes desde el punto de vista del análisis sismográfico.

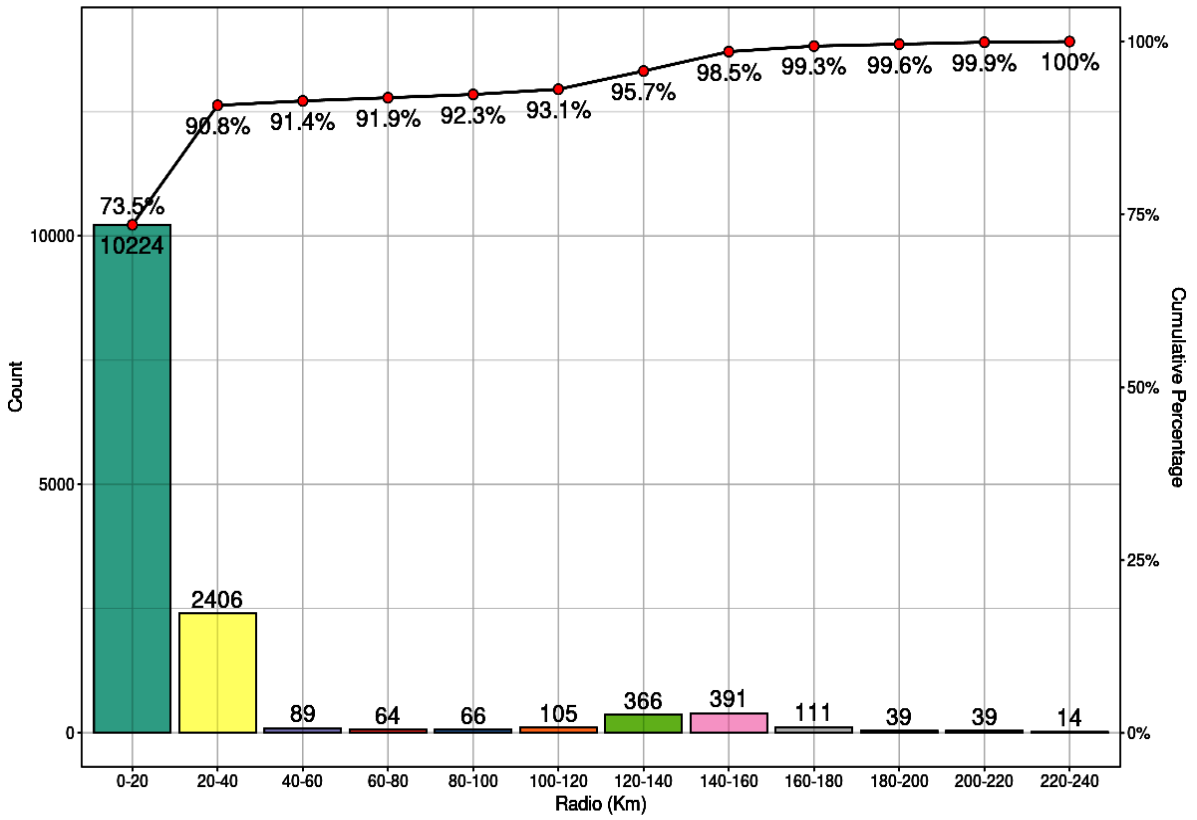

Figura 7: Conteo Acumulado de Sismos respecto a un radio en km (centrados en Punto Montalva).

Se observó por ejemplo que la energía sísmica media por semana durante el periodo del 01-12-2019 hasta el 15-01-2021 para la *región circular I* fue de 368.7 MJ; mientras que, para el mismo periodo, la energía sísmica media por semana de la *región II* fue de 3288.7 MJ. Por lo tanto, el promedio para la *región I* es $0.073\ \frac{\text{MJ}}{\text{km}^2}$ y $0.043\ \frac{\text{MJ}}{\text{km}^2}$ para la región *II;* es decir que, la región *I* mostró 1.7 veces más propensión a la actividad sísmica que la *región II;* a pesar de que la *región I* es 15 veces más pequeña que la *región II.*

Considerando estas relaciones se puede determinar que, un terremoto de magnitud igual a 8.0 Mw libera energía equivalente a 10^{11} MJ; como ejemplo de esto tenemos que, la energía liberada por una explosión nuclear de 10 kilotones es de 10^{6} MJ y equivale a un terremoto de magnitud igual a 5.5 Mw.

Con el análisis anterior, se puede observar que la *región I*, que comprende la parte suroeste de la isla de Puerto Rico, mantuvo una importante actividad sísmica durante el año 2020. Por otro lado, de acuerdo al comportamiento de las series de tiempo de la Figura 8, Figura 9 y Figura 10, existen indicios fuertes para estimar que la actividad sísmica fue también significativa durante el resto del 2021.

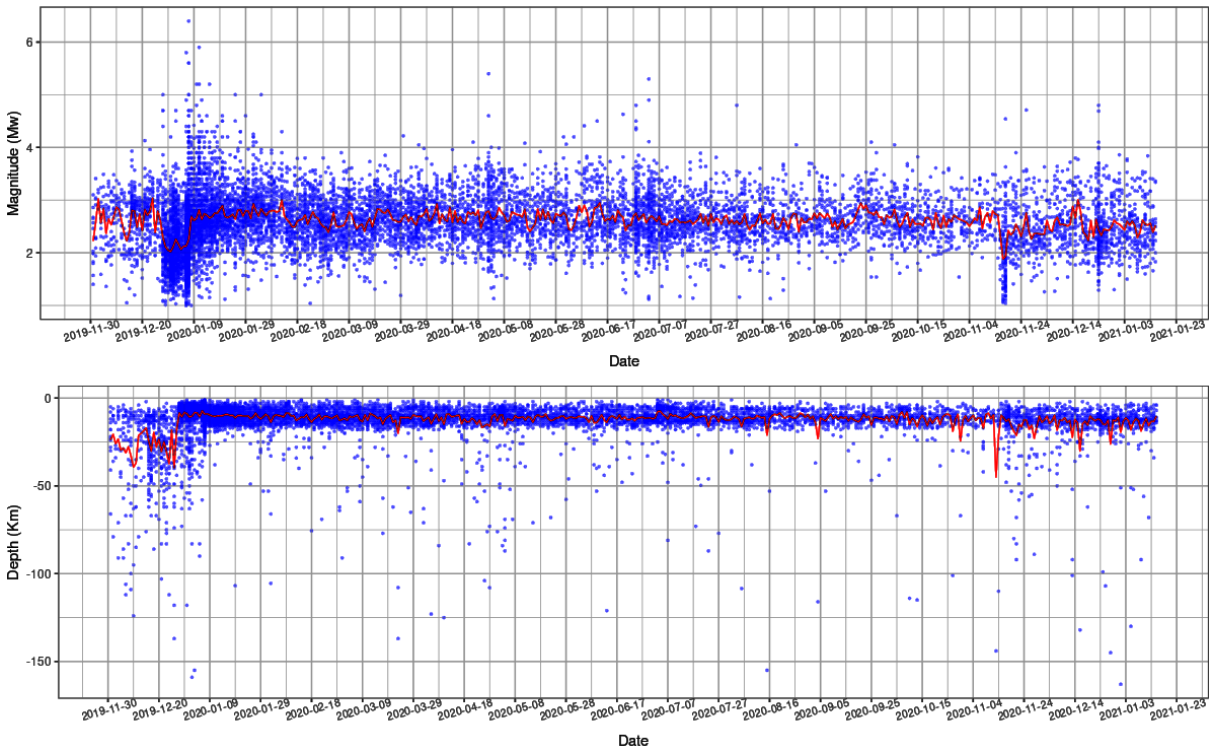

Figura 8: Serie de tiempo de la actividad sísmica en la Falla Punto Montalva (NBBPMfz) por magnitud y profundidad (01-12-2019 a 15-01-2021).

La Figura 8, además de resaltar los sismos más significativos que fueron sentidos en Puerto Rico, muestra a su vez la variación de la magnitud y profundidad de estos a través del tiempo. Esta figura presenta la serie de tiempo de la magnitud y profundidad de los sismos ocurridos sobre la Falla Punto Montalva (NBBPMfz); y respecto a ambas variables podemos distinguir un cambio importante y significativo desde el 28-12-2019 al 20-01-2020, en donde se nota un fuerte aumento en la cantidad de sismos registrados. No obstante, la magnitud promedio de estos sismos no es muy elevada hasta los días 6 y 7 de enero de 2020 que fueron las fechas en las cuales ocurrieron los dos eventos más destacados del período bajo estudio, un sismo de 5.80 Mw a las 6:32 a.m. hora local el día 06-01-2020 y el terremoto de 6.4 Mw del 07-01-2020 con una duración de 37 segundos y que es el tercer terremoto más fuerte de la historia de Puerto Rico. Ambos sismos ocurrieron en la falla de Punto Montalva (NBBPMfz) y fueron secundados días después por un tercer sismo de magnitud mayor que 5 Mw ocurrido en la mañana del sábado 15-01-2020. Estas tres fechas forman parte de este primer intervalo de tiempo de cambio significativo en esta serie de tiempo. Por otro lado, en la parte inferior de la Figura 8, también vemos que surgió un aumento en el promedio de la profundidad de los sismos a partir del 01-12-2019 hasta el 08-01-2020.

Se puede destacar que el aumento del promedio en la profundidad de los sismos coincide con el aumento de la cantidad y la magnitud de ellos; un ejemplo de esto es que dentro del primer periodo de cambio desde fines de diciembre hasta unos días después del terremoto del 07-01-2020 se reportaron los sismos con mayor profundidad de ese periodo; siendo los tres más profundos mayores a 25 km; dos de ellos ocurrieron en los días 29-12-2019 y uno el 02-01-2020. Posteriormente a este primer periodo, las series de la magnitud y de la profundidad de los sismos se estabilizaron para nuevamente mostrar un aumento en la magnitud el día 02-05-2020 con un sismo de 5.4 Mw como su punto máximo. Más adelante, hubo un nuevo incremento del promedio de los sismos alrededor del 03-07-2020 a las 4:49 p.m., con un sismo de magnitud 5.30 Mw también en la falla de Punto Montalva (NBBPMfz). Finalmente, tenemos un incremento del promedio en las vecindades de la fecha del día 27-12-2020. Existe un punto de cambio en la serie de la magnitud del total de sismos estudiados ocurridos en Puerto Rico los cuales son presentados en la Figura 9; este punto se da el día 07-01-2020 a las 3:29 a.m. en donde se registra un sismo de 2.48 Mw, con una profundidad de 3 Km ocurrido en la región de la falla Punto Montalva (NBBPMfz).

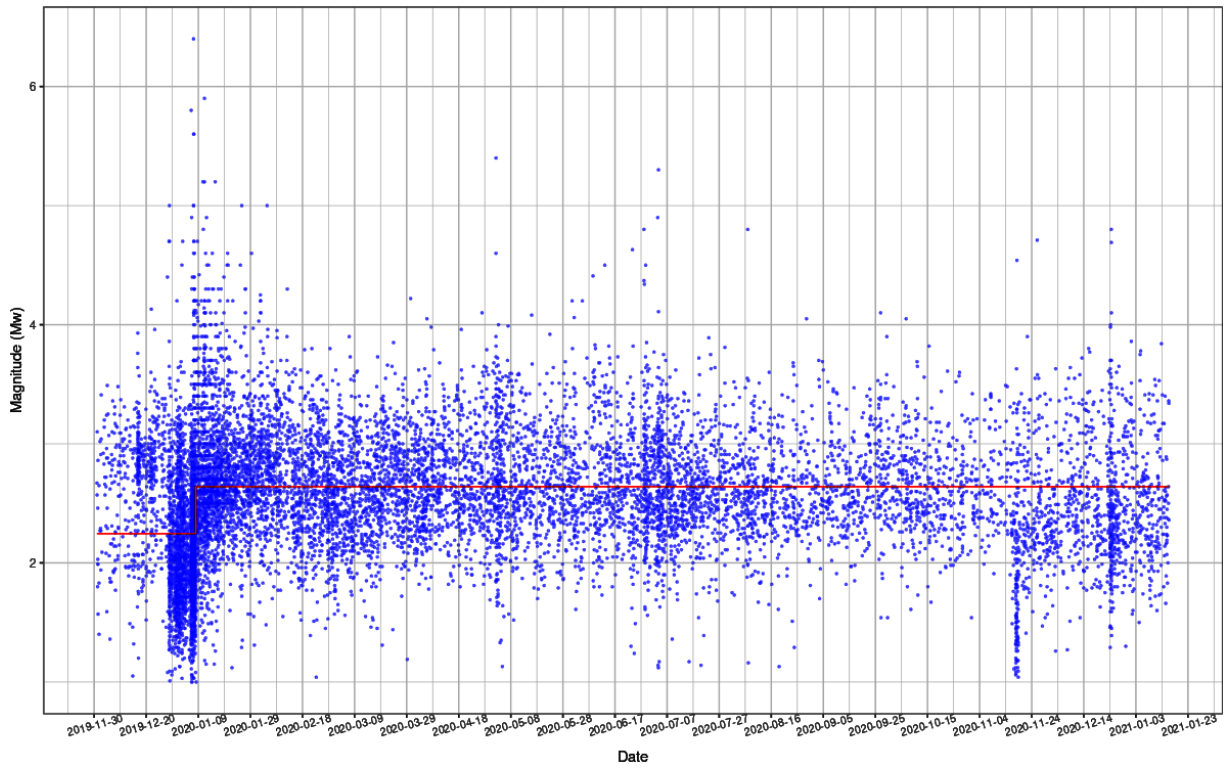

Figura 9: Detección del punto de cambio en la serie de tiempo de la actividad sísmica en Puerto Rico según magnitud (01-12-2019 a 15-01-2021). Se usó el algoritmo PLT del paquete zoo de R para detectar el punto de cambio.

Esta ruptura es la antesala del aumento en la magnitud promedio de los sismos en la serie que fue de 2.25 Mw; y posteriormente aumenta a 2.64 Mw para mantenerse estable en lo sucesivo hasta el día 07-11-2020, fecha en la que hay un descenso del promedio de la magnitud de los sismos que fue de 1.91 Mw (ver Figura 9). Esta disminución se dio por sólo tres días: entre el 16-11-2020 y 18-11-2020; luego regresó a un promedio de 2.43 Mw, el cual es sólo ligeramente inferior a la inicial.

Un comportamiento similar ocurrió con el promedio en la profundidad de sismos, que era de 27.3 km antes del punto de ruptura y que pasó a ser 10.88 km posteriormente (Figura 10).

Ahora, también se puede determinar que durante los tres días en los que el promedio de la magnitud cayó, también la profundidad tuvo un cambio considerable siendo este valor de 12.32 km sobre la superficie.

De la Figura 10, es relevante resaltar que posterior al punto de cambio, con una diferencia de tan sólo 55 minutos, se presenta el evento más importante de nuestro periodo de estudio, el cual fue el terremoto de 6.4 Mw y el cual tuvo una profundidad de 8.95 km (ver Figura 10).

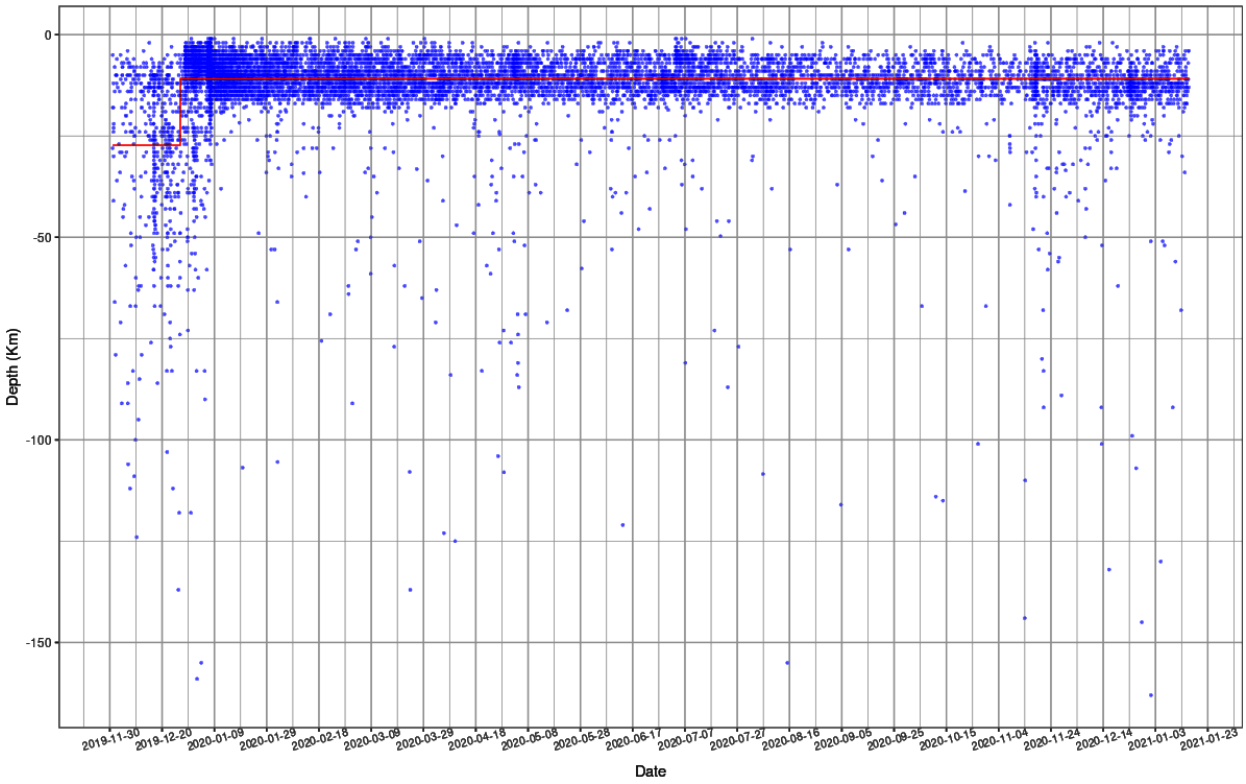

Figura 10: Detección del punto de cambio en la serie de tiempo de la actividad sísmica en Puerto Rico según profundidad (01-12-2019 a 15-01-2021). Se usó el algoritmo PLT del paquete zoo de R para detectar el punto de cambio.

CONCLUSIONES

Con base en los resultados de análisis de los datos sísmicos ocurridos en Puerto Rico entre el 01-12-2019 y el 15-01-2021 estudiados en la presente investigación, destacamos las siguientes conclusiones.

Con respecto al número de sismos ocurridos por mes, sobresale el mes de enero de 2020 con más de 4500 sismos, y entre los cuales están dos de los sismos más fuertes (5.8Mw y 6.4Mw) que históricamente hayan afectado a Puerto Rico. Por otro lado, de los 3687 sismos ocurridos en tierra, Guánica y Guayanilla fueron los pueblos con mayor registro, acumulando juntos 2487 de ellos (67.5%). Respecto a las fallas, se observó que el 88% del total de sismos con magnitud mayor a 4.00 Mw tuvo como epicentro a la Falla Punto Montalva. Finalmente, las dos conclusiones más importantes fueron: determinar que el aumento del promedio en la profundidad de los sismos registrados coincide con el aumento de la cantidad y la magnitud de ellos; y encontrar que la *región I* que comprende la parte suroeste de la isla de Puerto Rico pese a ser 15 veces más pequeña que la *región II*; mostró ser 1.7 veces más propensa a la actividad sísmica.

Estos datos deben conllevar al gobierno puertorriqueño a tomar medidas de protección que consideren el bienestar físico y mental de la población. Deben adaptarse los planes de acción para que haya un manejo más eficiente de cara a eventuales movimientos sísmicos en Puerto Rico. Los planes de acción no deben limitarse sólo a la seguridad física que incluye infraestructura, servicios de emergencia, distribución de agua, alimentos y medicamentos, sino también protocolos y servicios para que la población sufra lo menos posibles efectos psicológicos adversos. Las medidas preventivas deben aplicarse a todo Puerto Rico y se debería comenzar en la región suroeste por ser altamente vulnerable.

REFERENCIAS

Bommer J. J & Martínez-Pereira A. (1999). "The effective duration of earthquake strong motion", *Journal of Earthquake Engineering*, Vol. 3 No.2, pp. 127-172.

Red sísmica de Puerto Rico, Universidad de Puerto Rico "RSPR". (2019). Recinto de Mayagüez, Departamento de Geología, "Informe de la actividad sísmica en la región de Puerto Rico e Islas Vírgenes durante el mes de diciembre de 2019" https://redsismica.uprm.edu/spanish/sismicidad/reportes/2019/boleDiciembre2019.pdf

López, A.M., Hughes, K.S., & Vanacore, E. (2020). "Puerto Rico's Winter 2019-2020 Seismic Sequence Leaves the Island on Edge", Temblor, http://doi.org/10.32858/temblor.064.

USGS. (2020). United States Geological Survey – Latest Earthquakes. Disponible en: https://www.usgs.gov/programs/earthquake-hazards/earthquakes.

Voces del Sur. (2019). https://www.vocesdelsurpr.com/2019/12/temblor-ampliamente-sentido-en-puerto-rico/.

DW. (2020). https://www.dw.com/es/puerto-rico-carece-de-un-plan-de-acción-ante-terremotos-aseguran-expertos/a-52064237.

RESEÑA DE AUTORES

S. Huanca-Ochoa

Candidata doctoral del Programa Graduado de Bioingeniería en la Universidad de Puerto Rico – Mayagüez (UPRM). Obtuvo el Bachillerato en Matemática mención Estadística en la Universidad Nacional de San Antonio Abad del Cusco, Perú y la Maestría en Ciencias en Matemática Estadística en la UPRM. Miembro de "The Applied Optimization Group" del Departamento de Ingeniería Industrial de la UPRM. Las líneas de investigación incluyen el análisis de datos biológicos, el modelamiento y optimización de sistemas biológicos.

R. Trespalacios-Alies

Profesor e investigador del Departamento de Ciencias Básicas de la Universidad Tecnológica de Bolívar, Colombia. Egresado de la Universidad de Cartagena, Colombia donde obtuvo su Bachillerato en Matemáticas y la Maestría en Ciencias en Matemática Estadística en la Universidad de Puerto Rico – Mayagüez (UPRM) con planes de reanudar sus estudios doctorales en UPRM. Miembro de "The Applied Optimization Group" del Departamento de Ingeniería Industrial de la UPRM. Las líneas de investigación incluyen estadística computacional, análisis funcional, y minería de datos.

Z. Acevedo-Figueroa

Estudiante del Bachillerato de Ingeniería Industrial (ININ) en la Universidad de Puerto Rico – Mayagüez (UPRM). Miembro de "The Applied Optimization Group" del Departamento de Ingeniería Industrial de la UPRM. Las líneas de investigación incluyen la manufactura esbelta, el mejoramiento continuo y el análisis estadístico de datos.

RESEÑA DE AUTORES (CONT.)

D. Alizo-Alique

Egresada de la Universidad de Puerto Rico – Mayagüez (UPRM) donde obtuvo su bachillerato en Ingeniería Industrial en 2021. Miembro de "The Applied Optimization Group" del Departamento de Ingeniería Industrial de la UPRM. Las líneas de investigación incluyen la manufactura, la mejora continua de negocios y el emprendimiento empresarial.

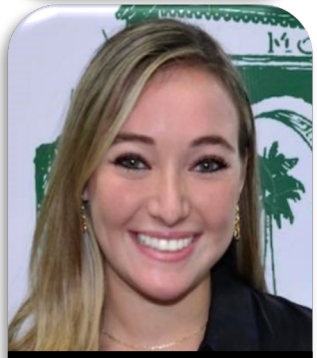

A. Nieves-Jiménez

Estudiante egresada en *Colorado State University* y su enfoque es en Meteorología Tropical. Terminó sus estudios de Bachillerato en Ingeniería Industrial en la Universidad de Puerto Rico – Mayagüez (UPRM) y participará de la graduación de Junio 2022. Fue miembro de "The Applied Optimization Group" del Departamento de Ingeniería Industrial de la UPRM durante sus años subgraduados y el enfoque de sus investigaciones fue combinando Ingeniería Industrial y Ciencias Atmosféricas. Las líneas de investigación incluyen el anejo de emergencias, planificación de desastres y huracanes.

C. Isaza

Catedrática Auxiliar en el Departamento de Biología de la Universidad de Puerto Rico – Mayagüez (UPRM). Egresada de la Universidad de los Andes, Colombia donde obtuvo el Bachillerato en Física y egresada de *The Ohio State University* donde obtuvo el Doctorado en Biofísica. Realizó el Postdoctorado en *Ponce Health Sciences University*, después del cual fungió como Catedrática Auxiliar del Programa de Salud Pública y del Departamento de Ciencias Básicas en la misma universidad. Fue Profesora Investigadora en la Facultad de Ciencias Biológicas de la Universidad Autónoma de Nuevo León, México del 2005 al 2008. Es actualmente Codirectora de "The Applied Optimization Group" del Departamento de Ingeniería Industrial de la UPRM. Las líneas de investigación incluyen el análisis de datos biológicos, la biofísica, la salud pública y el estudio de condiciones neurodegenerativas y su posible relación con infecciones virales.

M. Cabrera-Ríos

Catedrático en el Departamento de Ingeniería Industrial y en el Programa Graduado de Bioingeniería en la Universidad de Puerto Rico – Mayagüez (UPRM). Obtuvo la Maestría en Ciencias y el Doctorado en Ingeniería Industrial y de Sistemas en *The Ohio State University* (OSU); su Bachillerato fue en la misma disciplina en el Instituto Tecnológico y de Estudios Superiores de Monterrey (ITESM) en México y realizó el postdoctorado en OSU. Fue Profesor Investigador en el Programa de Posgrado en Ingeniería de Sistemas de la Universidad Autónoma de Nuevo León, México del 2003 al 2008. Es actualmente Codirector de "The Applied Optimization Group". Sus intereses incluyen la caracterización, la modelación y la optimización multicriterio de sistemas de manufactura, biológicos y decisionales.

DYNAMIC SEISMIC RESPONSE OF LA MISSION BRIDGE IN BAJA CALIFORNIA, MÉXICO [1]

Song Hoon [2], Carlos I. Huerta-López[3], Alejandro García-Gastélum[4]

ABSTRACT: The analytical and experimental seismic response of La Mission Bridge, and the site sub-surface characterization on its neighborhood is presented in this paper. SAP 2000 (Structural Analysis Program) was used to model and characterize numerically the expected response of the bridge in terms of their vibration natural frequencies and maximum displacement. It was also generated the scenario of the bridge response upon strong motion. In both cases, ambient vibration measurements were used for the experimental studies. The stiffness matrix method was used for the analytical study (forward modeling) of wave propagation in layered media. The relevant characteristics of the results are next succinctly described: For the bridge: the theoretical fundamental frequency of vibration was 3.10 Hz., and the estimated experimental fundamental vibration frequency was 3.30 Hz. For the site characterization, our results are described starting at the north end of the bridge going through its south end: (i) The site S1_2, which is the site where the soil was artificially compacted, has a dominant frequency of 2.5 Hz and an average shear wave velocity of 195 m/s. (ii) For sites S3_1 and S2_4, the dominant frequency was 1.5 Hz and the average shear wave velocity was 115 m/s and 123 m/s, respectively. (iii) Site S2_2, the dominant frequency was 3.5 Hz and an average shear wave velocity 275 m/s. (iv) Site S2_5, in this site two clear peaks at frequencies of 1.5 and 3.75 Hz were observed, regarding to the average shear wave velocity it was 128 m/s. (v) Site S2_3, the dominant frequency was 4.0 Hz and the average shear wave velocity was 346 m/s. All the experimental sites were in soils at natural conditions, but the site S1_2, which was artificially compacted. The soil characteristics along the 163 m length of the bridge, clearly shows a rigidity change of the soil sub-surface conditions. That condition is an indication that different amplifications of the ground response will probably be experienced, being in the range of the 4.0 Hz at the south-end side of the bridge, and 1.5 Hz on the portion of the north-end of the bridge. In no case the fundamental vibration frequency of the bridge matches the fundamental vibration frequency of the ground surface. However, they are somehow no too far apart each other.

Keywords: ambient vibration, natural frequency, layered media, shear wave velocity, dominant frequency

RESPUESTA SÍSMICA DEL PUENTE LA MISIÓN EN BAJA CALIFORNIA, MÉXICO

RESUMEN: La respuesta sísmica analítica y experimental del puente La Misión, en Baja California, México y la caracterización del terreno en la vecindad del puente se presenta en este artículo. Se utilizó el programa SAP 2000 para modelar numéricamente y caracterizar la respuesta esperada del puente en función de sus frecuencias naturales de vibración, sus desplazamientos máximos ante movimientos débiles y fuertes, así como las frecuencias de vibraciones teóricas y experimentales. Respecto del terreno, se utilizaron mediciones de vibración ambiental para su caracterización experimental. El análisis de la respuesta teórica del terreno se realizó mediante el modelado directo de la propagación del campo total de ondas que utiliza las matrices de rigidez para medios estratificados. De los resultados obtenidos sobresalen las siguientes

[1] Article received on March 29, 2022, and accepted for publication on April 15, 2022.
[2] Doctoral Student, Oceanological Research Institute (IIO), Autonomous University of Baja California (UABC). Campus Ensenada B.C. México. Email: hsong@uabc.edu.mx
[3] Associate Professor/Researcher, Civil Engineering and Surveying Department, University of Puerto Rico-Mayaguez (UPRM), Email: carlos.huerta@upr.edu, and Adjunt Professor, Faculty of Engineering Sciences and Technology, Autonomous University of Baja California (FCITEC-UABC), Campus Tijuana B.C. México. Email: m-huerta@alumni.utexas.net
[4] Professor/Researcher, Faculty of Marine Sciences, Autonomous University of Baja California (UABC), Campus Ensenada B.C., México. Email: agarcia@uabc.edu.mx

características del puente (i) la frecuencia de vibración del modo fundamental del modelo del puente es de 3.1 Hz. El valor experimental estimado fue de 3.3 Hz. De la caracterización del terreno se da a continuación la descripción de los hallazgos: partiendo del extremo norte del puente (su inicio) hacia el extremo sur (final) del puente. Se observó que en el sitio S1_2 (parte norte) que es una zona compactada artificialmente, la frecuencia dominante es de 2.5 Hz, con una velocidad promedio de ondas de corte no mayor a 190 m/s. En los sitios intermedios S3_1 y S2_4 la frecuencia dominante estimada fue de 1.5 Hz y la velocidad promedio de ondas de corte varió respectivamente de 115 m/s a 123 m/s. En el sitio S2_2 se obtuvo una frecuencia dominante de 3.5 Hz y una velocidad promedio de ondas de corte 275 m/s. Para el sitio S2_5 se observaron dos picos espectrales, uno a 1.5 Hz y el otro a 3.75 Hz. Por otra parte, la velocidad promedio de las ondas de corte fue de 128 m/s. Finalmente, en el extremo sur del puente, para el sitio S2_3 se tiene una frecuencia dominante a 4.0 Hz y una velocidad promedio de las ondas de corte de 346 m/s. Todos los sitios donde se hicieron las mediciones experimentales están en condiciones naturales del terreno, a excepción del sitio S1_2 que fue compactado artificialmente. Lo antes descrito, muestra que a lo largo de los 163 m que tiene el puente, hay un claro cambio en la rigidez de los materiales del subsuelo y que el comportamiento esperado de la respuesta del terreno tenderá a amplificar significativamente los movimientos del terreno en el rango de frecuencias del orden de los 4 Hz en la porción sur del puente, mientras que para la porción norte del puente la amplificación significativa se espera pueda ocurrir alrededor de los 1.5 Hz. En ninguno de estos dos casos la frecuencia dominante de vibración del puente coincide con la del terreno circundante. Sin embargo, éstas no son muy diferentes unas de otras.

Palabras Clave: vibración ambiental, frecuencia natural, medios estratificados, velocidad de ondas de corte, frecuencia dominante

INTRODUCTION

The accelerated urban growth of border cities between California, USA and Baja California, México, as well as along the shoreline between San Diego-Tijuana-Ensenada (the largest bi-national conurbation shared between USA and México), and the construction on the Mexican side (government and/or private) of dwellings (whether authorized or not) high-rise condominium buildings, and industrial estates on hilltops and slopes has been ongoing for the last 40 years, but communication roads/highways between Tijuana and Ensenada. For example, for Tijuana the mean territorial expansion currently is 2.25 hectares/day, and the population grew at 4.7% on average annually. Overpopulation and rapid, unplanned urban development of the region both mean that human activity has become a key triggering factor in terrain instability. The economic activity of the border region, which includes San Diego-Tijuana-Rosarito-Ensenada depends mainly on the Tijuana-Ensenada scenic road, which was built in the early 60's.

The natural conditions due to the seismo-tectonic and geological conditions at which the region is exposed, as well as the known on-shore and off-shore mapped fault systems (related to the interaction between the North-America and the Pacific plates) are clear indications of the regional hazard at which all civil infrastructure is exposed.

Results of experimental and theoretical dynamic properties and response upon seismic loads, of La Mission Bridge (located at Km 50+1 on the scenic road Tijuana-Ensenada), as well as soil-site characterization in its neighborhood are here presented. Ambient Vibration (AV) measurements of the structure and the free-field were collected and digital signal processing (DSP) spectral analysis were conducted for the estimation of the experimental vibration frequencies of the bridge, and the horizontal to vertical spectral ratio (HVSR) for the site vibration frequencies characterization. For the estimation of theoretical vibration frequencies and response of the bridge to weak and strong ground motions, the code SAP2000 (which solves the Eigen-value problem considering the geometry, and the physical properties of the structural elements) was used. For the soil-site characterization, forward modeling by means of the stiffness matrix method developed by Kausel and Roesset (1981), was used.

LA MISSION REGION AND LA MISSION BRIDGE DESCRIPTION

La Mission Bridge

The characteristics and dimensions of the studied bridge are: (i) 163.26m of length and 23.50m wide of deck including the guardrail, (ii) bridge beams are type V of AASHTO, (iii) piers as supporting at intermediate points, (iv) the left shoulder is an abutment (Tijuana-Ensenada direction), and (v) the right shoulder is and abutment with deep pile foundation (Ensenada-Tijuana direction). Figures 1 and 2 provides auto-cad figures of profiles and cross sections, and pictures of the bridge and its structural elements, respectively. The bridge physical descriptions are next provided.

The spans between abutments and piers of the five sections of La Mission bridge are:

Left shoulder - Pier 1(beam one): 32.65m;
Pier one – Pier 2 (beam two): 32.65m;
Pier two – Pier 3 (beam three): 32.65m;
Pier three – Pier 4 (beam four): 32.65m;
Pier four – Right shoulder (beam five): 32.55m

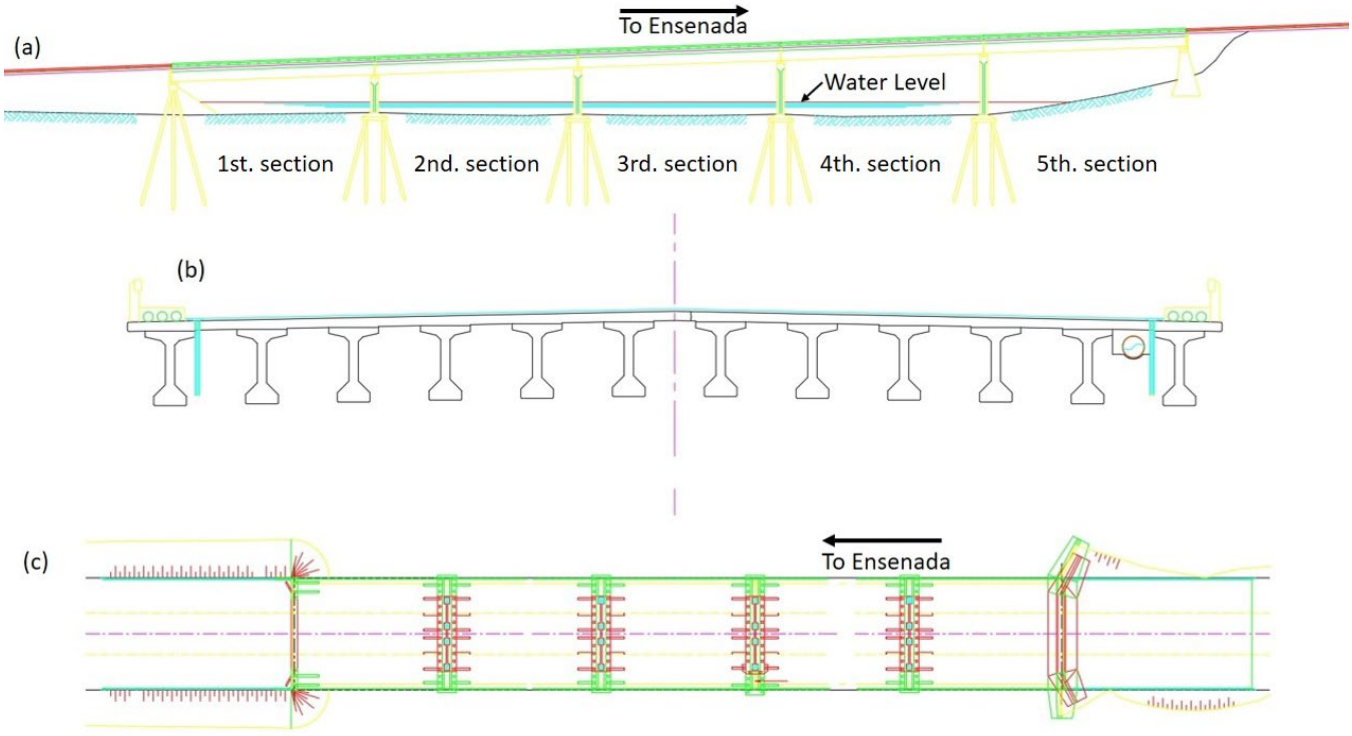

Figure 1: La Mission Bridge.
(a) longitudinal profile bridge, (b) Transverse Cross-Section of superstructure bridge, and (c) Plane of bridge.

The bridge has a slope approximately of four percentage (4%) in Tijuana-Ensenada direction. The deck is a continuous 20 cm thickness reinforced concrete all along the bridge. The beams are perforated pre-cast and pre-stressed independent structural elements, separated at each supporting pier. Neoprene plates were placed at each supporting pier location, acting as an articulation. Because the beams are discontinuous no moments are produced, but axial loads.

Along the wide direction of the bridge deck (23.50m) at 1.97m, 12 beams type V of AASHTO were placed in each section, because there are 5 sections a total of 60 beams type V of AASHTO were installed. At each one third of each section, diaphragms were constructed to provide lateral rigidity.

Deep pile foundation was installed in each intermediate pier and at the right shoulder. In the right shoulder, an array of 12 piles was installed as follows: three at each end, one vertical and two non-vertical at 15^0, and groups of three vertical deep pile foundation at each 1.97m. In each intermediate pier (piers: one, two, three, and four), 4 piles were installed as follows: four at each end (two vertical and two non-vertical at 15^0), and groups of two vertical piles at each 1.97m. Each pier has 38 deep pile foundation, giving a total of 126 deep pile foundation for the whole bridge.

Figure 2: La Mission Bridge. (a), (b) and (c) Road view, (d) pier view and (e) neoprene plates.

La Mission Region Description

The site is located in the area named as La Mission, showing either historical or recent earthquake activity, which is a consequence of the regional relative motion between the North-American and the Pacific Plates. The region is characterized for several well identified and mapped regional and local fault systems shown in Figure 3, which also shows the catalog of epicentral locations of historical M>6 earthquakes, as well as all M>2 instrumental detected seismicity up to 08/2017. Either the historical and instrumental documented seismic activity, was compiled from the seismological agencies: (i) *Red del Noroeste de México* (*RESNOM*) from the 1970's, and the (ii) Southern California Seismic Network (SCSN) from the 1960's.

The potential occurrence of M>6 earthquakes in the region, is clearly shown in Figure 3, and from the compiled information of earthquakes catalog geographically filtered for the Northern Baja California – Mexico, and Southern California –USA regions and the temporal window of 1970's to 08/2017, and 1932 to 08/2017, respectively.

The relationship between the epicentral locations and the mapped faults (or fault zones) clearly shows the ones that are more seismic active in the whole region. The regional structural-tectonic frame in the neighborhood of the studied region, shown in Figure 4, is formed by: (i) at the North by the: Rose Canyon, la Nacion, Agua Caliente, Garcia, Vallecitos-San Miguel, Los Buenos, Miramar, and Coronado Bank (off-shore), and (ii) at the South by the: Agua Blanca, Tres Hermanos, San Diego Through and San Clemente, both West-South-West off-shore. The historical and local seismic activity in the vicinity of La Mission region is low in comparison with the rest of the region.

GEOLOGICAL DESCRIPTION OF LA MISSION REGION

The site in which the studied structure (bridge) is located, is within a region characterized by parallel normal faults (horst-graben systems) along the shore-line forming plateaus. In the work of Minch *et-al* (1984), a detailed description of the Miocene for the Northwestern Baja California Peninsula is provided about the stratigraphy and depositional ambient of the California-Baja California Continental Borderland.

The Rosarito Beach formation unit and is correlated lithological units were deposited within the California-Baja California Continental Borderland and the Range provinces. The Rosarito Beach shows a great variety of lithology and fauna that goes from sub-aerial basalt flows, pyroclastic sediments (Loophole, Tuff, Volcanic ash, Lapilli tufs), as well as diatomaceous sediments, sandstone tuff, conglomerates, and coquina with abundant invertebrate mega-fossils as gasteropods, pelycypods, crustaceous, and vertebrates as fish, birds and mammals. There is also, abundant diatomeus siliceous micro-fossils, silico flagellates and radiolarian by Demere *et-al*. (1984). The Rosarito beach formation, is divided in seven units, based in its lithology and fauna variations by Minch *et-al*. (1984), being La Mission and Los Indios the subsoil lithological units present at the studied site, in which Quaternary Alluvial sediments formed by gravel, sands, clay and silt rests. The basalts and pyroclastic rocks of Rosarito Beach formation are exposed all along the shore-line between Tijuana and Ensenada, forming plateaus within the La Mission region, and covering a local area, which is representative of the period of explosive volcanic episodes during the Mid-Miocene and the early stage of the formation of the California-Baja California Continental Border line during the Miocene.

Seismicity and Local Geology

The study area is clearly evident tectonic active in terms of its seismic activity. As an example, according to RESNOM, during 04/28/1982 to 12/13/2008, 118 earthquakes of $0.6 \leq M \leq 4.1$ occurred in La Mission area. Figures 3 and 4, show the local and regional mapped faults, as well as the epicentral locations nearby the studied site.

Locally, in the studied site at La Mission area, the surficial layers are of alluvial deposits produced by the erosion and weathering of the typical intrusive igneous rocks of the region. The geomorphological relief of the region shows a quite flat topographic relief. On Figure 5, the location of the studied bridge, the regional and the local geological conditions are shown.

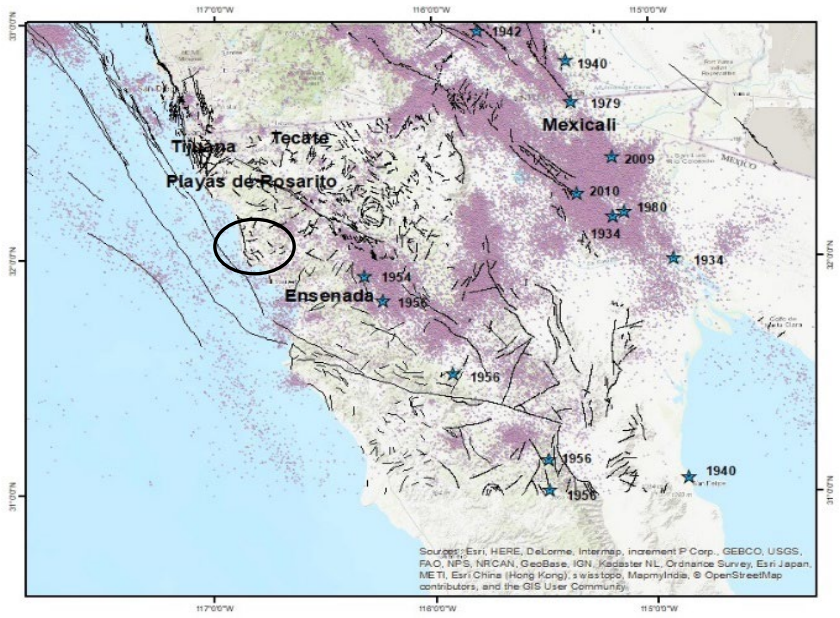

Figure 3: Principal northern Baja California, Mexico urban centers. Regional and local northern Baja California, Mexico and southern California, USA fault systems. Black oval show la Mission region. Stars show the historical M≥6. earthquakes, and small pink dots the accumulated all magnitudes seismicity from 1932-2017 (august). Source of epicentral locations: *Red Sísmica del Noroeste de México* (RESNOM), Southern California Seismic Network (SCSN) and United States Geological Survey (USGS).

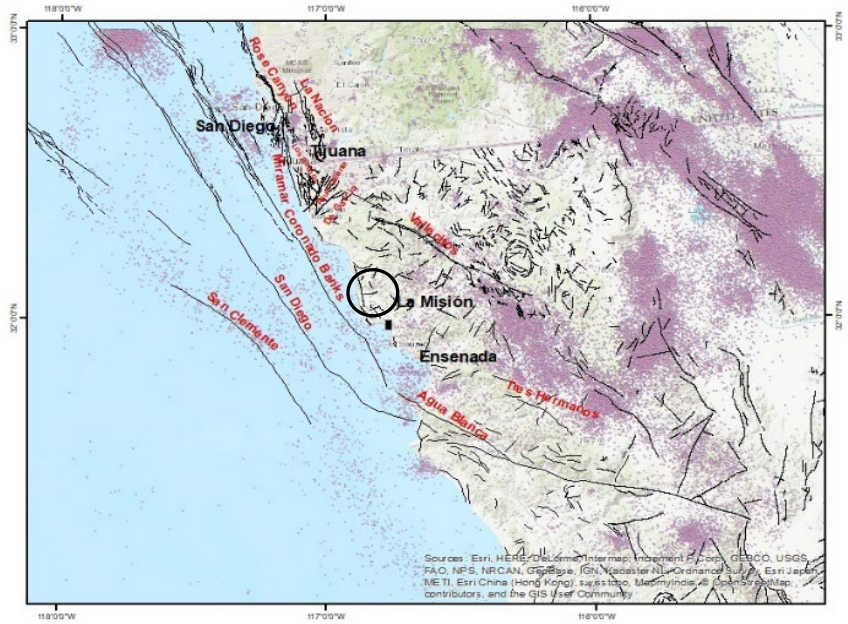

Figure 4: Regional structural frame work of La Mission Region, the accumulated seismicity reported by RESNOM and USGS for 1973 to 2017 (august) is shown in pink solid dots. The study site is shown with black oval, and faults with black lines.

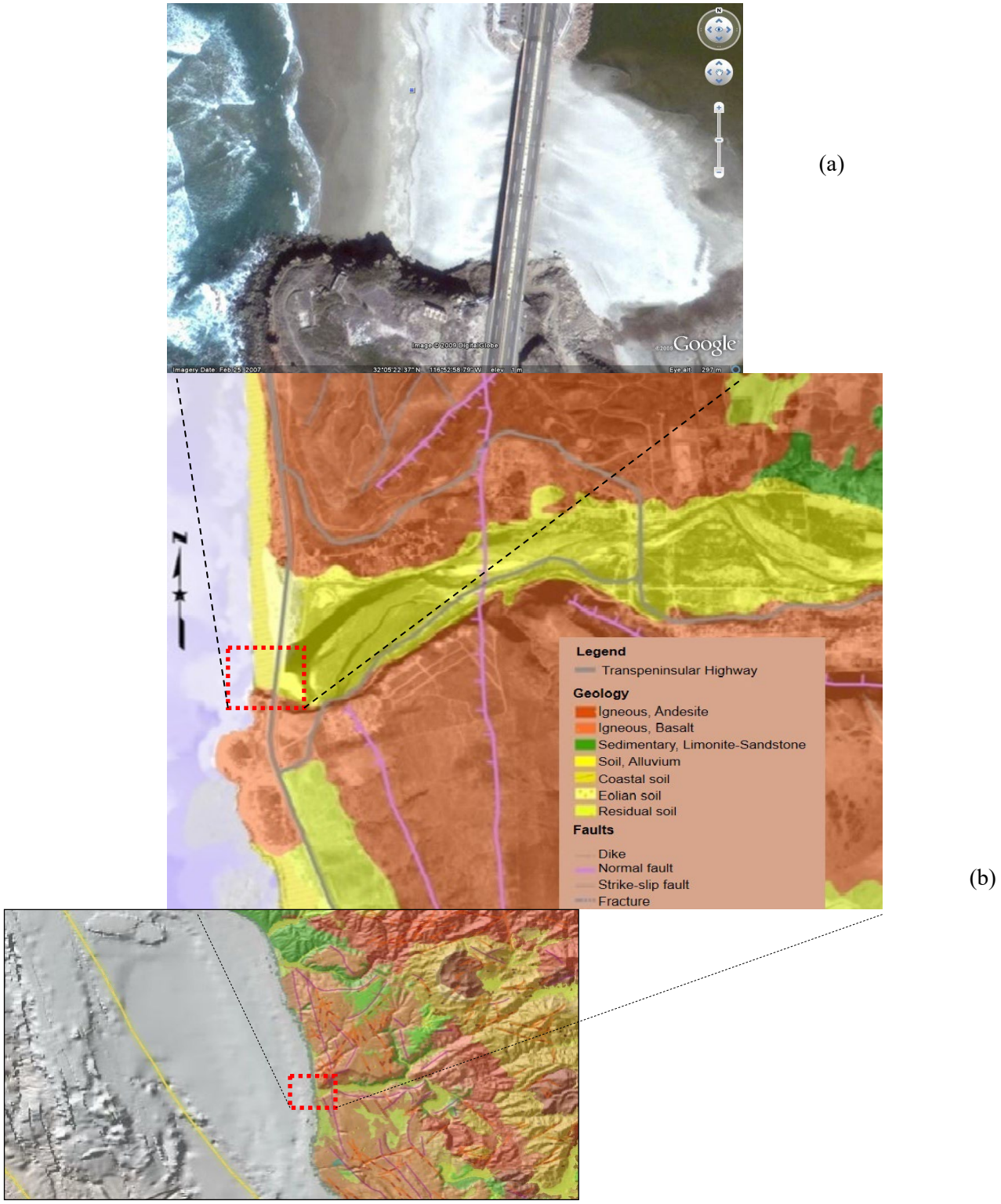

Figure 5: Regional geology of studied site, La Mission Bridge. (a) Bridge location, (b) Local geology at La Mission Bridge, and (c) Regional geology.

DATA PROCESSING AND MODELING

Numerical Modeling for the Soil-Site Characterization

The wave propagation Stiffness Matrix method developed by Kausel and Roesset (1981) was used for the site-soil forward modeling of layered media. The Stiffness Matrix method is essentially a modified wave propagation method developed by Thomson (1950) and Haskell (1953). It is a more efficient code that works in a similar way as codes used in structural analysis. Here, the main purpose of using the Stiffness Matrix method is the sub-soil-site characterization in terms of the: (i) geometry and physical properties of layered soil system, (ii) dominant vibration frequency, and (iii) its transfer function in the frequency domain.

The analysis and characterization of layered soil system response was conducted by means of the 1-D wave propagation method based on the stiffness matrix. This linear wave propagation method, developed by Kausel and Roesset (1981), was used because among of its particular numerical and computational features, it provides the freedom of:

(i) Use the total wave field (P, SV, SH) or any of particular interest of them,
(ii) Can be used for modeling thin layers in the layered soil systems,
(iii) Normal and non-normal incident wave field at the soil system-half space interface can be used,
(iv) The behavior of the propagation wave field through and at the interfaces of the layered soil system can be traced.

As a final step, this method was implemented in a code written in Fortran language to estimate the site shear-wave velocity profile versus depth as developed by Kausel and Roesset (1981), and implemented by Huerta López et al., (2005).

Numerical Study of "La Mission" Bridge

In SAP 2000, before the analytical model is developed, it is necessary identify and compute the centroidal axis of structural elements, it is said: beams, piers, deck, abutments, and shoulders, among others.

Before the bridge structural elements are developed the following steps should be conducted: (i) the first step is to design the grid for easy location of structural elements, and then (ii) according to the design specifications the structural elements are developed. As an example, to develop a type V AASHTO beam, the SAP 2000 protocol is: *Define > SectionProperties > Framesections > AddFrameProperty > Framesectionpropertytype > Concrete > Precast I > Set SectionDimensionsshellon a Standard Section> AASHTO Beam I – Type V >Ok.*

For the case of shear wall and/or the deck the *shell* function should be used. Once all the bridge structural elements are developed (following the design specifications of the structural maps), the nodes of the deck and beams should be joined as a rigid element with no weight or by using the function "*constraint*" of type "*body*".

For this study case, rigid elements with no weight were used. As mentioned before, because the beams are discontinuous elements, the function "*AssignFrameReleases*" was used to release the moments. Once the whole bridge structure was developed, the code was executed to obtain the nodal results.

Collecting and Processing of Experimental Data

The collected data was recorded in raw binary format (.SSR) in counts digital units. In preparation for the digital signal processing (DSP) data was converted to acceleration (by applying the joint sensor-recorder constant of $3.8147e10^{-6}$ g(m/s^2)/counts) physical units and converted to ASCII format.

The first step for the data processing consisted in time domain visual inspection of the time series plots, in order to identify non characteristic ambient vibration signals (anthropogenic undesired vibrations) for manually removal. Our DSP procedure does not require the transient signals being manually removed.

The frequency domain analysis was conducted by computing the Power Spectral Density (PSD), mean removal and base line correction was first applied to the time series. Instrument correction was not needed to apply due that the transfer function frequency response of the accelerometers is within ~DC-200 Hz, wide enough of the frequency band of our interest.

PSD estimation was conducted following the standard Fourier analysis as described on signal processing books like: Kanasewish (1981), Oppenheim and Shafer (1975), and Bendat and Piersol (1971).PSD were estimated using time series of 86272 total length of data points using sub-segments of 4096 points with overlap of 50% and 75% until complete the total data length of the recorded time series. The more stable PSD's were the ones obtained with the largest overlap.

The mean value of each sub-segment was removed and Hanning window of equal number of points was applied to each sub-segment either. Final spectral amplitudes of the average PSD was normalized by the frequency increment (Δf) and the amplitude scaling factor (due to the symmetry of the discrete Fourier Transform) dived by the data points number (N). Appendix A provides details for the Discrete Fourier Transform (DFT) analytical derivation. Details of description provided above are in the Appendix A.

NAKAMURA H/V SPECTRAL RATIO ESTIMATION

The horizontal to vertical spectral ratio (HVSR) using ambient vibration (AV) as developed by Nakamura (1989), is an efficient and well proved method for the estimation of fundamental vibration mode of soil systems.

The Nakamura's fundamental hypothesis is based on empirical observations of computed HVSR that allows the estimation/identification of the fundamental vibration mode, which at the same time is interpreted an indicator of the local site response. He also states that by doing the HVSR the source and path effects are canceled (minimized) and the Rayleigh waves on the ambient noise. The hypothesis also implies that for small strains of the ground motions (site response) on vertical component are not significantly affected by the soft materials that constitute the soil.

The data acquisition field work for the Nakamura HVSR method requires ambient vibration (micro-tremors) measurements at single location with an orthogonal sensors array deployed at the ground surface. Its general hypothesis states that in rigid soils (rock) the ground response of horizontal and vertical components are very similar, which can be interpreted that there is no preferential direction of particle motion in the wave propagation phenomena, and that any observed amplification at the ground surface is a consequence of the presence of soft soils and can only be explained because the previous statement.

The academic community widely accepts the fundamental hypothesis of the Nakamura method, Nakamura (1989), which states that both the horizontal and the vertical ambient vibration signals are amplified independently from multiple reflections of shear- and compression-waves, respectively. Even though the debate about if the local site response is due to Surface Rayleigh waves still on discussion among the academic community, Nakamura (2000), and Huerta-Lopez *et al.* (2003) provides evidence that the contribution of surface Rayleigh waves has little or no contribution at the fundamental vibration mode.

EXPERIMENTAL HVSRS COMPUTATIONS

To compute the hvsrs from ambient vibration by nakamura (1989) psds computed as described in section of collecting and processing of experimental data, and carefully analyzed as described in sub-section nakamura h/v spectral ratio estimation. We used series of scripts written on the matlab environment following the procedure described by chatelain et al. (2008) and documented on sesame (2004) project. The quadratic arithmetic mean of both horizontals h1 and h2 psds, and the vertical v psd were use to estimate the final hvsr, as stated in equation (1):

$$R = \frac{\sqrt{\frac{H_1^2 + H_2^2}{2}}}{V} \tag{1}$$

RESULTS: ANALYSIS AND COMPARISON

Bridge Comparison of Numerical and Experimental Results

Figure 6 provides the location of sensors array deployed on the bridge sections, associated with the node of the finite element model, while Figure 7 shows both the theoretical pseudo-spectral acceleration of longitudinal, transversal, and vertical (PSA at 0%) and the experimental PSDs estimated from the two Ambient Vibration (AV) measurement campaigns.

The first column on Figure 7, corresponds to the longitudinal (first row), transversal (second row) and vertical (third row) of PSDs and PSAs of bridge first section. On same Figure 7, second, third, and fourth columns correspond to the second third and fifth bridge sections, following the same order described above.

Figure 7 shows the following: (i) First column-bridge first section, show good agreement between PSDs and PSAs at 3.25 Hz, the fundamental vibration frequency (FVF) for longitudinal, transversal and vertical components. On the transversal component, a second PSA peak at 4.3 Hz peak is not evident on the longitudinal and the vertical PSDs, (ii) Plot second column-bridge second section, show good agreement between PSDs and PSAs at the FVF for longitudinal, and transversal components at 3.2 Hz but for vertical component where the PSA is slighted shifted to 3.65 Hz, (iii) Plot third column-bridge third section in a very similar way of bridge second section, the results show good agreement between PSDs and PSAs at the FVF for longitudinal, and transversal components (3.2 Hz) but for vertical component where the PSA is slighted shifted to 3.65 Hz, (iv) Plot fourth column-fifth bridge section show good agreement between PSDs and PSAs at the FVF for longitudinal, transversal and vertical components (3.25 Hz).

Regarding to the FVF, the best agreements (almost perfect match) were obtained for all longitudinal components in all bridge sections. For the transversal components a second PSA peaks are shifted to high frequencies from the FVF, which is not present in the PSDs is evident in all bridge sections. On the vertical component good agreement was obtained for first and fifth bridge sections, but for second and third bridge sections in which the FVF of PSA is shifted to high frequencies from the FVF.

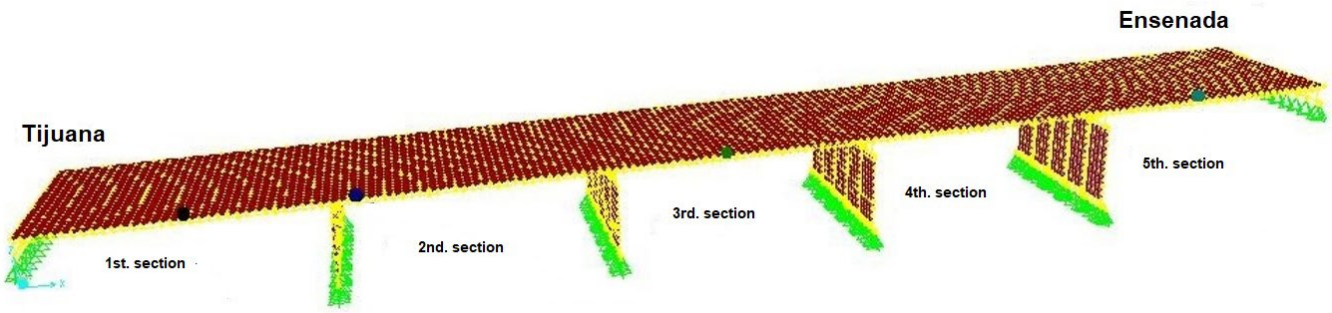

Figure 6: La Mission Bridge sensors array location with the associated node of the structural elements of the bridge sections.

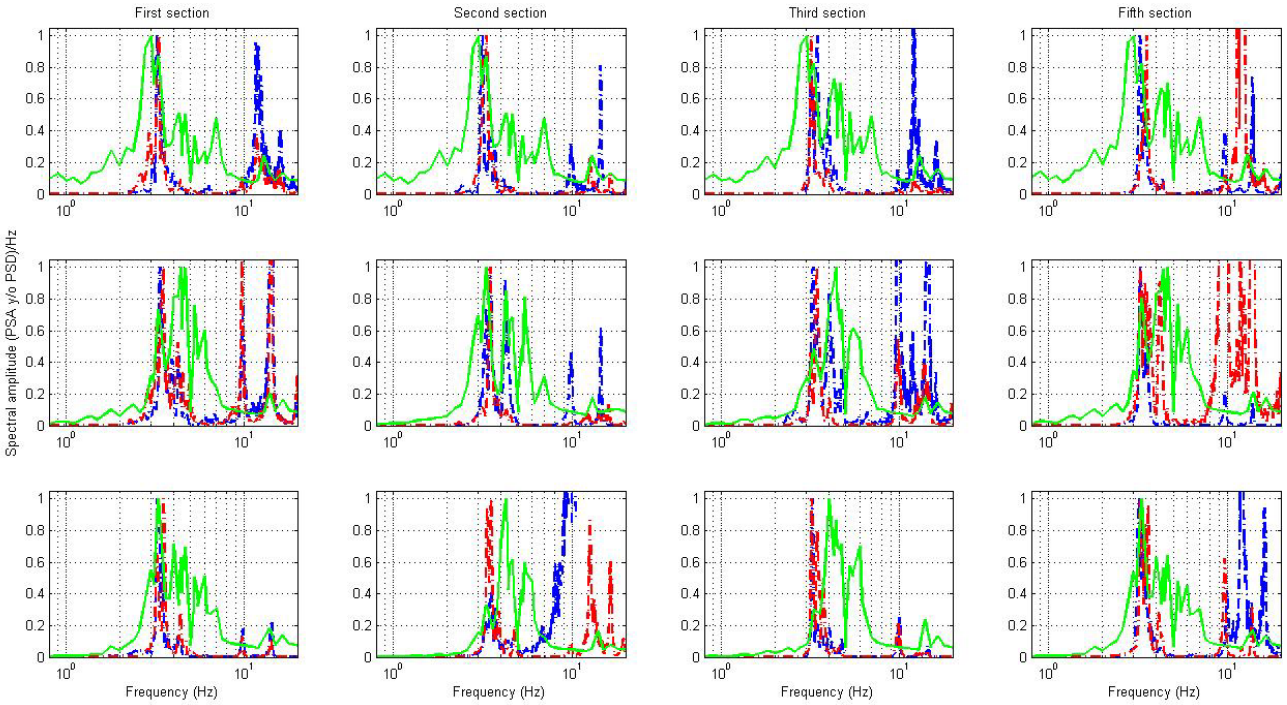

Figure 7: Experimental PSD spectrum and theoretical PSA, both are normalized with respect to its maximum. Longitudinal (first row), transversal (second row) and vertical (third row). Green line is the theoretical PSA. Dashed blue line data from first measurements campaign, and dashed red line the second measurements campaign.

Site Characterization: Comparison and Interpretation of Theoretical and Experimental HVSRS

This section describes the site characterization in terms of the pseudo-transfer function obtained by means of SRHV at the free-field locations shown in Figure 8, and the site physical properties and geometrical layered soil models from the numerical results of the 1D wave propagation modeling by means of the stiffness matrix method by Kausel and Roesset (1981) described in section of numerical modeling for the soil-site characterization.

Experimental results of PSDs H/V [Average of L/V and T/V] ($H_{N\text{-}S}$/V [L/V], $H_{E\text{-}W}$/V [T/V]), as well as the theoretical spectral ratios of H_{SH}/P [SH/P], and H_{SV}/P [SV/P]) obtained by the stiffness matrix method by Kausel and Roesset (1981) are provided in Figure 8. The results for free-field modeled sites layered soil system of: (i) physical parameters, and (ii) geometry are provided in Table I.

Site S1_2 is shown in Figure 8, and the results are provided in Figure 9 "first column-first row". Clear and good agreement of both experimental and theoretical spectral ratios is observed at 2.5 Hz. However, the modeled transfer function did not match the experimental ratios at frequencies larger than 4 Hz. Site S3_1 is shown in Figure 8, and the results are provided in Figure 9 "second column-first row". The FVF is shown at 1.5 Hz with very good agreement between the SH/P and the T/V. Both experimental and theoretical spectral ratios preserves the general trend among them at frequencies range of 4 Hz up to 7 Hz. Site S2_4 is shown in Figure 8, and the results are provided in Figure 9 "second column-second row". In both, experimental and theoretical spectral ratios, good agreement of two clear amplitude peaks are observed at 1.5 Hz and 3.8 Hz (4 Hz in the theoretical). Site S2_5 is shown in Figure 8, and the results are provided in Figure 9 "third column-first row". On the experimental spectral ratios, two spectral amplitude peaks are observed at 1.5 Hz and in the range of 3 to 5.3 Hz. On the theoretical spectral ratios, the spectral amplitude are observed at 1.5 Hz and 3.9 Hz, Both results, theoretical and experimental agrees well for the 1.5 Hz, and quite well for the one on the range of 3 to 5.3 Hz with the theoretical at 3.9 Hz. Site S2_2 is shown in Figure 8, and the results are provided in Figure 9 "third column-second row". A dominant spectral amplitude peak is observed at 4 Hz and a second spectral amplitude peak of lower amplitude at 9Hz. The general trend between both, the theoretical and the experimental spectral ration shows good agreement. Site S2_3 is shown in Figure 8, and the results are provided in Figure 9 "fourth column-first row". For the theoretical spectral ratios, the largest spectral amplitude is located at 4 Hz, followed by a second one with lower amplitude at 9.5 Hz. For the experimental spectral ratios the largest spectral amplitude is located at 4 Hz, followed by a second one with lower amplitude at 7 Hz. The general trend between both, the theoretical and the experimental spectral ration shows good agreement.

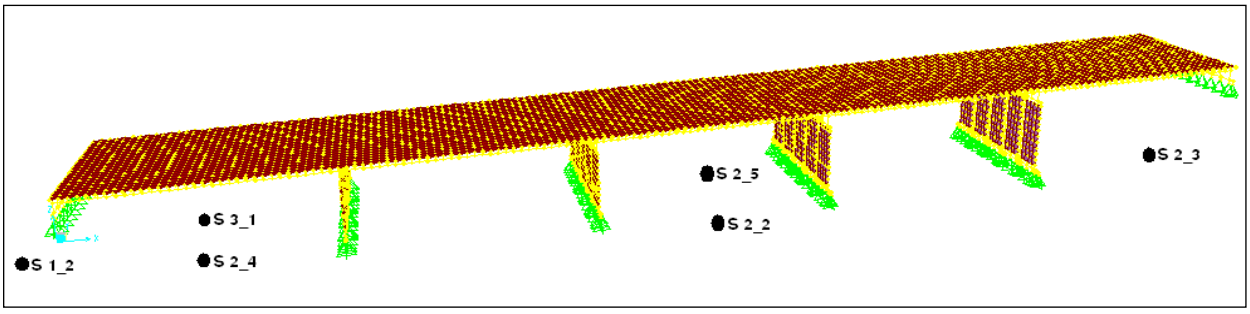

Figure 8: Free-field sensors array configuration nearby La Mission Bridge. S1_2 located at the beginning of the bridge on artificially compacted soil, S3_1 located at 11.9m on longitudinal direction and at 6.3m on transversal direction, S2_4 located on soil natural conditions at central point of first section, S2_5, and S2_2 located in soil natural conditions at longitudinal and transversal central point of third section, S2_3 located half way of fifth section on natural soil conditions.

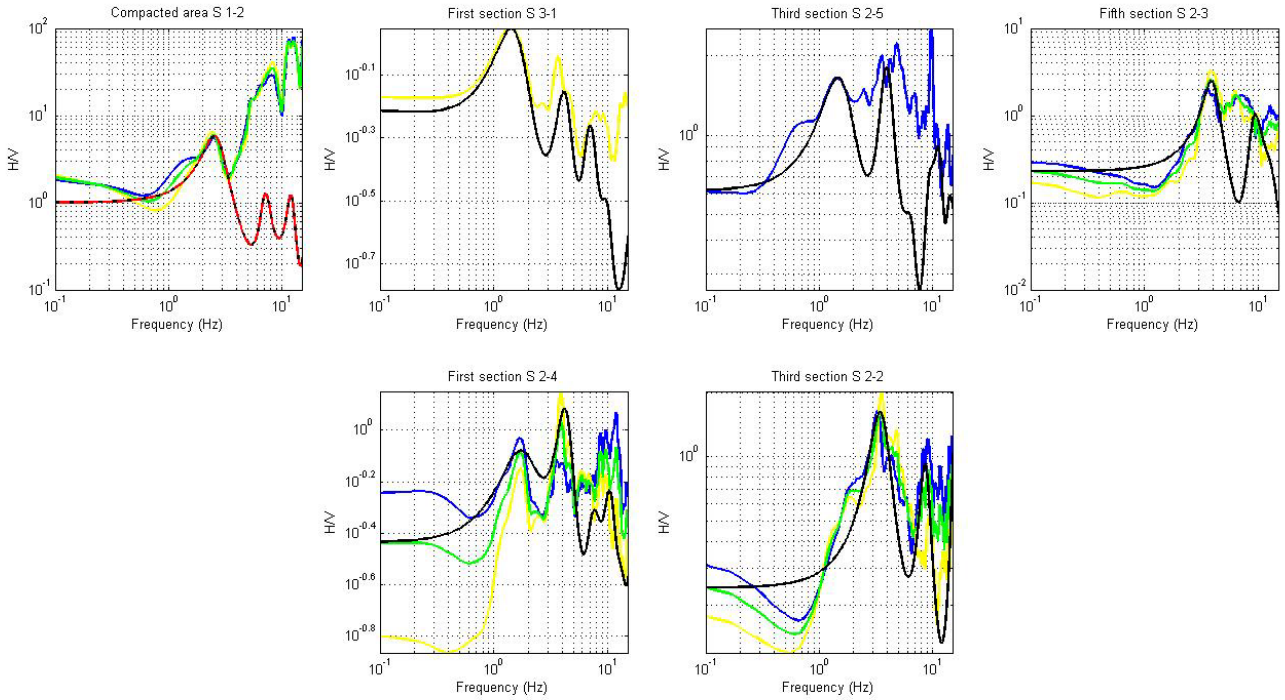

Figure 9: Free-field sites experimental spectral ratios, L/V, T/V, and H/V; and theoretical SV/P and SH/P spectral ratios. Blue line L/V spectral ratio. Yellow line T/V spectral ratio. Green line H/V spectral ratio. Black line SV/P spectral ratio, and dashed red line SH/P spectral ratio.

Table 1: Free-field sites modeling results: sites estimated physical properties, geometry, and average values for an equivalent single layer model.

Site	*h (m)*	*Vs (m/s)*	ρ *(tn*seg²/m⁴)*	ξ *(%)*	σ	$f_{d\,(Hz)}$	$\overline{Vs}$, $\overline{h}$
S 1_2	7	170	0.1569	0.04	0.30		
	13	210	0.1627	0.02	0.40	2.5	196, 20
	0	550	0.1850	0.0	0.25		
S 3_1	7	100	0.1500	0.10	0.30		
	13	122	0.1600	0.10	0.40	1.5	114.3, 20
	0	200	0.2000	0.0	0.25		
S 2_4	7	100	0.1500	0.05	0.26		
	13	135	0.1700	0.09	0.36	1.5	122.75, 20
	0	200	0.1850	0.0	0.25		
S 2_5	7	100	0.1500	0.035	0.29	1.5	128.083, 24
	13	138	0.1600	0.045	0.38		

	4	145	0.1800	0.025	0.29		
	0	200	0.2000	0.0	0.25		
S 2_2	2.6	200	0.1500	0.05	0.26		
	7	220	0.1600	0.06	0.35		
	7.4	350	0.1700	0.03	0.37	3.5	274.859, 21.4
	4.4	280	0.1700	0.033	0.38		
	0	800	0.2000	0.0	0.25		
S 2_3	3	100	0.1500	0.05	0.26		
	7	175	0.1800	0.05	0.28		
	6.5	450	0.1850	0.005	0.28	4.0	346.511, 21.5
	5	600	0.1900	0.005	0.26		
	0	970	0.2000	0.0	0.25		

ρ : density, ξ : damping, σ : Poisson ratio, Vs: shear-wave velocity, h: thickness, f_d: fundamental vibration frequency, $\overline{Vs}$: average shear-wave velocity, $\overline{h}$: average thickness

CONCLUSIONS

Site characterization nearby La Mission Bridge most relevant issues are documented on Table I and next described as follows:(i) Free-field sites nearby to bridge first and second sections shows FVF lower than sites nearby bridge sections three and five, (ii) at site S1_2 the associated FVF is 2.5 Hz, while at sites S3_1 and S2_4 the FVF is 1.5 Hz,(iii) on the site S2_2 (facing to the sea) the FVF is 3.5 Hz, and 1.5 Hz for the site S2_5 (facing to the lagoon), these two sites are nearby the bridge third section, just at the middle of the bridge, (iv) for site S2_3 (nearby the bridge fifth section) the FVF is 4 Hz, which is the most rigid soil conditions of the soil along the bridge.

Regarding to results description provided in section Bridge comparison of numerical and experimental results, the bridge experimental (PSDs), and theoretical (PSAs) mean value of the FVF estimated on all bridge sections is 3.15 Hz, and 3.10 Hz, respectively. These values are close enough for its use in the analysis of the dynamic behavior of civil structures to estimate the experimental structural dynamic behavior using AV measurements.

DATA AND RESOURCES

We used time series of ambient vibration (AV) measurements collected with epi-sensor accelerometers from the engineering, architecture, and design faculty of UABC-Ensenada. Seismic catalogs can be obtained from https://resnom-mf.cicese.mx/, and Southern California Seismic Network (SCSN) and United States Geological Survey (USGS). MATLAB is available at www.mathworks.com/products/matlab (last accessed July, 2020). Geology (home-vectorised data) for the northern Baja California were obtained from INEGI web-site https://www.inegi.org.mx. SAP2000 V10., (2000) Computers and structures, Inc.

ACKNOWLEDMENTS

This study was supported by the Mexican National Council of Science and Technology (CONACyT) and the doctoral scholarship of Hoon Song at the *Universidad Autónoma de Baja California*. We are grateful to the Puerto Rico Strong Motion Program of the Civil Engineering and Surveying Department of the University of Puerto Rico for supporting Hoon Song during his stay at the University of Puerto Rico as student exchange and the student's mobility program of CONACyT. This manuscript has benefited from thoughtful suggestions and detailed comments by our reviewers and the anonymous reviewers for valuable suggestions. To the *Secretaría de Transporte y Comunicación* (SCT) authorities for their invaluable support detouring the vehicles traffic while collecting the AV data.

REFERENCES

Alfaro A., Goula X., Susagna T., Pujades L. G., Canas J. A. Navarro M. and Sánchez J. (1998). *Estimación del Período Predominante del Suelo a Partir de Microtemblores*, Aplicación a Barcelona, IX Asamblea Nacional de Geodesia y Geofísica, Aguadulce (Almería, España), Febrero 9-13.

Alain W., Le Page M., Chávez V. G., Vela G. R., Castañeda S. R., and González V. C. (2000). *Aportes para un escenario sísmico en Tijuana, ¿y si un terremoto de magnitud 6.5 se produjera en la falla La Nación?*, El Colegio de la Frontera Norte y el Institu de Recherchepour le Développement, 74 p.

Bendat, J. S., and Piersol A. G. (1971). *Random data: Analysis and measurements procedures,* John Wiley & Sons, Inc. New York, 407 p.

Chatelain J. L., Guillier B. F. C., Duval A. M., Bard K. A. P. Y. and The WP02 SESAME team. (2008). *Evaluation of the influence of experimental conditions on H/V results from ambient noise recordings*, Bull Earthquake Eng. 6: 33–74 p.

Chopra Anil K. (2007). *DYNAMICS OF STRUCTURES-Theory and Applications to Earthquake Engineering,* Third Edition, Prentice Hall. 1 – 48, 208 – 212, 244 – 245 p.

Demere T.A., Roeder M. A., Chandler R.M., and Minch J. A. (1984). *Paleontology of the Middle Miocene Los Indios Member of the Rosarito Beach Formation, Northwestern Baja California, Mexico*; Minch J.A., Ashby J.R. (eds.), *Miocene and Cretaceous Depositional Environments, Northwestern Baja California, Mexico*, Pacific Section A.A.P.G., San Diego, California, 54, 47-56 p.

Esparza Fuentes M., Huerta López C. I., Lomelí Limón D. S., Baltasar Cifuentes Y., Contreras Porras R. S., Espinoza Barreras F., and Song H. (2007). *Theoretical and experimental vibration frequencies of a nine story building located near the Tijuana's river zone* (Estimación teórica y experimental de la vibración de un edificio de nueve niveles localizado en la vecindad de la zona río de Tijuana, B.C.), Memorias del XVI Congreso Nacional de Ingeniería Sísmica, Ixtapa Zihuatanejo, México. Oct/31-Nov/3, 2007, CD proceedings paper Nov-14, 1-19 p.

Espinoza Barreras F., Huerta López C. I., Juárez García J. R., Contreras Porras R. S., Reynaga Márquez A., Ramírez González E., González Ortega J. A., Baltasar Cifuentes Y., Figueroa Martínez M., and Baltasar Rodríguez R. (2007). *Ambient vibrationson Ensenada B.C. urban bridges* (Vibración ambiental en puentes urbanos de Ensenada, B.C.), Memorias del XVI Congreso Nacional de Ingeniería Sísmica, Ixtapa Zihuatanejo, México, Oct/31-Nov/3, 2007. CD proceedings paper Nov-13, 1-12 p.

Hallin M. W., Ball A., Esplín R., and Hsieh K. (2004). *Modal analysis and modeling of highway bridges*, 13th World Conference on Earthquake Engineering, Vancouver, B.C., Canada, August 1-6, paper # 2996.

Haskell N. A. (1953). *The dispersion of surface waves on multilayered media*, Bull. Seismol. Soc. Am. 43, 17-34.

Huang C. S. (2000). *Modal identification of structures using ARMV model for ambient vibration measurement*, 12th World Conference on Earthquake Engineering, Auckland, New Zealand, paper # 1702.

Huerta López C. I., Roësset J. M., Stokoe K. H., and Acosta J. G. (1994). *In-situ determination of soil damping from earthquake records*, A. A. Balkema/Rotterdam/Brookfield (ISBN 90 5410 392 2), Editor S. A. Savidis, Proceedings of the Second International Conference in Earthquake Resistant Construction and Design (ERCAD), 1, 8, 227-234 p.

Huerta López C. I., Roësset J. M., and Stokoe K. H. (1998). *Evaluation of the random decrement method for in-situ soil properties estimation*, A. A. Balkema/Rotterdam/Brookfield (ISBN 90 5809 030 2), Editors: KojiroIrikura, Kazuyoshi Kudo, Hiroshi OkadaandTsutomu Sasatani, Proceedings of the Second International Symposium on The effects of Surface Geology on Seismic Motion, Recent progress and new horizon on ESG study, Vol. 2, 749-756p.

Huerta López C. I., Pulliam J., Nakamura Y., and Yates B. (2001). *Modeling amplification effects of marine sedimentary layers via horizontal/vertical spectral ratios*, Society of Exploration Geophysicist (SEG) (ISSN 1052-3812), Proceedings of the 71st SEG meeting, Vol. 1, 825-828 p.

Huerta López C. I., Pulliam J., Stokoe K. H., Roësset J. M., and Valle-Molina C. (2003). *Spectral characteristics of earthquakes recorded on the Gulf of Mexico seafloor and soft sediment characterization*, ASME invited lecture at the Offshore Geotechnics Workshop of the 22nd Offshore Mechanics and Arctic Engineering International Conference, (ISBN 0-7918-3672-X), Proceedings of the 22nd Offshore Mechanics and Arctic Engineering 2003 International Conference in CD proceedings, paper # 37504, 1-9p.

Huerta López C. I., Stokoe K. H., Jay Pulliam, José M. Roësset, and Valle-Molina C. (2005). "Modeling of seafloor soft marine sediments and spectral characteristics of earthquakes recorded on the Gulf of México", *Journal of Offshore Mechanics and Arctic Engineering,* American Society of Mechanical Engineers ASME, (ISSN 0892-7219) 127, 1, 59-67 p.

Irie Y., and Nakamura K. (2000). *Dynamic characteristics of a r/c building of five stories based on microtremor measurements and earthquake observations*, 12th World Conference on Earthquake Engineering, Auckland, New Zealand, paper # 0500.

Kanasewich, E. R. (1981). *Time series analysis in geophysics, Third Edition*, University of Alberta Press, Edmonton, Alberta, 480 p.

Kausel E. and Roësset J. M. (1981). "Stiffness matrices for layered soils", Bull. Seism. Soc. Am. 71. (6): 1743-1761p.

Midorikawa S. (1990). *Ambient vibration tests of buildings in Santiago and Viña del Mar. Report of the Chilean-Japan Joint Study Project on Seismic Design of Structures*, Sponsor, JICA, Departamento de Ingeniería Estructural, Escuela de Ingeniería, Pontifica Universidad Católica de Chile, Santiago, Chile.

Minch J. A., Ashby J. R., Demere T. A., and Kuper H. T. (1984). *Correlation and depositional Environments of the Middle Miocene Rosarito Beach Formation of Northwestern Baja California, Mexico*; Minch J.A., Ashby J.R., (eds.), (1984), *Miocene and Crestaceous Depositional Environmets, Northwestern Baja California, Mexico*, Pacific Section A.A.P.G., San Diego, California, 54, 33-46.

Muriá-Vila D., Fuentes O. L., and Gonzáles A. R. (2000). *Uncertainties in the estimation of natural frequencies of buildings in México City*, 12th World Conference on Earthquake Engineering, Auckland, New Zealand, paper # 2092.

Nakamura Y. (1989). *A method for dynamic characteristics estimation of subsurface using microtremor on the ground surface*, Quarterly Report of Railway Technical Research Institute, 30. (1): 25-33 p.

Oppenheim, A. V., and R. W. Schafer (1975). *Digital signal processing*. Prentice-Hall, Englewood Cliffs, New Jersey, 556 p.

Ren W. X., Zatar W., and Harik I. E. (2004). "Ambient vibration-based seismic evaluation of continuous girder bridge", *Engineering Structures* vol. 26, 631-640 p.

Rojas R. R., Jara G. J. M., and Hernández B. H. (2006). *Estudio analítico y experimental de un puente peatonal en la ciudad de Morelia. Revista Ciencia Nicolaita*, Universidad Autónoma de Morelia, México, 143-140 p.

Roësset J. M., Huerta López C. I., and Stokoe K. H. (1995). *Effect of magnitude and type of damping in soil amplification. University of Missouri-Rolla* (ISBN 1887009019), Editor Shamsher Prakash, Proceedings of the Third International Conference on Recent Advances in Geotechnical Earthquake Engineering and Soil Dynamics. 725-732 p. 04/1995.

SAP2000 V10. (2000). Computers and structures, Inc.

SESAME. (2004). Guidelines for the implementation of the H/V spectral ratio technique on ambient vibration: measurements processing and interpretation. http://sesame-fp5.obs.ujf-grenoble.fr/Delivrables/Del-D23-HVUserGuidelines.pdf, accessed on Feb/09.

SESAME European project, (2004). Overall comparisons for test sites. Deliverable D17.10.

Thomson W.T. (1950). Transmission of elastic waves through a stratified solid medium, J. Appl. Phys. 11, 87-180.

APPENDIX A

The power spectrum estimation is calculated using Discrete Fourier Transform (DFT) of each realization (sample) here denoted by $x^{(k)}[n]$, where *n = 0, 1, 2, 3, ..., N-1*. Each realization is $T = N\,t_s$ seconds in duration, *N* denotes the total sample size, and t_s the sampling interval. l^{th} the simple value of the Continuous Fourier Transform (CFT) $X_T(l\Delta f)$ is related to the DFT by

$$X_T(l\Delta f) = \frac{X[l]}{\Delta f}, \text{ ..... } l = 0, 1, 2, 3, \ldots, N-1, \tag{A.1}$$

Where $\Delta f = \frac{1}{T}$. The expression for the k^{th} sampled spectrum, then can be rewritten as

$$S^{(k)}(l\Delta f) = \tfrac{1}{T} \mid X_T^{(k)}(l\Delta f) \mid^2, \tag{A.2}$$

$$S^{(k)}(l\Delta f) = \tfrac{1}{T} \frac{|X^{(k)}[l]|^2}{(\Delta f)^2}, \tag{A.3}$$

$$S^{(k)}(l\Delta f) = \tfrac{1}{\Delta f} \mid X_T^{(k)}[l] \mid^2. \tag{A.4}$$

$S^{(k)}(l\Delta f)$ is then the PSD representation of the sample. We now introduce the discrete power spectrum $S^{(k)}[l]$,

$$S^{(k)}[l] = S^{(k)}(l\Delta f)\Delta f, \tag{A.5}$$

Combining equations A.4andA.5, we arrive at the expression for the discrete case of the simple power spectrum,

$$S^{(k)}[l] = \mid X^{(k)}[l] \mid^2, \quad l = 0, 1, 2, 3, \ldots, N-1, \tag{A.6}$$

where $X^{(k)}[l]$ is the DFT of the k^{th} realization consisting of *N*samples, for example

$$X^{(k)}[l] = \tfrac{1}{N} \sum_{n=0}^{N-1} x^{(k)}[n] e^{-i2\pi nl/N}. \tag{A.7}$$

The estimate of the discrete power spectrum $S^{(k)}[l]$ is given by the average of the set of all discrete power spectra. This is,

$$\hat{S}^{(k)}[l] = \tfrac{1}{M} \Sigma \sum_{k=1}^{M} \mid X^{(k)}[l] \mid^2, \qquad l = 0, 1, 2, 3, \ldots, N-1, \tag{A.8}$$

$\hat{S}[l]$ denotes the power associated with those frequencies of bandwidth Δf, centered on $f = l\Delta f$.

AUTHORS BIOSKETCH

S. Hoon

Doctoral student at Oceanological Research Institute (IIO) of the Autonomous University of Baja California, Mexico. His research interests include the study of dynamic behavior of soils, civil structures vulnerability and natural risk for earthquakes.

C. Huerta-López

Associate professor and researcher in the Civil Engineering and Surveying Department of the University of Puerto Rico at Mayagüez (UPRM). Experience in industry, teaching and research dates back to the 1980's. His areas of expertise include Earth sciences, Seismology, Geophysics and Engineering seismology. His recent scientific productivity includes 38 publications in referred journals and proceedings with 76 cites out of 21 of these publications, three books, and seven book chapters, and several presentations in conference meetings. He had advised 34 students as supervisor as well as committee member, and from 2007 to current date, he was granted with five research projects by National Council for Science and Technology/México (CONACyT) and private industry also in Puerto Rico. He is member of the Seismological Society of America (SSA), and has the distinction as National Scientific Researcher I since 2006-present, granted by the Mexican government through CONACyT, by the "Sistema Nacional de Investigadores" (SNI).

A. García-Gastélum

Professor and researcher at the Faculty of Marine Sciences of the Autonomous University of Baja California, Mexico. His main interest is the training of human resources in the assessment of vulnerability and natural risks and environmental indicators. His main research and work are in natural risks assessments like drought, earthquakes, tsunamis and coastal and marine floods, geodiversity studies, at the regional and local levels. Consulting work with municipal, state and federal governments in studies like atlas of municipal natural risks, anti-drought measures program at river basin council level, and management programs. His teaching work is focused on Environmental Indicators, Natural Risks, Remote Sensing and Geographic Information Systems, at the bachelor's, diploma, master's and doctorate levels.

NA-TECH EVENTS IN THE COASTAL REGION OF SÃO PAULO, BRAZIL: DATA AND FREQUENCY[1]

José Carlos de Moura Xavier [2], Wilson Cabral de Sousa Junior[3]

ABSTRACT: The scientific literature on events involving the loss of containment of hazardous materials due to a natural event (known as na-tech events) is recent and limited in Brazil. Evidence was sought of the occurrence of these events in the coastal region of the state of São Paulo. The study identified fifteen na-tech events between 1940 and 2015, and showed that the events predominantly affected bodies of water. A method was then proposed to estimate the frequency of these events, relativizing them to the number of companies that generated them. Relativization allows the quantitative comparison among locations with different numbers of companies and the transfer of the estimated frequency among locations. The method also allows attributing less uncertain frequency estimates to na-tech accident hypotheses, favoring risk-based decisions. Consistent databases combined with the method allow the construction of na-tech hypotheses appropriate to the location during a quantitative risk assessment of an industrial facility.

Keywords: database, frequency, Na-tech, precipitation, quantitative risk assessment, vulnerability

EVENTOS NA-TECH EN LA REGIÓN COSTERA DE SÃO PAULO, BRASIL: DATOS Y FRECUENCIA

RESUMEN: La literatura científica sobre eventos que involucran la pérdida de contención de materiales peligrosos debido a un evento natural (conocidos como eventos na-tech) es reciente y limitada en Brasil. Se buscaron evidencias de la ocurrencia de estos eventos en la región costera del estado de São Paulo. El estudio identificó quince eventos na-tech entre 1940 y 2015, y mostró que los eventos afectaron predominantemente a cuerpos de agua. Se propuso entonces un método para estimar la frecuencia de estos eventos, relativizándolos al número de empresas que los generan. La relativización permite la comparación cuantitativa entre localidades con diferente número de empresas y la transferencia de la frecuencia estimada entre localidades. El método también permite atribuir estimaciones de frecuencia menos inciertas a las hipótesis de accidentes de na-tech, favoreciendo las decisiones basadas en el riesgo. Las bases de datos consistentes combinadas con el método permiten la construcción de hipótesis na-tech apropiadas para la ubicación durante una evaluación cuantitativa de riesgos de una instalación industrial.

Palabras clave: base de datos, frecuencia, na-tech, precipitación, evaluación cuantitativa de riesgos, vulnerabilidad

INTRODUCTION

The scientific literature on events involving the loss of containment of hazardous materials due to a natural event is recent and limited in Brazil. Nascimento and Alencar (2016) showed, based on a systematic literature review of the 2000-2015 period, the lack of publications by authors affiliated with research institutions in South America. Similarly, Suarez-Paba et at. (2019), who conducted a literature review from 1960-2018, explicitly mentioned only two articles referring to Brazil, including the study by Xavier and Sousa Junior (2016), discussed ahead.

[1] Article received on January 19, 2022 and accepted for publication on May 1, 2022.
[2] Engineer, São Paulo State Environment Company (CETESB), Av. Professor Frederico Hermann Júnior, 345, São Paulo, CEP 05459-900, Brazil. Email: jxavier@sp.gov.br
[3] Professor, Technological Institute of Aeronautics (ITA), Praça Marechal Eduardo Gomes, 50, São José dos Campos, CEP 12228-900, Brazil. Email: wilson@ita.br

These events are known in the scientific literature as na-tech (natural and technological) events, a term coined by Showalter and Myers (1992, 1994), who used it in research on the perception of emergency management agencies of 50 American states regarding the relationship between natural disasters and technological emergencies. Throughout the text, discussing the results of the research, the authors used the term na-tech event when referring to the occurrence of a natural event (earthquake, hurricane, flood, tornado) and the secondary effect of release of hazardous chemical substances to the environment, including of nuclear origin, making a clear distinction between natural events, technological events and na-tech events.

Xavier and Sousa Junior (2016) investigated na-tech events in the strategies of the agencies responsible for the prevention of accidents involving hazardous materials in Brazil. They showed, for example, that the accident databases operated by these agencies, designed to separately record accidents of natural and technological origin, were not prepared to record and quickly retrieve na-tech events. The immediate implication was the limitation in knowing the intensity of the damage caused by na-tech events and estimating their frequency of occurrence and, as a result, not allowing one to both (i) discern the risk posed to humans by na-tech hypotheses in the quantitative risk assessment (QRA) of industrial facilities that handle hazardous materials (the na-tech risk), and (ii) elucidate the potential damage to the environment that is not typically considered in a QRA. Nevertheless, the authors advocated the use of data from Brazilian sources such as the aforementioned Brazilian accident databases, newspapers, and the technical and scientific literature rather than international data in order to estimate the contribution of na-tech events within a QRA.

The interest in clarifying the relevance of na-tech events in Brazil motivated the development of this research. As starting point, it covered the coastal region of the state of São Paulo. The reasons are both the intense industrialization and the environmental characteristics of the region as an annual mean rainfall between 1100 and 1500 mm, with maximum annual rainfalls of greater than 4000 mm, the presence of overlapping soils, and tropical forest covering layers of coastal hills, being subject to the strongest erosion and transport of soil within Brazil (Ab'Sáber, 2005a, 2005b).

The research sought evidence of the occurrence of na-tech events between 1940 and 2015. It also investigated the correlation between the frequency of occurrence of the identified events and rainfall intensity, as well as the need to correct this frequency based on the rainfall trend in the 2007-2040 period for the RCP4.5 and RCP8.5 greenhouse gas emission scenarios proposed by the Intergovernmental Panel on Climate Change (IPCC). Then, based on the identified na-tech events, the na-tech risk and possible damage to the environment were discussed.

This article presents the initial stages of research related to the identification of na-tech events and the estimation of their frequency of occurrence. The other research stages will be presented in due course.

NA-TECH EVENT IDENTIFICATION

The coastal region of the state of São Paulo comprises the municipalities of Bertioga, Cananéia, Caraguatatuba, Cubatão, Guarujá, Iguape, Ilha Bela, Ilha Comprida, Itanhaém, Mongaguá, Peruíbe, Praia Grande, São Vicente, Santos, São Sebastião and Ubatuba. Figure 1 shows the location of these municipalities.

The study was limited to the 1940-2015 period (76 years). The reason for 1940 was to be able to investigate the presence of na-techs before 1955, the date of the beginning of the operation of the Presidente Bernardes Refinery (RPBC, for its acronym in Portuguese), which led to intense industrialization in Cubatão in the following decades. Between 1940 and 1955, there were few industries in the coastal region of São Paulo and four or five in Cubatão.

As a research method, we adopted the reading of regional printed newspapers from the coastal region of the state of São Paulo, reading of the websites of newspapers with state/national coverage and access to the databases of the National Civil Defence, State Civil Defence, São Paulo State Environment Company (CETESB, for its acronym in Portuguese) and Centre for Research on the Epidemiology of Disasters (CRED). The page-by-page reading of printed newspapers sought to find historical evidence of the occurrence of na-tech events. In the websites, the keywords "municipality name" and "flood" were used. In the databases, the keywords "municipality name" and "cause (natural, leak)" were used, and "Brazil" in the CRED database.

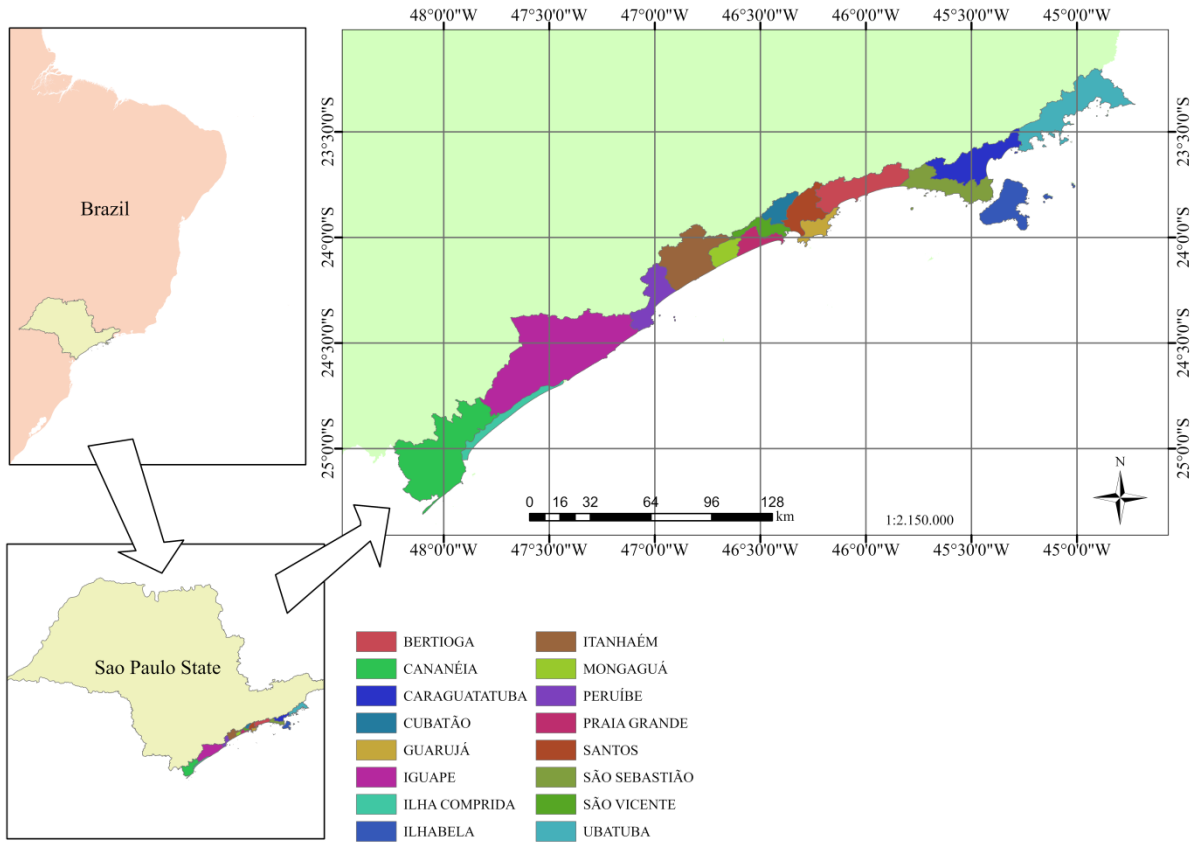

Figure 1: Municipalities of the coastal region of the state of São Paulo.

The search in newspapers proved to be the appropriate option to access old data with accurate date of occurrence of the natural event, since the cited databases did not retrieve events occurring at the beginning of the period of interest and did so in a limited way for the following decades. The approach is similar to that reported by Petrova (2011) on the implementation of a database of technological accidents and disasters in Russia, by Kumasaki et al. (2016), who investigated cascading natural disasters in Japan, or by Chaumillon et al. (2017), who investigated storm-induced marine flooding in France and worldwide.

Approximately 500 reports that mentioned heavy rains, some associated with floods and landslides, were identified. In others, there was mention of strong winds. Some news items appeared in more than one newspaper. There was also some overlap between newspapers and databases, especially the CETESB database.

Based on these news stories, fifteen na-tech events were identified, evidenced by the mention of loss of containment of a reservoir that stored a hazardous material due to a natural event. The appendix and Figure 2 show, by municipality, the na-tech events. There are also twelve news stories that suggest na-tech events, all occurring in Cubatão.

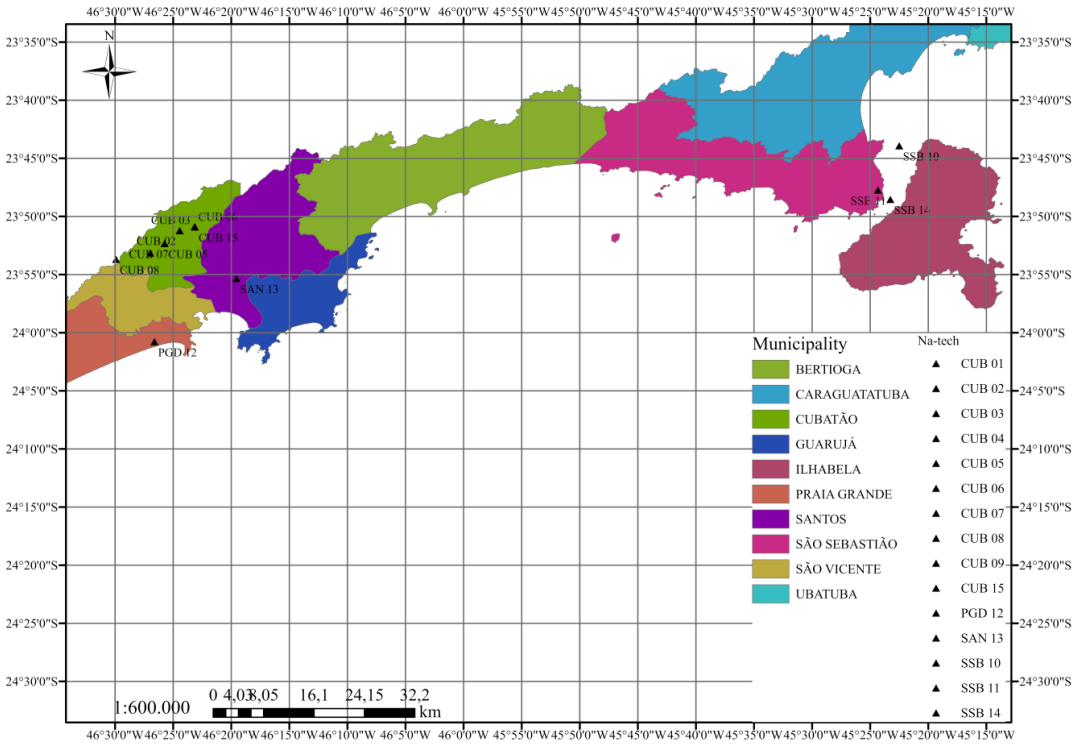

Figure 2: Location of na-tech events in the coastal region of the state of São Paulo.

The reports in the appendix were not refined. Many of them maintain the journalistic language, with emphasis on aspects of the natural event such as impact and time of occurrence. Few of them mention the leaked substances and their quantities. This type of record was preferred to maintain the characteristics of the available information, often conflicting, such as leaked quantities (SSB 10) or equipment where the leak occurred (CUB 05). Refinement can be performed in the future when building a database.

Of the fifteen na-tech events that occurred in the coastal region of São Paulo, ten occurred in Cubatão. The higher incidence in the municipality of Cubatão is compatible with the larger number of companies (25 to 27 starting in the 1980s) compared to São Sebastião (three na-tech events) where there is only one company, although the two municipalities have similar geographic characteristics. The predominance of na-tech events (10 out of 15) occurring in Cubatão combined with the number of companies makes it reasonable to express the occurrence of these events in Cubatão in the period of interest using a quantitative index (a frequency), explained in detail next.

NA-TECH EVENT FREQUENCY

From a methodological perspective, the frequency of occurrence of na-tech events can be estimated similarly to the frequency of pipeline leaks present in *European Gas Pipeline Incident Data Group* (EGIG) and *European Petroleum Refiners Association* (CONCAWE), databases that report leaks in natural gas and oil/oil product pipelines, respectively, in Europe. For example, EGIG (2018) reports a frequency of 0.31 annual occurrences per 1000 km of pipeline. This estimate results from the record of 1366 occurrences during the 1970-2016 period in approximately 143,000 km of pipelines (current length), equivalent to an exposure in the period of 4.41E + 03 km×year.

Following a similar reasoning, where the number of leaks is normalized by the length of the pipelines, equation 1 allows estimating TN_n, the frequency of occurrence of na-tech events accumulated over time and normalized by the number of companies based on the chronological ordering of the events in the 1940-2015 period.

The underlying reasoning for normalization derives from the definition of a na-tech event, i.e., it only occurs in the presence of at least one company, from which there will be loss of containment of the hazardous material. This logic is evident in Santella et al. (2011) or Girgin and Krausmann (2016).

$$TN_n = \left(\sum_{i=1}^{n} \frac{N_i}{E_i}\right)\left(\sum_{i=1}^{n} P_i\right)^{-1} \quad (1)$$

where (i) period of interest, (N_i) number of na-tech events in period i, (E_i) number of companies in period i and (P_i) number of years in each period i.

As a premise, the equation 1 requires independent na-tech events. Based on the employment of the term na-tech by Showalter and Myers (1992, 1994), the independence is reached by assigning only one identifier code (see the first column in the appendix) for each natural event regardless the number of secondary effects, i.e., the releases of hazardous materials to the environment (or the technological events).This approach can be observed in both SAN 13 and CUB 08 na-tech events mentioned in appendix. The first one indicates a natural event (lightning) and a cascading secondary event involving three storage tanks. The second, CUB 08, reports a natural event (heavy rain) and secondary events in three different locations.

To determine the TN_n for Cubatão, the period 1940-2015 (76 years) was divided into five-year periods, except for the first period which comprised six years. The periods were chosen after applying the method proposed by Sturges (1926). The initial fifteen-year periods derived from the method were reduced for five-year periods after exploring na-tech events distribution and the number of companies in different periods. The number of na-tech events and companies in each period was determined, and the frequency was calculated using equation 1. Table 1 shows the estimated TN_n.

Table 1: Frequency of occurrence of na-tech events in Cubatão accumulated over time and normalized by the number of companies (TN_n).

i	***P_i***	***E_i***	***N_i***	**Event in the period (occurrence/ company × year)**	***TN_n* (occurrence/ company × year)**
1940-1945	6	4	0	0	0
1946-1950	5	4	0	0	0
1951-1955	5	5	0	0	0
1956-1960	5	11	0	0	0
1961-1965	5	12	0	0	0
1966-1970	5	15	0	0	0
1971-1975	5	21	0	0	0
1976-1980	5	28	0	0	0
1981-1985	5	27	2	1.48E-02	1.61E-03
1986-1990	5	27	2	1.48E-02	2.90E-03
1991-1995	5	27	1	7.41E-03	3.31E-03
1996-2000	5	26	2	1.54E-02	4.30E-03
2001-2005	5	26	0	0	3.97E-03
2006-2010	5	25	0	0	3.69E-03
2011-2015	5	25	3	2.40E-02	4.97E-03

Legend: (i) period of interest, (P_i) number of years in each period i, (E_i) number of companies in period i, and (N_i) number of na-tech events in period i.

The frequency is increasing and reflects the record of na-tech events starting in the 1981-1985 period. Since then, zero to three occurrences per period have been observed, with a temporal trend shown in Figure 3. The frequency point value, e.g., 4.97E-03 occurrence/company × year, indicates the number of na-tech events normalized by the number of companies present in each period and counted over the entire period of interest.

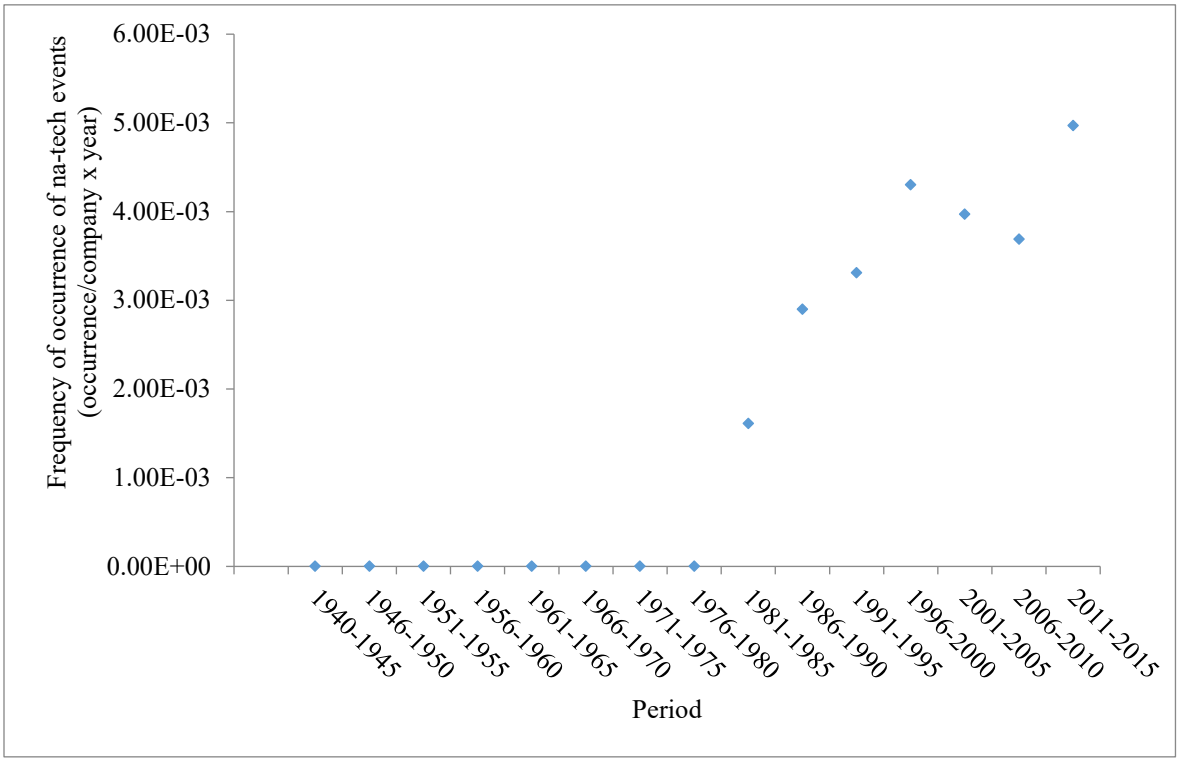

Figure 3: Frequency of occurrence of na-tech events in Cubatão.

Next, similar to the QRA of pipelines, where the frequencies of the accidental hypotheses are estimated from databases such as EGIG and CONCAWE (BSI, 2009; CETESB, 2014), a hypothesis related to the loss of containment of equipment due to a natural event can be formulated and the frequency (TN_n) assigned to it as an estimate of the frequency of occurrence of the hypothesis.

NA-TECH EVENT DAMAGE

In the na-tech events identified in the coastal region of São Paulo, there is no mention of people affected by fire, explosion or atmospheric dispersion of the substances. There is no mention of monitoring of the water bodies in the days following na-tech events, although it is reasonable to infer some damage to the fauna near the leak sites.

The absence of human fatality was also noted by Girgin and Krausmann (2016) when investigating the occurrence of na-tech events in the onshore pipeline network for the transport of hazardous liquids in the United States between 1986 and 2012. This finding is relevant because the metric adopted in the QRA to express risk has as reference values (or end points) toxic substance concentrations, thermal radiation intensity or overpressure intensity sufficient to cause human fatality.

The finding that water bodies were affected by the leaks is in line with the findings of Cozzani et al. (2010), who, in a survey of European and American databases, identified water contamination as the most

recorded effect. Girgin and Krausmann (2016), in turn, showed that 48% of na-tech events resulted in releases to the ground, 28% to water bodies and 14% to the atmosphere.

From the appendix, Table 2 was constructed, which contains the substances and equipment involved in the spills, in addition to the immediate causes of the spills.

Eight of the fifteen na-tech events have floods as an immediate cause. Soil movement was the immediate cause of four na-tech events. Wind, stream, rainfall and lightning also appear as immediate causes.

The floods reached open equipment installed at ground level, as in the case of effluent treatment stations and storage sheds. These equipments can be added to those identified by Cozzani et at. (2010) and suggest, due to their construction and location characteristics, a higher probability of loss of containment.

Nevertheless, regarding the equipment, there is no report of the involvement of pressurized tanks, and only SAN 13 mentions an atmospheric tank hit by lightning.

The na-tech event SAN 13 affected two tanks, where the first was hit by lightning and the second by a domino effect resulting from the explosion and movement of the roof of the first tank.

Table 2: Equipment and substances involved in na-tech events.

Identifier	Date	Substance leaked	Equipment	Immediate cause
CUB 01	01.25.1985	Ammonia	Pipeline	Land slide
CUB 02	03.09.1988	Tail gas	Pipeline	Land slide
CUB 03	02.05.1989	Ammonia	Pipeline	Land slide
CUB 04	01.16.1992	Oily waste	Effluent treatment station	Flood
CUB 05	02.08.1998	Oily waste	Effluent treatment station	Flood
CUB 06	01.11.1999	Unidentified	Solids storage warehouse (supposedly)	Flood
CUB 07	01.15.2011	Oily waste	Effluent treatment station	Flood
CUB 08	02.22.2013	Oily waste	Effluent treatment station (site 1)	Flood
		Oily waste	Effluent treatment station (site 2)	Flood
		Chlorine	900kg cylinder (site 3)	Land slide
CUB 09	03.17.2013	Oily waste	Effluent treatment station	Flood
SSB 10	03.18.1974	Crude oil	Ship tank	Wind and stream
SSB 11	01.14.2010	Oily waste	Filter drainage tanks	Rainfall
PGD 12	04.13.2007	Diesel	Underground tanks	Flood
SAN 13	10.10.1991	Acrylonitrile, hexane	Vertical atmospheric tank	Lightning
SSB 14	08.19.1976	Crude oil	Unloading arms	Wind
CUB 15	02.01.1983	Sulphate, Urea (??)	Solids storage warehouse (supposedly)	Flood

The loss of containment of the toxic gases ammonia and chlorine in na-tech events CUB 01, CUB 03 and CUB 08 suggests the possibility of harm to humans, although the records mentioned only odour perception in CUB 08.

DISCUSSION

Seven of the 15 na-tech events were identified in the CETESB database (CETESB 2022). Another seven by reading the *A Tribuna* printed newspaper and one on the website of the *Folha de São Paulo* newspaper (Folha de São Paulo, 2022). Only three events had concurrent records in two sources.

The underreporting noted by Rasmussen (1995) or the identification of the na-tech event only after an intense examination of records reported by Girgin and Krausmann (2016) were also identified in this study. For example, in the na-tech event CUB 08, the *A Tribuna* newspaper did not mention the dragging of five chlorine cylinders and the loss of content from one of them (underreporting). Additionally, na-tech event CUB 07 was located after personally consulting the Emergency Response Sector of CETESB and using the keyword "overflow" to search its database (identification).

Despite the lack of a specific database for na-tech events, the existing databases, such as those of CETESB, National Civil Defence (Brazil, 2021) and State Civil Defence of São Paulo (São Paulo, 2022), do not have search keywords with immediate association with this type of event. In the case of the CETESB database, events were identified through searches with keywords such as overflow, tank or pipeline transport, different from the expected for an event triggered by a natural cause. The keyword "natural" was introduced in 2012 and allowed retrieval of three records, all na-tech events.

Specific databases, such as the one managed by the Joint Research Centre (JRC) (European Commission, 2011), a European Union research center, allow the targeted search of these events. The counterpoint is the need to feed these databases with past records for statistical analysis. Alternatively, the existing databases can be improved (Xavier and Sousa Junior, 2016) by inserting search keywords that lead directly to na-tech events. In the same way as for a specific database, the existing records should be reviewed to qualify them based on the new search keyword.

The systematic recording of these events makes it possible to broaden the analysis of their occurrence on the temporal and spatial scales in order to determine the damage states and the frequency of occurrence, which are essential for a QRA of an industrial facility that handles hazardous materials installed in an area prone to occurrence of na-tech events. It would also help to determine the contribution of these events to the risk imposed by the facility on humans and to elucidate possible damages to the environment that are not commonly considered in a QRA.

Normalizing the frequency of occurrence of na-tech events by the number of companies allows to properly compare the frequency of events occurring in Cubatão with those estimated for locations with greater or lesser presence of companies. It also allows attributing less uncertain frequency estimates to na-tech accidental hypotheses, which favours risk-based decision making.

Unlike hypotheses whose causes are attributed to human or equipment failures, as occurs in traditional QRA, with numerical probability and frequency values that can be used in industrial facilities located in different countries, na-tech hypotheses consider local and regional specificities such as the geographic, hydrological and industrial and occupation characteristics. Therefore, the frequency of occurrence of na-tech events is limited to Cubatão and its surroundings and shows a growing trend, as indicated in Figure 3. Adopting the values found for other regions is not recommended but adopting the proposed method is, as it can guide other estimates, preferably at the local or regional level, so that they reflect the characteristics of regions.

The research did not identify reports of injured or dead people. It did find that na-tech events predominantly affected water bodies close to companies. Therefore, this risk should be managed, regardless of the metric used for its expression.

For Cubatão, the strategy for the protection of industrial enterprises established in 1986 and still in force with the creation of the special commission for the restoration of Serra do Mar region in Cubatão should be expanded. The commission proposed that year a contingency plan to monitor the amount of rainfall and adopt measures in companies potentially affected by landslides (São Paulo, 1986).

Landslides are not the main cause of na-tech events in Cubatão. As shown in Table 2, six of the ten events that occurred in the municipality resulted exclusively from floods and affected open equipment installed at ground level.

Therefore, the public and private management of the Cubatão industrial park should also include the identification of flood-prone regions and observation of the presence of equipment storing or processing hazardous substances. Equipment installed at ground level and near water bodies should take priority in protection using physical barriers or be moved to suitable locations.

The results of the research can be used in the decision-making processes of companies and regulatory agencies. Companies, as already mentioned, can assist in the location of the new projects or in the management of the existing projects. For regulatory agencies, this is an important result in that it expands the scope of the QRA, even though the metrics of that tool do not consider the impacts on environmental goods other than humans but which are observed in the identified na-tech events.

These results can be improved by expanding databases with records from other sources. It is understood that the companies involved in na-tech events can contribute accurate information about the equipment involved, the amounts of substances released into the environment, the measures adopted before and after the na-tech event, the damage to human life and to other environmental goods, economic impacts and effects on the company's image and, last, the lessons learned. This information is relevant for understanding the dynamics of na-tech events, estimating na-tech risk and proposing management measures.

CONCLUSIONS

The fifteen na-tech events presented in the appendix and twelve other suggestive reports confirm the initial interest of the research regarding the occurrence of na-tech events in the industrialized areas of the coastal region of São Paulo.

The difficulty in identifying these events, as well as the observed increasing trend in the number of na-tech events, reinforces the need for Brazilian accident databases to include these events, making it possible to broaden the discussion about their relevance in the risk to humans imposed by enterprises that handle hazardous materials in places prone to the occurrence of na-tech events.

The proposed method for estimating the frequency of occurrence, which relativizes the events found by the number of companies that generated them, is relevant because it allows the quantitative comparison of locations or regions with different numbers of companies. The comparison and eventual adoption of the numerical value will be more robust if these locations or regions have similar geographic, hydrological and industrial land occupation characteristics.

Consistent databases combined with the proposed method for frequency estimation will allow the construction of na-tech hypotheses appropriate to the location or region in which a traditional QRA is performed, making it possible to determine the contribution of these hypotheses to the risk imposed by companies to humans.

REFERENCES

Ab'Sáber, A.N. (2005ª). Os domínios de natureza do Brasil: potencialidades paisagísticas [The domains of nature in Brazil: landscape potential], São Paulo: Ateliê Editorial 3rd ed.

Ab'Sáber, A. N. (2005b). Litoral do Brasil [Brazilian Coastline], São Paulo: Metalivros.

Ministério da Integração Nacional. (2021). Sistema Integrado de Informações sobre Desastres – S2iD, accessed Oct 18, 2021 at:. https://s2id-search.labtrans.ufsc.br/.

BSI, British Standard Institution. (2009). BSI PD 8010-3:2009. Steel pipelines on land - Guide to the application of pipeline risk assessment to proposed developments in the vicinity of major accident hazard pipelines containing flammables.

CETESB. (2014). Risk of accident of technological origin. Method for decision-making and reference terms, accessed May 06, 2022 at: https://sistemasinter.cetesb.sp.gov.br/normas/11/2013/11/P4261.pdf.

CETESB. (2022). Sistema de Informações sobre Emergências Químicas, accessed May 06, 2022 at:.https://sistemasinter.cetesb.sp.gov.br/emergencia/relatorio.php.

Chaumillon, E.; Bertin, X.; Fortunato, A. B.; Bajo, M.; Schneider, J. L.; Dezileau, L.; Walsh, J. P.; Michelot, A.; Chaveau, E.; Créach, A.; Hénaff, A.; Sauzeau, T.; Waeles, B.; Gervais, B.; Jan, G.; Baumann, J.; Breilh, J. F.; Pedreros, R. (2017). *Storm-induced marine flooding: Lessons from a multidisciplinary approach, Earth-Science Reviews*, v. 165, 151-184. http://dx.doi.org/10.1016/j.earscirev.2016.12.005.

Cozzani, V.; Campedel, M.; Renni, E.; Krausmann, E. (2010). "Industrial accidents triggered by flood events: analysis of past accidents", *Journal of Hazardous Materials*, v. 175, 501–509. https://doi.org/10.1016/j.jhazmat.2009.10.033.

EGIG. (2018). EGIG gas pipeline incidents: 10th Report of the European Gas Pipeline Incident Data Group (period 1970–2016), accessed May 06, 2022 at:. https://www.egig.eu.

European Commission. (2011). *Natech accident database*, Joint Research Centre, Institute for the Protection and Security of the Citizen, Italy, accessed May 06, 2022 at: https://enatech.jrc.ec.europa.eu/.

Folha de São Paulo. (2022). São Paulo: UOL, 1921, accessed May 06, 2022 at: http://acervo.folha.uol.com.br/.

Girgin, S.; Krausmann, E. (2016). "Historical analysis of U. S. onshore hazardous liquid pipeline accidents triggered by natural hazards", *Journal of Loss Prevention in the Process Industries*, v. 40, 578-590. http://dx.doi.org/10.1016/j.jlp.2016.02.008.

Kumasaki, M.; King, M.; Arai, M.; Yang, L. 2016. Anatomy of cascading natural disasters in Japan: main modes and linkages. Natural Hazards, v. 80, 1425-1441. DOI 10.1007/s11069-015-2028-8.

Nascimento, K. R. da S.; Alencar, M. H., (2016). "Management of risks in natural disasters: a systematic review of the literature on NATECH events", *Journal of Loss Prevention in the Process Industries*, v. 44, 347-359. http://dx.doi.org/10.1016/j.jlp.2016.10.003.

Petrova, E. G. (2011). Natural factors of technological accidents: the case of Russia. Natural Hazards and Earth System Sciences, v. 11, 2227–2234. https://doi.org/10.5194/nhess-11-2227-2011.

Poffo, I. R. F. (2000). Vazamentos de óleo no Litoral Norte do estado de São Paulo: análise histórica (1974 a 1999). Master's Dissertation, University of São Paulo, Brazil, 2000, accessed May 06, 2022 at: https://cetesb.sp.gov.br/emergencias-quimicas/wp.

Rasmussen, K. (1995). "Natural events and accidents with hazardous materials", *Journal of Hazardous Materials*, v. 40, 43-54. https://doi.org/10.1016/0304-3894(94)00079-V.

Santella, N.; Steinberg, L. J.; Aguirra, G. A. (2011). "Empirical estimation of the conditional probability of na-tech events within the United States", *Risk Analysis*, v. 31, (6), 951–968. https://doi.org/10.1111/j.1539-6924.2010.01561.x.

São Paulo. (1986). Comissão Especial para a Restauração da Serra do Mar na Região de Cubatão. Plano de Ações de Emergência 1985/1986: Relatório de Situação. Printed copy available at CETESB library

São Paulo. (2022). Governo do Estado de São Paulo. Sistema Integrado de Defesa Civil – SIDEC, accessed May 06, 2022 at:. http://www.sidec.sp.gov.br/. (in Portuguese)

Showalter, P. S.; Myers M. F. (1992). Natural disasters as the cause of technological emergencies: a review of the decade 1980–1989. Working paper 78. Natural Hazards Research and Applications Information Center. Institute of Behavioral Science. University of Colorado.

Showalter, P. S.; Myers M. F. (1994). "Natural disasters in the United States as release agents of oil, chemicals, or radiological materials between1980–1989: analysis and recommendations", *Risk Analysis*, v. 14, (2), 169–182.

Sturges, H. A. (1926). "The choice of a class interval", *Journal of the American Statistical Association*, v. 216, n. 153, 65-66.

Suarez-Paba, M. C.; Perreur, M.; Munoz, F.; Cruz, A. M. (2019). "Systematic literature review and qualitative meta-analysis of Natech research in the past four decades", *Safety Science*, v. 116, 58-77. https://doi.org/10.1016/j.ssci.2019.02.033.

Xavier, J. C. de M.; Sousa Junior, W. C. (2016). Recognising na-tech events in Brazil: moving forward. Natural Hazards (Dordrecht), v. 82, 493-506. https://doi.org/10.1007/s11069-016-2194-3.

APPENDIX
Identified na-tech events

Identifier	Date	Municipality	Location		Company	Description
			UTM-N	UTM-E		
CUB 01	01.25.1985	Cubatão	7361270	356682	Ultrafértil	Rupture of a three-inch pipeline transporting ammonia between Ultrafértil's Jardim São Marcos and Fafer units. Leakage of 15t in approximately three hours due to landslide resulting from rainfall. It occurred at 11:45 pm at km 60 of Piaçaguera-Guarujá highway, at Sector 8.
CUB 02	03.09.1988	Cubatão	7361270	356682	Copebras/ Union Carbide	Small leaks of tail gas in a pipeline that connects Copebras to Union Carbide due to landslide. Detection occurred during testing of the pipeline performed prior to its operation. The leaks occurred at dawn, at km 60 of Piaçaguera-Guarujá highway, in Sector 8.
CUB 03	02.05.1989	Cubatão	7361270	356682	Ultrafértil	Rupture of a three-inch pipeline transporting ammonia between Ultrafértil's Jardim São Marcos and Fafer units. It resulted from landslide. It occurred at km 60 of Piaçaguera-Guarujá highway, in Sector 8.

APPENDIX
Identified na-tech events (continued)

Identifier	Date	Municipality	Location		Company	Description
			UTM-N	UTM-E		
CUB 04	01.16.1992	Cubatão	7359213	354505	Petrobras	Heavy rain led to the overflow of Cubatão River. Its waters reached the effluent treatment station of Presidente Bernardes Refinery (RPBC). The contaminated waters reached the residences of Vila Elizabeth, near the RPBC. Over the past 72 hours, rainfall in the region of the refinery reached 342 mm. Peak rainfall in Cubatão occurred at 4 pm with 147.4 mm (1 h). Approximately 1000 people were forced out of their homes, mainly in Vila Parisi and Morro Mazargão.
CUB 05	02.08.1998	Cubatão	7359213	354505	Petrobras	Heavy rain caused the overflow of oily waters from the RPBC effluent treatment station, which reached the Cubatão River. The leaked volume was not reported or estimated. According to CETESB, (i) the spill impregnated with oil an approximately 5-km extension of the right bank of Cubatão River; (ii) preliminary evaluation indicated severe damage to the environment and (iii) the leakage resulted from the operation of only two of the five pumps that control the arrival of oil in the treatment station. According to Petrobras, the spill had no connection with the pumps. It was due to the rupture of the lid of a passage box through which runs a pipeline carrying oil to the treatment station.

APPENDIX
Identified na-tech events (continued)

Identifier	Date	Municipality	Location		Company	Description
			UTM-N	UTM-E		
CUB 06	01.11.1999	Cubatão	7361874	358913	Solorrico	Heavy rain associated with the opening of the floodgates of the Billings dam flooded part of the Cubatão industrial complex. The opening contributed to the partial flooding of the company and of the main access roads to the complex. The flooding was also due to restrictions to the flow of Piaçaguera River, near Solorrico. A note from the company reported that at 5 pm its industrial area was threatened by water, with material losses.
CUB 07	01.15.2011	Cubatão	7359213	354505	Petrobras	Heavy rain led to the overflow of the waste retention pond of the RPBC effluent treatment station.

APPENDIX
Identified na-tech events (continued)

Identifier	Date	Municipality	Location		Company	Description
			UTM-N	UTM-E		
CUB 08	02.22.2013	Cubatão	7359213	354505	Petrobras	Heavy rain caused (i) flooding of the RPBC areas, including the effluent treatment station (industrial wastewater treatment station and effluent accumulation basin), carrying oily material to Cubatão River; (ii) mudslide and a landslide at Serra do Mar near the Pilões water treatment station of Sabesp. Among the consequences, there was the dragging of five chlorine storage cylinders with individual storage capacity of 900 kg. The cylinders were recovered from the water bodies of the region. One of them had a ruptured valve and lost its contents. There were complaints of odour from the Vila dos Pescadores community; and (iii) flooding of Transpetro's Cubatão Terminal. As a result, there was flooding of the water-oil separator (WOS), pump house, sump tank and rupture of the levees of tanks TQ 14011 and TQ 14023. There was mud accumulation in the WOS, sump tank and waste yard, with drums carried from this yard to the street (Pescada Street) and accumulation of debris contaminated with oily sludge. On February 25,500 people were temporarily forced out of their homes and 4,000 were made homeless.
			7356622	347438	Sabesp	
			7357676	352436	Transpetro	

APPENDIX
Identified na-tech events (continued)

Identifier	Date	Municipality	Location		Company	Description
			UTM-N	UTM-E		
CUB 09	03.17.2013	Cubatão	7359213	354505	Petrobras	Heavy rain caused flooding of the RPBC areas, including the effluent accumulation basin of the effluent treatment station, carrying oily sludge to Cubatão River.
SSB 10	03.18.1974	São Sebastião	7375331	461814	Transpetro	Strong winds and stream led to the breaking of the moorings of the Takamiya Maru tanker, from Japan, and Conoco Canada tanker, of Liberian flag, at approximately 11 am, which were anchored next to the piers of the São Sebastião Waterway Terminal (TA/SSE). The Conoco, after hitting a rock, drifted and ran aground on a sand bank near Ilha Bela municipality. The Takamiya, which also hit the rock, had a broken hull and, according to the *Folha de São Paulo* newspaper, poured approximately 15t of oil into the sea. In turn, the newspaper *A Tribuna* reported 15,000t and Poffo (2000) reported a leakage of 6,000t.
SSB 11	01.14.2010	São Sebastião	7368370	458685	Transpetro	Heavy rain caused the overflow of the surge tank of the auxiliary filters' drainage tanks of the OSVAT pipeline located at TA/SSE. A small amount of oily sludge reached Outeiro creek, which flows into São Sebastião Channel.

APPENDIX
Identified na-tech events (continued)

Identifier	Date	Municipality	Location		Company	Description
			UTM-N	UTM-E		
PGD 12	04.13.2007	Praia Grande	7343599	353177	Centro Automotivo Veraneio	Heavy rain caused flooding of the three tanks of this gas station. The gas station was deactivated, and the tanks' lids were opened, removed by vandals. The leaked product was diesel oil, which flowed to the nearby rain water drains.
SAN 13	10.10.1991	Santos	7353785	365022	Granel Química	Lightning sparked a fire in two 1,400m^{3}tanks shortly after 6:30 a.m. The lightning hit tank 51, containing 500t of acrylonitrile. An explosion followed, and the tank's roof hit and ruptured a valve in tank line 57, which contained hexane. The hexane jet hit tank 61, which was partially destroyed. There were no victims.
SSB 14	08.19.1976	São Sebastião	7366873	460582	Transpetro	Winds of up to 110 km/h broke the moorings of the Energy Transmission tanker, of Liberian flag, anchored on the TA/SSE pier, at approximately 7:40 a.m. Three of the five unloading arms broke, and oil spilled into São Sebastião Channel.
CUB 15	02.01.1983	Cubatão	7361874	358913	Solorrico	Heavy rain led to the overflow of the Piaçaguera River. Rainfall fell more intensely after 4:00 am. At 5:00 am, the waters reached 50cm in the industrial and administrative area of the company, flooding the raw material storage and production sectors, forcing it to stop fertilizer production. Tons of urea and sulphate were lost.

AUTHORS BIOSKETCH

J. de Moura-Xavier

Graduated in chemical engineering; pharmacy and biochemistry from University of São Paulo, Brazil. He obtained a Master and Doctorate in Science both from Technological Institute of Aeronautics. Actually, he works at *São Paulo State Environment Company* in activities related to risk management of industrial enterprises that handle hazardous materials.

W. de Sousa-Junior

Associate professor at Technological Institute of Aeronautics working mainly on the following topics: environmental and ecological modeling, enviromental management instruments, economic-environmental analysis of infrastructure projects and climate change. He is graduated in oceanology with a Master in remote sensing and Doctorate in economics. Also, he works as a professor at the graduate program in natural disasters at São Paulo State University and coordinate the HabITAs project, which aims to break paradigms in Brazilian civil construction towards sustainability. Author of the book "Water management in Brazil: reflections, diagnoses and challenges", among other.

VULNERABILITY OF SCHOOLS IN PUERTO RICO TO TSUNAMIS[1]

Gustavo E. Pacheco-Crosetti[2], Omaira Collazos-Ordóñez[3], Verónica A. Torres Rodríguez[4], Joel A. Cohen Vázquez[4]

ABSTRACT: The archipelago of Puerto Rico is a region of high danger to tsunamis (ATC, 2019). Recognizing that the school population in Puerto Rico is around 600,000 people (including students and teachers, according to 2016 data), and that schools are essential facilities to safeguard against extreme events, the objective of the research has been to evaluate if the Puerto Rican schools are vulnerable to tsunamis. In the first instance, a comprehensive database of schools in Puerto Rico that could be affected by tsunami events was developed and critical municipalities were identified. The municipalities of San Juan and Cataño were selected as case studies in which a more detailed evaluation was carried out. This evaluation included the analysis of the evacuation time required to move from each schoolyard to a safe place as the main vulnerability factor. The shortest route and several alternative routes were evaluated for each school. The analysis included as a complementary factor the status of the critical school evacuation route in each of the two municipalities. In addition, a survey form was developed and administered to collect data on school evacuation preparedness. The study found that the most vulnerable schools in each study municipality present excessive evacuation times and unsafe and inadequate evacuation routes for the evacuation process. Several additional study areas have been identified to improve the vulnerability assessment of schools. Therefore, a second phase of the research is being developed to obtain better estimates of evacuation times, including all stages of the evacuation process (evacuation timeline), analyzing the factors that affect pedestrian dynamics and simulation of each of these phases and integrating data from evacuation drills. The results of these investigations are expected to contribute to the rehabilitation processes of coastal schools by providing refined tools to decide if vertical evacuation is required.

Keywords: tsunamis, tsunamis effects, school vulnerability, school safety, community resilience

VULNERABILIDAD DE ESCUELAS DE PUERTO RICO A EVENTOS DE TSUNAMI

RESUMEN: El archipiélago de Puerto Rico es una región de alto peligro a tsunamis (ATC, 2019). Reconociendo que la población escolar en Puerto Rico es de alrededor de 600,000 personas (incluyendo estudiantes y maestros, según datos de 2016), y que las escuelas son instalaciones esenciales para salvaguardar frente a eventos extremos, el objetivo de la investigación ha sido evaluar si las escuelas de Puerto Rico son vulnerables a los tsunamis. En primera instancia, se desarrolló una base de datos integral de las escuelas de Puerto Rico que podrían verse afectadas por eventos de tsunamis y se identificaron los municipios críticos. Se procedió a seleccionar los municipios de San Juan y Cataño como casos de estudio en los que se realizó una evaluación más detallada. Esta evaluación incluyó el análisis del tiempo de evacuación requerido para moverse desde cada patio escolar hasta llegar a un lugar seguro como principal factor de vulnerabilidad. Se evaluó la ruta más corta y varias rutas alternativas para cada escuela. El análisis incluyó como factor complementario el estado de la ruta de evacuación de la escuela crítica en cada uno de los dos municipios. Además, se desarrolló y administró un formulario de encuesta destinado a recopilar datos sobre la preparación para la evacuación de las escuelas. El estudio encontró que las escuelas más vulnerables en cada municipio de estudio presentan tiempos de evacuación excesivos y rutas de evacuación inseguras e inadecuadas para el proceso de evacuación. Varias áreas de estudio adicionales han sido identificadas para mejorar la evaluación de la vulnerabilidad de

[1] Article received on April 30, 2022 and accepted for publication on May 16, 2022.
[2] Professor, Department of Civil and Environmental Engineering and Land Surveying, Polytechnic University of Puerto Rico, San Juan, PR 00918. Director, *Transportation Infrastructure Research Center*. E-mail: gpacheco@pupr.edu
[3] Professor, Department of Civil and Environmental Engineering and Land Surveying, Polytechnic University of Puerto Rico, San Juan, PR 00918. E-mail: ocollazos@pupr.edu
[4] Undergraduate Students, Civil Engineering Program, Polytechnic University of Puerto Rico, San Juan, PR 00918.
E-mails: torres_110592@students.pupr.edu, cohen_112931@students.pupr.edu

las escuelas. Por tanto, se está desarrollando una segunda fase de la investigación para obtener mejores estimaciones de los tiempos de evacuación, incluyendo todas las etapas del proceso de evacuación (línea de tiempo de evacuación), analizando los factores que afectan a la dinámica peatonal y la simulación de cada una de estas fases e integrando datos de simulacros de evacuación. Se espera que los resultados de estas investigaciones contribuyan a los procesos de rehabilitación de las escuelas costeras brindando herramientas refinadas para decidir si se requiere evacuación vertical.

Palabras clave: tsunamis, efectos de tsunamis, vulnerabilidad de escuelas, seguridad de escuelas, resiliencia comunitaria

INTRODUCTION

Any construction in Puerto Rico (PR) could experience very strong shakings due to earthquakes (NIBS, 2010). This high seismic hazard is due to PR being located on a microplate sandwiched between the edge of the North American Tectonic Plate and the extreme northwest of the Caribbean Tectonic Plate. The interaction between these two plates has generated several significant faults in the region, (Figure 1, showing only the offshore faults). Some of these faults have the potential to generate local tsunamis, including the Puerto Rico trench (NOAA, 2010) or a repeat of the 1918 tsunami in the Mona Canyon (Reid and Taber, 1919).

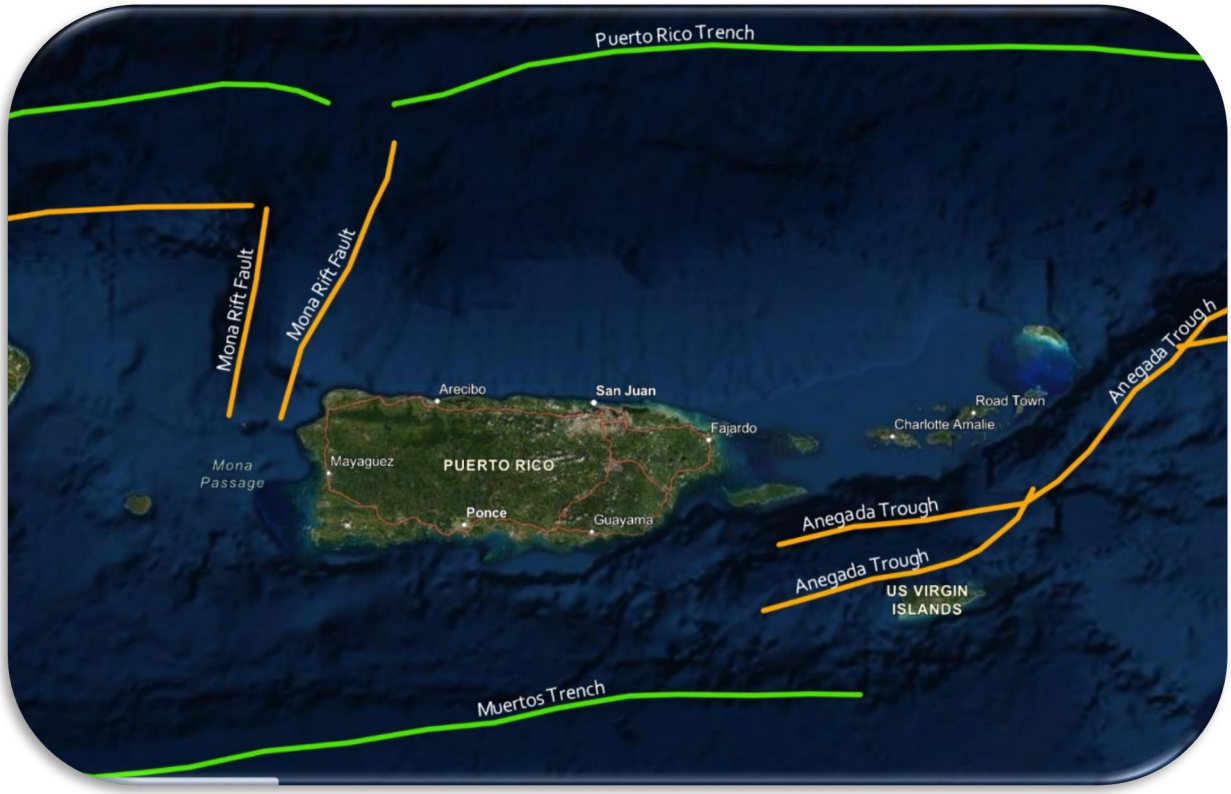

Figure 1: Puerto Rico Offshore Seismic Faults (QuakeFeed App, Artisan Global LLC., n.d.).

On January 7, 2020, a 6.4 magnitude earthquake affected PR, with high intensities in the southern west area, as presented in Figure 2, causing damages and collapse on diverse types of buildings and facilities in several municipalities. Figure 3 presents examples of the collapse of houses mounted on stilts located in Guánica, while Figure 4 presents the collapse of Agripina Seda School in Guánica.

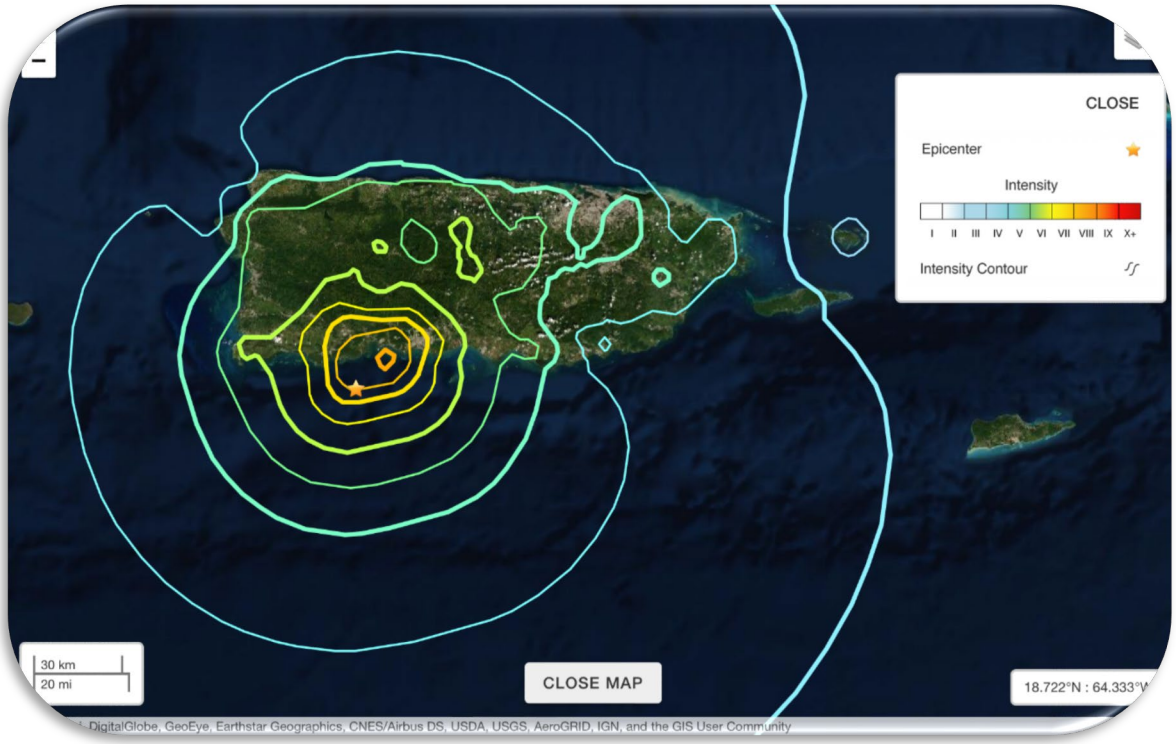

Figure 2: Intensity contours due to January 7, 2020 M6.4 Earthquake (USGS, 2020a and 2020b)

Figure 3 : Examples of Collapse and Damages to Houses in Guánica due to January 7, 2020 Earthquake (Pacheco-Crosetti, 2020).

Figure 4 : Collapse of Agripina Seda School in Guánica due to January 7, 2020 Earthquake (Pacheco-Crosetti, 2020).

After the earthquake of January 7, 2020, the damages on soils and structures have been extensively studied, documented and disseminated in papers, reports, and conferences (i.e., Bernal et al, 2020; Chen et al, 2022; Knoper et al, 2020; Miranda et al, 2020; Pacheco-Crosetti, 2020). Topics such as the impact of the informal construction, the lack of seismic steel detailing, the quality of materials, and the presence of intrusive elements in structural elements have been addressed. Considering the catastrophic collapse of the school in Guánica (Figure 4), significant damage to many other schools, and that many of the schools do not meet actual code requirements (Noticel, 2020), the identification of the vulnerabilities and the rehabilitating of schools has emerged as a societal priority. Nevertheless, the proposed improvements are considered not enough (CBEE, 2021), since they are focusing only on the presence of short columns instead of a comprehensive assessment of school rehabilitation needs.

Despite the fact that several topics associated to seismic design have been addressed as critical as a consequence of the 2020 events, the consideration of the possible impact of tsunamis has not emerged as a significant topic in general, and in schools' rehabilitation in particular. According to the report FEMA P-646 - Guidelines for Design of Structures for Vertical Evacuation from Tsunamis (ATC, 2019a), Puerto Rico is a region with a high hazard of experiencing tsunami impacts, as presented in Figure 5. Indeed, the effects of tsunamis can be very destructive (Figure 6, and as described in FEMA P-646 report).

Table 2-1 Qualitative Tsunami Hazard Assessment for U.S. Locations, (Dunbar and Weaver, 2015)

Region	Hazard Based on Historical Record and Earthquake Probabilities	Number of Reported Deaths
Alaska	High to Very High	222
Alaska Arctic Coast	Very Low	None
American Samoa	High	34
Guam and Northern Mariana Islands	High	1
Hawaii	High to Very High	293
Puerto Rico and U.S. Virgin Islands	High	164
U.S. Atlantic Coast	Very Low to Low	None
U.S. Gulf Coast	Very Low	None
U.S. West Coast	High to Very High	25*

* Excludes any deaths caused by the 1700 Cascadia tsunami on the U.S. West Coast.

Figure 5: Qualitative Hazard to Tsunamis in the US (ATC, 2019a).

Figure 6: Tsunami inundating Yamada, Japan, in 2011 (NOAA, 2019).

The most recent devastating tsunami in Puerto Rico occurred on October 11, 1918, due to the 7.3 magnitude San Fermin earthquake, in the Mona Passage. The earthquake resulted in 116 casualties and more than four million dollars in property loss, according to the US Congress Report (1919). The earthquake generated a tsunami. The waves travelled quickly, taking between just five to six minutes after the shaking to arrive to Aguadilla shoreline in northwestern Puerto Rico (Reid and Taber, 1919). Near Punta Agujereada (North to Aguadilla) the elevation of the wave was calculated to be approximately 20 feet (Reid and Taber, 1919). The simulation by Mercado and McCann (1998) replicated fairly well the observations by Reid and Taber. In the town of Aguadilla, 32 people drowned and nearly 300 existing ranches on the beach were destroyed (Figure 7); in the vicinity of Punta Agujereada, 8 people drowned (Reid and Taber, 1918; PRSN, 1918 Earthquake).

Figure 7: Effects of the 1918 Tsunami on Aguadilla Shoreline, La Ñamera Sector (Biblioteca Nacional de Puerto Rico, 1918).

The Puerto Rico Seismic Network (PRSN) has led the development of a comprehensive analysis of the possible impact of tsunamis on the coasts of Puerto Rico. Together with the local and state emergency management agencies it also has prepared evacuation zones maps for all the 46 municipalities of Puerto Rico at risk from tsunamis inundation and made them available in pdf format and digital format on their web page, as depicted in Figure 8 by the yellow areas.

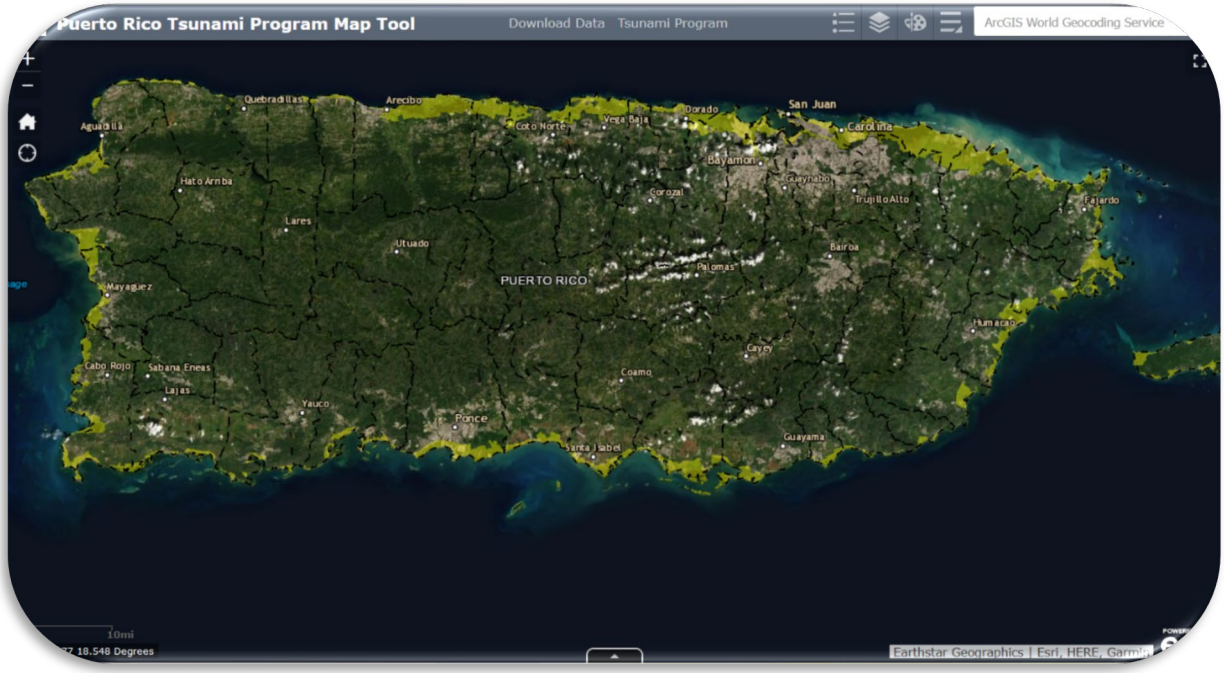

Figure 8: Puerto Rico Tsunami Program Map Tool, Evacuation Maps (PRSN, n.d. a, b and c).

According to Disdier-Flores and Cruz-Soto (2019), for the year 2016 there were more than 2,200 public and private schools in Puerto Rico, with a students and teacher population of around 600,000. Considering that schools should be treated as essential facilities, their exposed population, and that many are also used as shelters and voting centers (with a different and potentially larger exposed population), and the given tsunami hazard in PR, the objective of this research project was to evaluate the vulnerability of coastal schools of PR to this type of event. The main purpose has been to provide useful information that could contribute to the decision-making process of school's rehabilitation, both in assigning priorities (assessing more vulnerable schools) and in determining rehabilitation requirements (i.e., need of vertical evacuation due to excessive horizontal evacuation time, and/or evacuation routes improvements due to their poor condition). Reliable data that support planning contribute to safer and more resilient communities.

METHODOLOGY

This section presents a summary of the stages of the study that can be summarized as: (a) data gathering, (b) school's tsunami hazard identification, (c) case studies selection for detailed evaluation, (d) vulnerability analysis selection, selection and development of tools, (e) vulnerability assessment of case studies, (f) vulnerability assessment of other critical cases, and (g) analysis of results. After that, the summary and conclusions, and the recommendations for further studies are presented.

Data Gathering

The first stage consisted in obtaining the following data for public and private schools of Puerto Rico: (1) geolocation, (2) population, (3) usage as an emergency shelter, (4) usage as a voting center. Also obtained was the tsunami evacuation zone for the 46 at risk coastal municipalities.

The following sources were consulting: (a) the *Homeland Infrastructure Foundation-Level Data -HIFLD* (U.S. Department of Homeland Security, 2020), (b) *Profiles of USA Public Schools* (Public School Review, n.d.), (c) "Busca tu Escuela - 2018-2019" ("Departamento de Educación de Puerto Rico", 2019a), (d) "Plan Operacional para Emergencias e Incidentes Catastróficos 2018-2019" ("Departamento de Educación de Puerto Rico", 2019b), (e) "Centros de Votación" ("Comisión Estatal de Elecciones de Puerto Rico", 2020), (f) "Anuario Estadístico del Sistema Educativo" ("Instituto de Estadísticas de Puerto Rico", n.d.), (g) *Puerto Rico Tsunami Evacuation Maps and Puerto Rico Tsunami Program Map Tool* (Puerto Rico Seismic Network, n.d. b, c and d).

School's Tsunami Hazard Identification

The geolocation of schools obtained from the Homeland Infrastructure Foundation-Level Data -HIFLD for public schools (U.S. Department of Homeland Security, 2020) and the tsunami evacuation zone obtained from the Puerto Rico Tsunami Program Map Tool (Puerto Rico Seismic Network, n.d. b, c and d) were inserted as GIS layers in ArcGIS Online (Esri, n.d. a and b), as presented in Figure 9. With the two sets of data, every one of the 46 coastal municipalities at risk were evaluated to identify the schools in the tsunami evacuation zone (see Figure 10 for an example of San Juan municipality). **Note: for the purpose of this study, the tsunami evacuation zone was considered as equivalent to the tsunami hazard zone**.

After identifying each school in the tsunami evacuation zones, the information regarding the school population, and its usage as an emergency shelter and a voting center was obtained, from the references presented in the previous section. Table 1 presents the results for each coastal municipality, indicating the number of schools that are located in the tsunami evacuation zone and their total population (students, teachers and administrative and support staff) as well as the number of those schools that are also used as shelters and voting centers. The table highlights the municipalities with schools in the tsunami hazard zone (THZ) and distinguish between those municipalities with lower number of schools in the THZ (one to three) and those with a higher number of schools in the THZ (four or more), as a visual aid to identify municipalities that have more schools vulnerable to tsunamis.

It is important to point out that the first cycle of this research (August 2020-July 2021) focused only on public schools, since the geolocation of private schools was not available in any of the sources consulted. This article presents the findings of this first cycle. A second cycle of the research is currently under development (August 2021-present), and its objectives are briefly summarized in the Further Studies Section (at the end of the article). During this second cycle, the private schools placed in the tsunami evacuation zones were identified, locating each school manually (due to the lack of information in their geolocation). It was decided to also present these results in Table 1, to provide the reader with a more comprehensive view of tsunami hazards in the schools of Puerto Rico. But the remaining of the sections focus primarily on public schools.

Figure 9: ArcGIS Data Processing with Public Schools Locations and Tsunami Evacuation Zones.

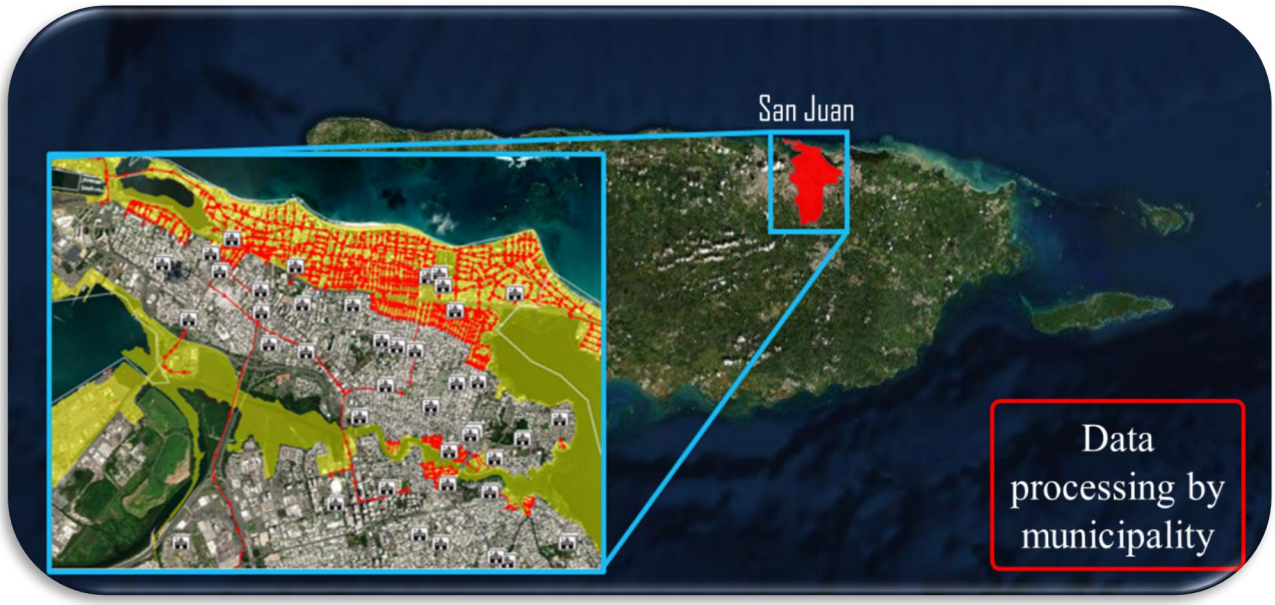

Figure 10: Example of Identification of Schools in the Tsunami Evacuation Zone in San Juan Municipality.

From the processed data it was determined that there are 74 public schools in the tsunami evacuation zone, located in 25 coastal municipalities (21 of the coastal municipalities do not have public schools in the hazard zone), and with a school population that may be affected by tsunami events of about 20,900; 34 of these schools are also used as voting centers, and nine are used as shelters.

It was also determined that there are 35 private schools in the tsunami evacuation zone, distributed among 12 coastal municipalities (34 of the coastal municipalities do not have private schools in the hazard zone), and with a school population that may be affected by tsunami events of about 6,600. Four of these schools are also used as voting centers, and none is used as shelter.

There is a total of 109 schools (public and private) in the tsunami evacuation zone. They located in 25 coastal municipalities, with a school population that may be affected by tsunami events of about 27,500; 38 of these schools are also used as voting centers, and nine are used as shelters.

Table 1: Summary of Schools in Tsunami Evacuation Zones.

Municipality	Public Schools				Private Schools				Public + Private Schools			
	Schools in Tsunami Hazard Zone	Voting Centers	Shelters	Population	Schools in Tsunami Hazard Zone	Voting Centers	Shelters	Population	Schools in Tsunami Hazard Zone	Voting Centers	Shelters	Population
Aguada	3	1	0	1,457	2	0	0	Unknown	5	1	0	1,457
Aguadilla	3	1	0	519	1	0	0	150	4	1	0	669
Añasco	1	0	0	0	0	0	0	0	1	0	0	0
Arecibo	1	0	0	97	3	0	0	110	4	0	0	207
Arroyo	0	0	0	0	0	0	0	0	0	0	0	0
Barceloneta	0	0	0	0	0	0	0	0	0	0	0	0
Bayamón	0	0	0	0	0	0	0	0	0	0	0	0
Cabo Rojo	3	1	0	931	0	0	0	0	3	1	0	931
Camuy	1	1	0	0	0	0	0	0	1	1	0	0
Canóvanas	0	0	0	0	0	0	0	0	0	0	0	0
Carolina	2	0	0	0	3	0	0	646	5	0	0	646
Cataño	4	2	0	1,465	1	0	0	0	5	2	0	1,465
Ceiba	0	0	0	0	0	0	0	0	0	0	0	0
Culebra	1	1	1	190	0	0	0	0	1	1	1	190
Dorado	1	0	1	937	1	1	0	668	2	1	1	1,605
Fajardo	0	0	0	0	0	0	0	0	0	0	0	0
Guánica	0	0	0	0	0	0	0	0	0	0	0	0
Guayama	1	0	0	115	0	0	0	0	1	0	0	115
Guayanilla	0	0	0	0	0	0	0	0	0	0	0	0
Guaynabo	0	0	0	0	0	0	0	0	0	0	0	0
Hatillo	1	0	0	0	0	0	0	0	1	0	0	0
Humacao	1	1	0	386	0	0	0	0	1	1	0	386
Isabela	0	0	0	0	0	0	0	0	0	0	0	0
Juana Díaz	2	1	0	529	0	0	0	0	2	1	0	529
Lajas	1	0	0	108	0	0	0	0	1	0	0	108
Loíza	8	4	3	2,401	2	1	0	394	10	5	3	2,795
Luquillo	3	1	0	596	0	0	0	0	3	1	0	596
Manatí	0	0	0	0	0	0	0	0	0	0	0	0
Maunabo	0	0	0	0	0	0	0	0	0	0	0	0
Mayagüez	9	5	1	3,247	0	0	0	0	9	5	1	3,247
Naguabo	0	0	0	0	0	0	0	0	0	0	0	0
Patillas	0	0	0	0	0	0	0	0	0	0	0	0
Peñuelas	1	0	0	245	0	0	0	0	1	0	0	245
Ponce	4	2	0	1,577	2	0	0	108	6	2	0	1,685
Quebradillas	0	0	0	0	0	0	0	0	0	0	0	0
Rincón	1	0	0	183	1	0	0	166	2	0	0	349
Río Grande	0	0	0	0	0	0	0	0	0	0	0	0
Salinas	4	3	0	541	0	0	0	0	4	3	0	541
San Juan	9	5	0	2,083	**7**	**1**	**0**	**2350**	16	6	0	4,433
Santa Isabel	1	1	1	486	1	0	0	Unknown	2	1	1	486
Toa Baja	8	4	2	2,802	**11**	**1**	**0**	**1987**	19	5	2	4,789
Vega Alta	0	0	0	0	0	0	0	0	0	0	0	0
Vega Baja	0	0	0	0	0	0	0	0	0	0	0	0
Vieques	0	0	0	0	0	0	0	0	0	0	0	0
Yabucoa	0	0	0	0	0	0	0	0	0	0	0	0
Yauco	0	0	0	0	0	0	0	0	0	0	0	0
Total	**74**	**34**	**9**	**20,895**	**35**	**4**	**0**	**6,579**	**109**	**38**	**9**	**27,474**

Municipalities with no schools in tsunami hazard zone

Municipalities with 1 to 3 schools in a tsunami hazard zone

Municipalities with 4 to more schools in a tsunami hazard zone

Total results

Case Studies Selection

Two municipalities were selected as case studies for a more detailed analysis on schools' vulnerabilities to tsunami events. The criteria for selection were that the municipalities have a relatively large number of schools in the THZ, that the schools have multiple uses (also used as voting centers and/or shelters), and that they are close to the San Juan Metropolitan Area (SJMA), so a visual inspection of evacuation routes could be performed. Cataño and San Juan municipalities were selected. Table 2 summarizes the school tsunami hazard found in the previous stage for both municipalities.

Table 2: Summary of School Tsunami Hazard for the Selected Case Studies.

	Cataño	San Juan	Totals
Schools in THZ	4	9	13
Student Population	1367	1920	3287
Teacher Population	98	163	261
Total Population	1465	2083	3548
Voting Centers	2	5	7
Shelters	0	0	0

Vulnerability Analysis Selection, Tools Adoption and Development

The ***required time to evacuate*** from the school's internal assembly area to a safe place was adopted as the primary factor to assess school vulnerability to tsunami events. Two analyses were performed: (1) the required time to evacuate from the internal assembly area to the point of exit of the tsunami evacuation zone, and (2) the required time to evacuate from the internal assembly area to the external assembly point.

To obtain this time, the procedures proposed in the USGS publication "*The pedestrian evacuation analyst: Geographic information systems software for modeling hazard evacuation potential*" (Jones, Ng, and Wood, 2014) were adopted. They propose four walking speed values, in mph, according to the walking type: (a) 2.46 mph for slow walk, (b) 2.70 mph for moderate walk, (c) 3.40 mph for fast walk, and (d) 2.50 mph for average walk.

The analysis consisted in: (a) Identifying the internal assembly area and the external assembly point. (b) Identifying possible evacuation routes. The shortest route was identified, and between two (2) to four (4) alternate routes were also evaluated, to see the impact of possible after earthquake obstructions to the shortest route. (c) Plotting each route and computing the required evacuation time according to the travel distance to the tsunami evacuation zone exit point and to the external assembly point. The ***Route Planner for walking, running, cycling*** provided by ***Ploaroute.com*** (n.d.) was used to trace the routes and compute the times. Figure 11 presents an example of the use of this web app.

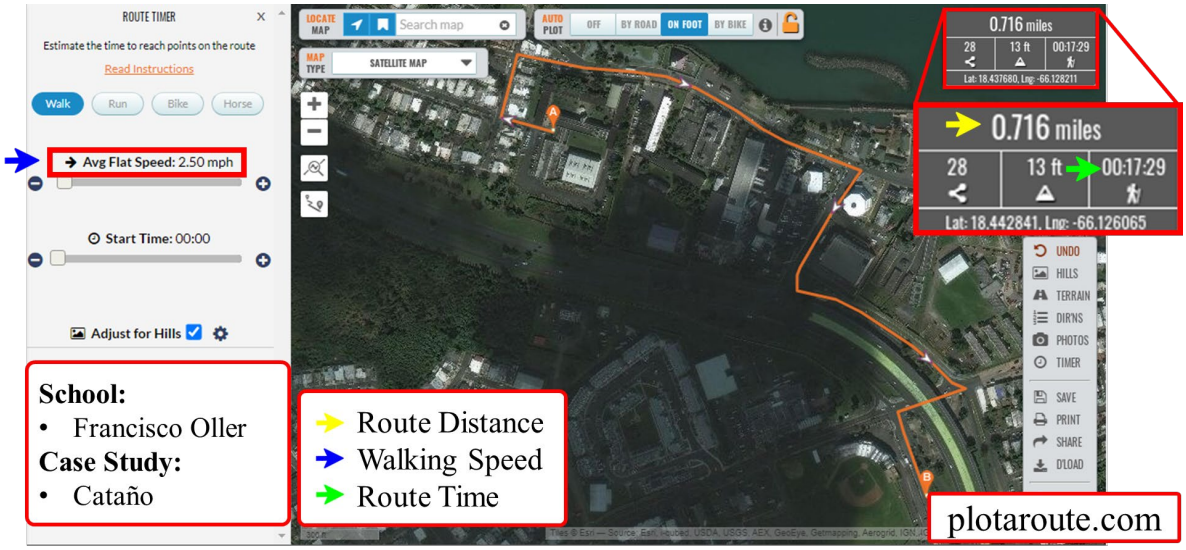

Figure 11: Example of Plotaroute Web App Usage for Francisco Oller School in Cataño.

The ***evacuation route condition*** was used as a complementary factor to assess school vulnerability to tsunami events. This analysis evaluated: (a) the percentage of the trace of the route that runs parallel to the shoreline, thus not moving away from the danger, (b) the presence of obstacles, discontinuities, or reduced effective width of the walkway, (c) the existence of evacuation signs along the route, (d) if the route passes near facilities that may represent, in the case of collapse, possible after earthquake obstacles that could force a change in evacuation route (i.e., electric lines and bridges), thus increasing the required evacuation time.

This analysis was originally envisioned to be carried out through field visits and visual inspections. But due to limitations in mobility and accessibility imposed by the COVID pandemic, a virtual tour using ***Google Earth Pro*** and its ***Street View*** capabilities was performed.

The ***school evacuation plans and evacuation drills*** were also considered as a complementary factor to assess school vulnerability to tsunami events. For that purpose, a detailed ***survey*** was developed in ***Google Forms***, that request information on: (a) municipality, (b) type of instruction (primary, secondary, high school), (c) building year of construction, (d) trainings on tsunamis received by school personnel, (e) tsunami evacuation plan, (f) drills practice, (g) evacuation time from the classrooms to internal assembly place, (h) external assembly point, (i) evacuation time from the internal assembly place to the external assembly point, (j) vertical evacuation plans, (k) vertical evacuation place, (l) evacuation time from the internal assembly place to the vertical evacuation place. The response was completely anonymous. The form was sent to all the schools of the case studies. The form can be accessed in: https://docs.google.com/forms/d/e/1FAIpQLSfoeD_VJwr3IGc2wfU0H3XBIrqrgc0qDLXfbIaX8Q0haDhGxQ/viewform

Vulnerability Assessment of Case Studies – Evacuation Time

The analysis was performed on the shortest evacuation route for each school, using the four (4) walking speeds of Jones, Ng, and Wood (2014). The results for Cataño public schools are presented first. Figure 12 summarizes the evacuation time, in minutes, from the internal assembly place to the point of exiting the tsunami hazard zone. Considering the average walking speed of 2.50 mph, the evacuation times range from 6 to 16 minutes, being Francisco Oller the school that requires the longest evacuation time.

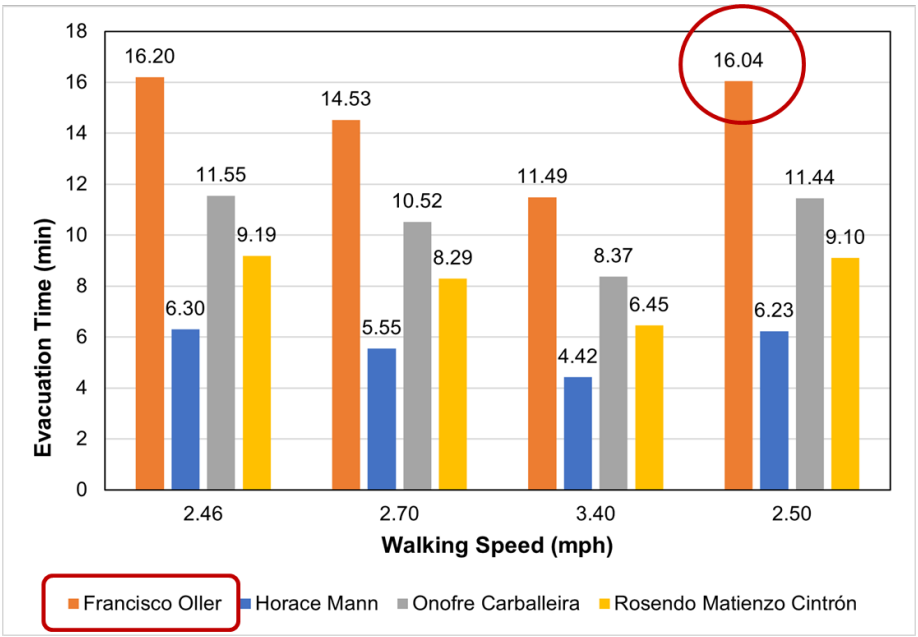

Figure 12: Evacuation time until exiting the tsunami evacuation zone for Cataño Public Schools.

Figure 13 summarizes the evacuation time, in minutes, from the internal assembly place to the external assembly point. Considering the average walking speed of 2.50 mph, the evacuation times range from 7 to 17 minutes, being Francisco Oller the school that requires the longest evacuation time. The external assembly point is close to the point where the THZ is left, so the increase in evacuation time from the previous analysis to this one is about one minute.

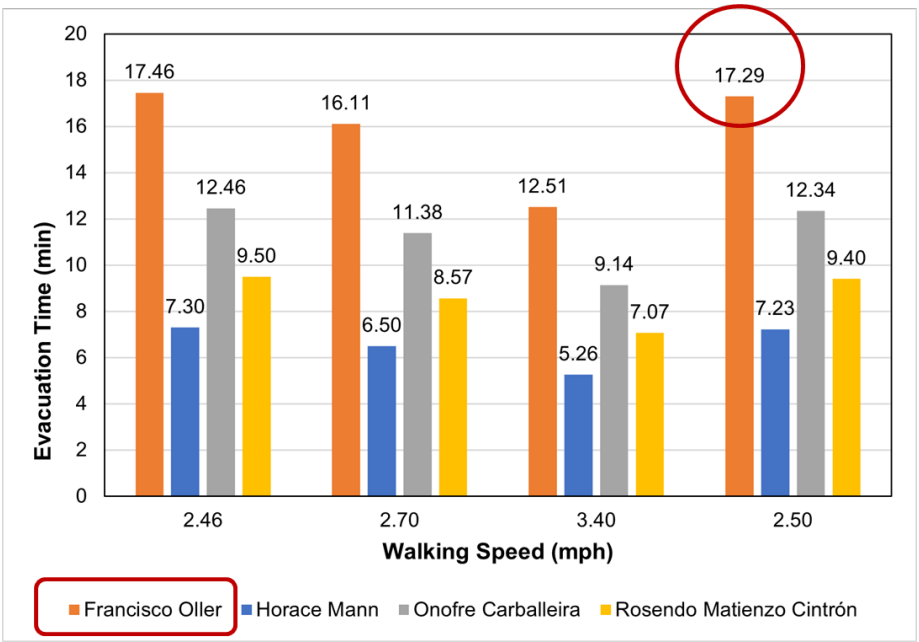

Figure 13: Evacuation time until reaching the external assembly point for Cataño Public Schools.

Second, the results for San Juan public schools are presented. Figure 14 summarizes the evacuation time, in minutes, from the internal assembly place to the point of exiting the tsunami hazard zone. Considering the average walking speed of 2.50 mph, the evacuation times range from 1 to 26 minutes, being Luis Llorens Torres the school that requires the longest evacuation time.

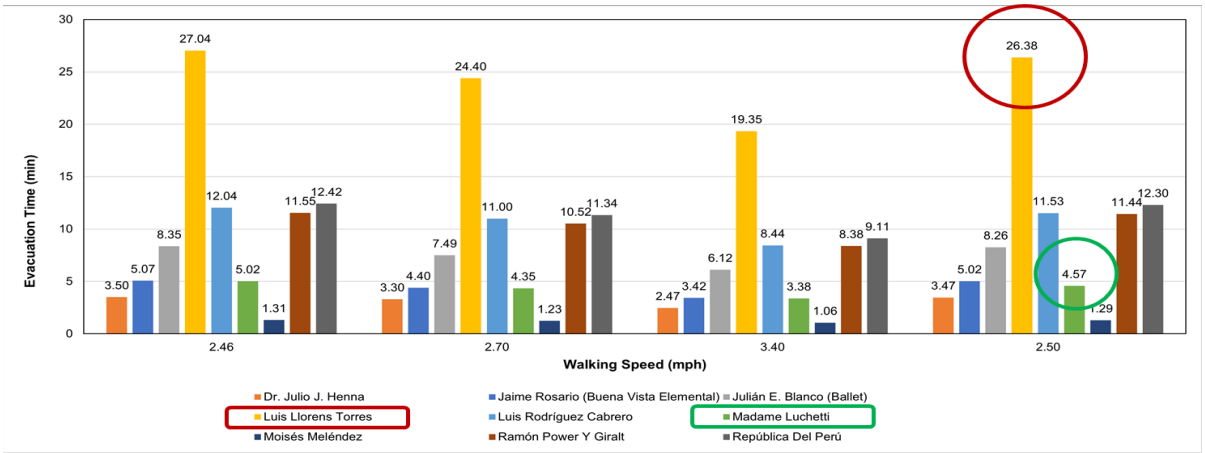

Figure 14: Evacuation time until exiting the tsunami evacuation zone for San Juan Public Schools.

Figure 15 summarizes the evacuation time, in minutes, from the internal assembly place to the external assembly point. Considering the average walking speed of 2.50 mph, the evacuation times range from 9 to 49 minutes, being Madame Luchetti the school that requires the longest evacuation time. The external assembly point is not close to the point where the THZ is left for most of the schools, so the increase in evacuation time from the previous analysis to this one ranges from 7 minutes to 45 minutes.

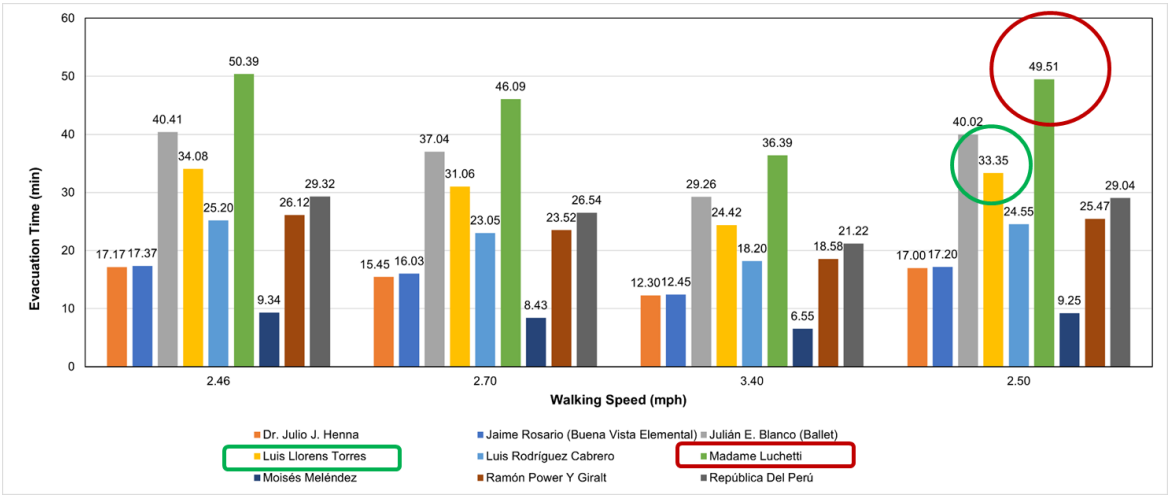

Figure 15: Evacuation time until reaching the external assembly point for San Juan Public Schools.

Finally, Table 3 presents, for both municipalities, a comparison between the evacuation time required until reaching the external assembly point following the shortest route, and the time required following alternate routes, using the time format (hh:mm:ss). Two to four alternative routes were evaluated for each school. There was always an increase in the evacuation time required by the alternate routes, increase that ranged between 1 minute to 33 minutes.

Table 3: Comparison of Required Evacuation Time until Reaching the External Assembly Point between the Shortest Route and Alternate Routes.

Municipality	School	Minimum Evacuation Route	Alternate Evacuation Routes				Difference between times			
			1	2	3	4	1	2	3	4
Cataño	Francisco Oller	00:17:29	00:19:35	00:35:22			00:02:06	00:17:53		
	Horace Mann	00:07:23	00:09:03	00:08:17			00:01:40	00:00:54		
	Onofre Carballeira	00:12:34	00:15:33	00:35:59			00:02:59	00:23:25		
	Rosendo Matienzo Cintrón	00:09:40	00:10:13	00:11:01	00:41:33		00:00:33	00:01:21	00:31:53	
San Juan	Dr. Julio J. Henna	00:17:00	00:18:23	00:18:33	00:49:57		00:01:23	00:01:33	00:32:57	
	Jaime Rosario	00:17:02	00:17:43	00:23:31	00:42:28		00:00:41	00:06:29	00:25:26	
	Julián E. Blanco	00:40:02	00:40:36	00:42:45			00:00:34	00:02:43		
	Luis Llorens Torres	00:33:35	00:37:58	00:37:00	01:06:34		00:04:23	00:03:25	00:32:59	
	Luis Rodríguez Cabrero	00:24:55	00:29:41	00:27:14	00:57:24		00:04:46	00:02:19	00:32:29	
	Madame Luchetti	00:49:51	00:55:46	00:56:21	01:14:12		00:05:55	00:06:30	00:24:21	
	Moisés Meléndez	00:09:25	00:10:25	00:11:03	00:29:02	00:33:12	00:01:00	00:01:38	00:19:37	00:23:47
	Ramón Power Y Giralt	00:25:47	00:30:31	00:26:53			00:04:44	00:01:06		
	República Del Perú	00:29:04	00:31:38	00:30:05			00:02:34	00:01:01		

Vulnerability Assessment of Case Studies – Route Condition

In each municipality of the case studies, the school that requires the longest time until exiting the tsunami evacuation zone was selected to perform a virtual tour exploring the conditions of the walkway and the alignment. The analysis was conducted on the shortest evacuation route. The principal findings can be summarized as follows:

Francisco Oller School in Cataño – Shortest evacuation route:

- The route has a distance of 0.656 miles to leave the tsunami hazard zone and 0.716 miles to get to the external assembly point, “Estadio Peruchin Cepeda”. There were two signs indicating the evacuation route along this route.
- It takes 16 minutes and 4 seconds to exit the tsunami hazard zone, and 17 minutes and 29 seconds to reach the external assembly site, considering an average walking speed of 2.50 mph.
- Travels approximately 0.300 miles parallel to the shoreline, representing a 46% of the 0.656 miles required to leave the tsunami hazard area. The layout of the route does not allow to move quickly away from the coast.
- Segments of the sidewalks presented unfitted conditions (Figure 16):
    - Has discontinuities of the walkway, and segments with reduced total width (in one segment, 28 in were measured; far less than the 36 in effective width required by ADA).
    - Has abundant presence of obstacles, such as urban furniture and cars that produce a reduction of the effective width.
    - There were damages to the walking surface, such as deterioration and cracks.
- Passes near power lines, and under a bridge located on the PR-165, that represent possible obstructions to the passage of pedestrians in case they collapse from the movement of the earthquake prior to the tsunami (Figure 17). This situation my force a change in the evacuation route.
- There could be conflicts with vehicular traffic, since the route moves along principal arteries of the zone.

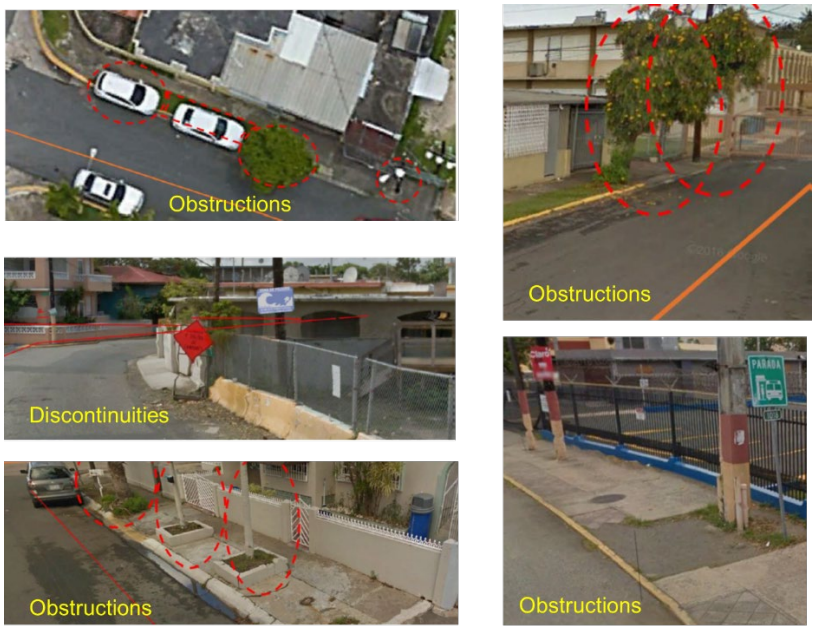

Figure 16: Obstruction, Reduced Effective Width, and Discontinuities on the Sidewalk for Francisco Oller Evacuation Route.

Figure 17: Obstruction on the Sidewalk and Potential After Earthquake Hazards for Francisco Oller Evacuation Route.

Luis Llorens Torres School in San Juan:

- The route has a distance of 1.074 miles to leave the tsunami hazard zone and 1.317 miles to get to the external assembly point, “Plaza Barceló”. This route only has a sign indicating that it is the tsunami evacuation route.
- It takes 26 minutes and 38 seconds to get out of the hazard zone, and 33 minutes and 35 seconds to get to the external assembly point for a walking speed of 2.50 mph.
- Travels 0.486 miles parallel to the shoreline, representing 45% of the 1,074 miles required to exit the tsunami hazard zone. The layout of the route does not allow to move quickly away from the coast.
- Segments of the sidewalks presented unfitted conditions (Figure 18):
    - Has discontinuities of the walkway, and segments with reduced total width (in one segment, 12 in were measured; far less than the 36 in effective width required by ADA).
    - Has profuse presence of obstacles, such as urban furniture and cars,that produce a reduction of the effective width.
    - There were damages to the walking surface, such as deterioration and cracks.
- Passes near power lines, and under a bridge located on the Pellín Rodríguez Street, that represent possible obstructions to the passage of pedestrians in case they collapse from the movement of the earthquake prior to the tsunami (Figure 19). This situation may force a change in the evacuation route.
- There could be conflicts with vehicular traffic, since the route moves along principal arteries of the zone.

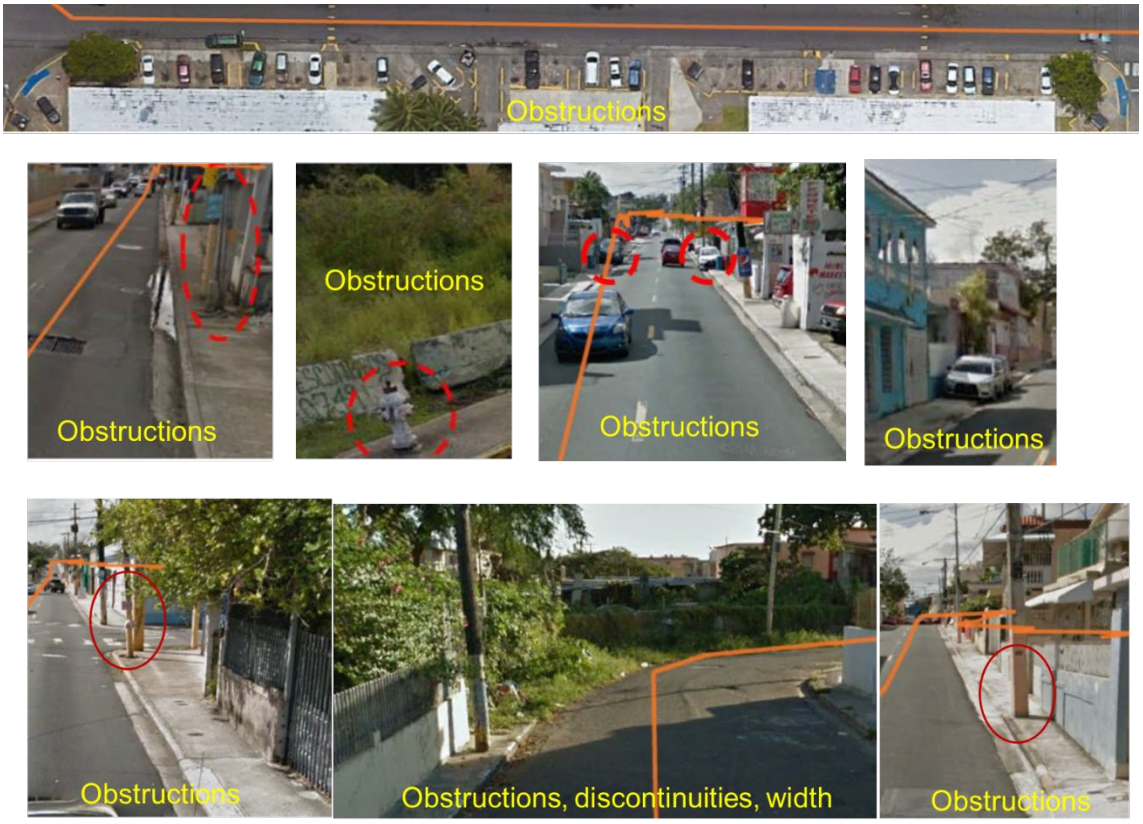

Figure 18: Obstruction, Reduced Effective Width, and Discontinuities on the Sidewalk for Luis Llorens Torres Evacuation Route.

Figure 19: Obstruction on the Sidewalk and Potential After Earthquake Hazards for Luis Llorens Torres Evacuation Route.

Vulnerability Assessment of Case Studies – School Survey

Two schools responded to the survey (a primary school in Cataño and a high school in San Juan. The information obtained is summarized as follows:

- Both schools were built before 1987 (therefore, considered pre code in terms of seismic details).
- Both schools have tsunami evacuation plans, and know their external assembly point (Parque Perucho Cepeda for the school in Cataño, and Plaza Barcelo Santurce for the school in San Juan).
- One school reported that during the drills the emergency siren to evacuate in case of tsunami events was not audible from the school.
- Both schools have conducted evacuations drills once a year or once every two years.
- Both schools reported evacuation times for the drills:
    - Cataño school: three minutes to evacuate from the classroom to the school internal assembly place, and eight minutes to evacuate from the school internal assembly place to the external assembly point.
    - San Juan school: one hour to evacuate from the classroom to the school internal assembly place, and one (hour to evacuate from the school internal assembly place to the external assembly point.
- One school reported that they have vertical evacuation plans, using the same school building as a shelter. Both schools reported vertical evacuation times.

Vulnerability Assessment of other Critical Cases - Evacuation Time

Two additional cases were analyzed, one in Loiza and one in Toa Baja, since the evacuation conditions of these municipalities were considered critical, and the computations confirm that assumption.

For the Mediania Alta public school in Loiza, considering the average walking speed of 2.50 mph, the evacuation time required to move from the internal assembly place until leaving the tsunami evacuation zone is one hour and 29 minutes (89 minutes), as presented in **Figure 20**.

Table 4 presents the total evacuation distance and summarizes the different evacuation times for this school. It is important to note that the evacuation route is along PR-187 Highway, the principal artery of the area. This may imply an increase in the pedestrian evacuation time due to interactions with vehicular traffic.

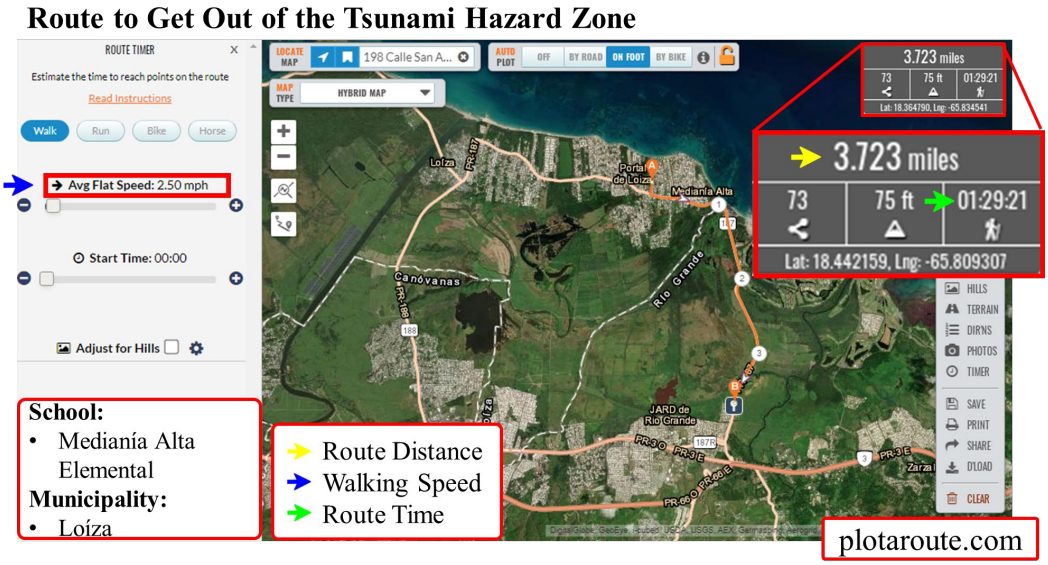

Figure 20: Plotaroute Web App Usage for Mediania Alta Public School in Loiza.

Table 4: Evacuation Times Summary for Mediania Alta Public School in Loiza.

Walking Speed USGS (mph)	Evacuation Time - PlotARoute (hr:min:sec)	
	Route to Get to the Assembly Place	Route to Get Out of the Tsunami Hazard Zone
2.46	2:00:44	01:30:48
2.70	1:50:00	01:22:44
3.40	1:27:21	01:05:42
2.50	1:58:48	01:29:21
Distance (miles)	4.950	3.723

For the Academia Espíritu Santo private school in Toa Baja, considering the average walking speed of 2.50 mph, the evacuation time required to move from the internal assembly place until leaving the tsunami evacuation zone is almost 51 minutes, as presented in **Error! Not a valid bookmark self-reference.**. Table 5 presents the total evacuation distance and summarizes the different evacuation time for this school. It is important to note that the evacuation route is along the PR-165 and PR-866 Highways, two of the principal arteries of the area, situation that may imply increase in the pedestrian evacuation time due to interactions with vehicular traffic.

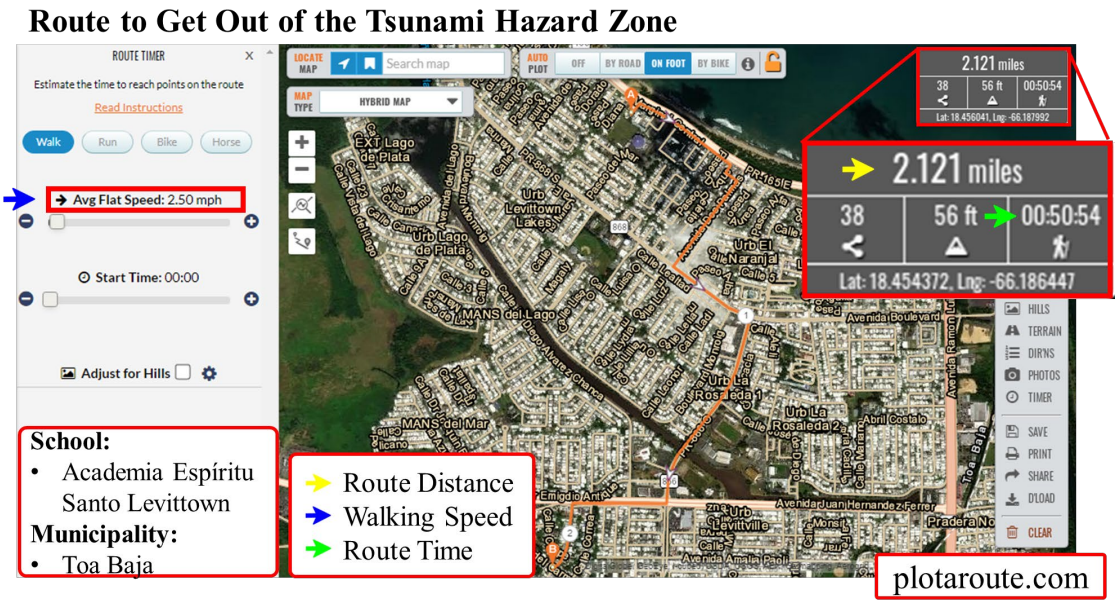

Figure 21: Plotaroute Web App Usage for Academia Espíritu Santo Private School in Toa Baja.

Table 5: Evacuation Times Summary for Academia Espíritu Santo Private School in Toa Baja.

Walking Speed USGS (mph)	Evacuation Time - PlotARoute (hr:min:sec)	
	Route to Get to the Assembly Place	Route to Get Out of the Tsunami Hazard Zone
2.46	01:04:34	00:51:37
2.70	00:58:49	00:47:02
3.40	00:46:43	00:37:21
2.50	01:03:45	00:50:54
Distance (miles)	2.656	2.121

Results Analysis

From the ***tsunami hazard identification stage***, one can consider the total number of schools in the THZ, the population of the schools, and their usage as shelters and voting centers as the parameters to differentiate between municipalities. Using this information one can identify that there are seven municipalities that may be considered critical for tsunami related rehabilitation of public schools, as presented in **Error! Reference source not found.**. The schools in these municipalities represent almost 70% of these parameters, considering the total number of public schools in the THZ. Of those seven municipalities, four are considered the most critical due to the number of schools in the THZ: Loiza, Mayagüez, San Juan and Toa Baja.

Table 6: Critical Municipalities Considering the Number of Public Schools in the THZ.

	Public Schools			
Municipality	**Schools in Tsunami Hazard Zone**	**Voting Center**	**Shelter**	**Population**
Cataño	4	2	0	1,465
Loíza	8	4	3	2,401
Mayagüez	9	5	1	3,247
Ponce	4	2	0	1,577
Salinas	4	3	0	541
San Juan	9	5	0	2,083
Toa Baja	8	4	2	2,802
Total	**46**	**25**	**6**	**14,116**
	62%	74%	67%	68%

If public and private schools are considered in the analysis, the critical municipalities increase to eleven, as presented in Table 7. These municipalities represent almost 80% of the previously mentioned parameters, considering the total number of public and private schools in the THZ. Of those eleven municipalities, the same four continue to be considered the most critical due to the number of schools in the THZ: Loiza, Mayagüez, San Juan and Toa Baja.

Table 7: Critical Municipalities Considering the Number of Public and Private Schools in the THZ.

	Public + Private Schools			
Municipality	**Schools in Tsunami Hazard Zone**	**Voting Center**	**Shelter**	**Population**
Aguada	5	1	0	1,479
Aguadilla	4	1	0	669
Arecibo	4	0	0	207
Carolina	5	0	0	646
Cataño	5	2	0	1,465
Loíza	10	5	3	2,795
Mayagüez	9	5	1	3,247

Ponce	6	2	0	1,685
Salinas	4	3	0	541
San Juan	16	6	0	4,433
Toa Baja	19	5	2	4,789
Total	**87**	**30**	**6**	**21,956**
	80%	79%	67%	80%

The ***evacuation time analysis*** results show one clear critical public school for each municipality: (a) School Francisco Oller in Cataño, with an evacuation time until exiting the THZ of 16.04 minutes considering an average walking speed of 2.50 mph. (b) School Luis Llorens Torres in San Juan, with an evacuation time until exiting the THZ of 26.38 minutes considering an average walking speed of 2.50 mph. Both evacuation times could result excessive in case of a local (near source generated) tsunami, that can arrive within 20 minutes (Christa von Hillebrandt, pers. communication, 2022), such as the case of the PR 1918 earthquake and tsunami, where tsunami inundation occurred within five and six minutes after the earthquake. Thus, vertical evacuation should be considered as an alternative evacuation strategy

For the public schools in Cataño, the difference in evacuation time until leaving the THN and until reaching the external assembly point do not differ significantly (about one minute for all the schools), but for the schools in San Juan the difference was substantial (ranging from seven minutes to 45 minutes for the different schools), due to the location of the external assembly point with respect to the schools' locations, and to the boundaries of the tsunami evacuation zones. For these cases, evaluating alternative assembly points could be advisable.

The critical school in San Juan has a significantly higher evacuation time until leaving the THZ than Cataño, but the average evacuation time is similar (9.4 minutes in San Juan vs 10.7 minutes in Cataño). The critical school in San Juan has a significantly higher evacuation time until reaching the external assembly point than Cataño, and also the average time is significantly higher (27.3 minutes in San Juan vs 11.6 minutes in Cataño).

If alternate routes have to be used (i.e., in the event of blockages due to the collapse of electrical infrastructure), the total evacuation time could be increased from about one minute to up to 32 minutes. This could lead to extremely excessive evacuation times.

Regarding the ***routes conditions analysis*** performed by virtual inspection tours, both routes presented similar situations. There is a significant length of the evacuation path that runs parallel to the shoreline (45% or more), thus the evacuation process does not move away quickly from the danger. Also, the conditions of the walkways are deficient in several segments due to the presence of obstacles, reduced effective width, discontinuities, and damages. Both shortest routes presented few tsunami evacuation route signs (Cataño two, and San Juan one).

The ***evacuation time analysis of other critical cases*** showed that Loiza and Toa Baja have significant more critical schools than Cataño and San Juan. The Mediania Alta public school in Loiza required 89 minutes to move from the internal assembly place until leaving the THZ (considering the average walking speed of 2.50 mph); this is 3.4 times the time required for the critical school in San Juan, and 5.5 times the time required for the critical school in Cataño. Academia Espíritu Santo private school in Toa Baja required almost 51 minutes to move from the internal assembly place until leaving the THZ (considering the average walking speed of 2.50 mph); this is almost 2 times the time required for the critical school in San Juan, and more than 3 times the time required for the critical school in Cataño.

The ***school survey*** was answered by only two schools, and the most relevant observations on their responses are:

- Both schools were built before 1987, situation that suggest special evaluation is required when assessing their seismic rehabilitation.
- Both schools have a tsunami evacuation plans and had correctly identified the external assembly point.
- The response that the tsunami evacuation siren was not audible in one school may suggest that the alarm system could require either maintenance, repair, or improvements.
- The discrepancies between the evacuation times from the classroom to the internal assembly place between both schools, and between having both horizontal and vertical evacuations may suggest that some questions were not adequately interpreted, and strongly suggest that the questionnaire should be reevaluated, and/or other strategies to collect and verify this critical data should be devised.

SUMMARY, CONCLUSIONS AND RECOMMENDATIONS

The study has assessed for all the 46 Puerto Rico coastal municipalities at risk from tsunamis: (a) the public and private schools in tsunami hazard (evacuation) zones, (b) their usage as voting centers, (c) their usage as shelters, and (d) the student and faculty population potentially affected. Critical municipalities in terms of quantity of schools, school population, and multiple usages of the school building have also been determined. These critical municipalities could serve as a basis in the planning process to prioritize school rehabilitation studies.

The study has assessed for all the four public schools that are in the THZ in Cataño, and all the nine public schools that are in the THZ in San Juan the time required to evacuate from the school internal assembly place until the point of exiting the tsunami hazard zone, and from the school internal assembly place until reaching the external assembly point. For each analysis, the four different walking speeds suggested by Jones et al (2014) were used. For each school, the shortest evacuation route and between two to four alternate routes were evaluated. The times to evacuate two additional schools, one in Loiza and one in Toa Baja, were also evaluated.

Schools with the longest times to leave the tsunami hazard zone are considered critical and more vulnerable to a tsunami event. These evacuation times may be used as one of the planning and decision-making criteria to prioritize rehabilitation funds, and also to evaluate the need for vertical evacuation. The total evacuation time until reaching external assembly point may mislead the assessment of critical schools, since reaching the external assembly point may imply a long walk outside the tsunami evacuation zones. Thus, it is recommended to use the evacuation time until exiting the tsunami evacuation zone for planning and decision-making analysis.

Critical schools in San Juan are more vulnerable than critical schools in Cataño. Although there are other municipalities with more vulnerable conditions, such as the cases presented for Loiza and Toa Baja.

Even though the results of the survey forms provided some useful information, such as that the schools have tsunami evacuation plans, validation of the external assembly points, showed that both schools were pre-code (1987), and participation in evacuation drills, two responses are considered not significant. Also, the reported evacuation times from drills, a critical information for this research, showed inconsistencies. It is recommended to perform one to one interview processes, to foster participation, clarify any doubt, validate the responses, and establish cooperative relationships with school administration.

The characteristics of the shortest evacuation route evaluated using Google Earth Pro for the two most critical schools showed that they may not be suitable for transit during the evacuation process due to the presence of obstacles, insufficient walkway width, pathway discontinuities, presence of potential after earthquake hazards, and routes layout parallel to the shoreline. An improvement of pedestrian facilities used

as evacuation routes could be advisable. Also, the improvement of evacuation routes identification should be evaluated, since few signs were found in the shortest evacuation routes.

The use of vehicular roads as evacuation facilities (and its implications) should be considered. This alternative would require the evaluation of vehicular traffic and its possible interaction with pedestrian movement, since many of the evacuation routes move along primary arteries of the zone, with large traffic volumes.

Google Earth Pro in conjunction with ArcGIS and PlotARoute resulted useful tools to perform the evacuation time analysis and the evaluation of the conditions of the characteristics of the schools' evacuation routes.

Regarding the limitations of the study, one can point out that: (a) The school data available was from 2016 (population may have varied; some schools may be closed due to the restructuration plans of the PR Department of Education in the last few years); (b) The geolocation used for public schools was from Homeland Infrastructure Foundation-Level Data (HIFLD), U.S. Department of Homeland Security. (2020); further analysis revealed that in some municipalities (not the case studies) few schools are misplaced in the dataset; the total number of schools identified in tsunami hazard zone may have a small variation.

The most significant barrier/problem encountered was the availability and reliability of school data: data were dispersed, data sources were not obvious, some data were not up to date or was not available (i.e., population). This strongly suggest that GIS based, broad and inclusive, centralized, accessible, and validated information is essential to support data-based decision processes, allow what-if analysis, and fosters research on community safety and resilience.

The computed evacuation times, following the guidelines of the USGS publication "*The pedestrian evacuation analyst: Geographic information systems software for modeling hazard evacuation potential*" (Jones, Ng, and Wood, 2014) are considered good initial evaluation values, that provide a ***lower bound estimate*** of the total evacuation time required, since:

- Other studies showed different (and lower) average evacuation speeds, and propose speeds that vary with age (i.e., UNESCO 2020).
- The computed time consider only one stage of the evacuation process, not the complete evacuation procedure timeline triggered immediately after the earthquake event occurred, i.e., the reaction time and the time required to move from the classroom to the school patio/internal assembly site.
- Different scenarios that consider the effect of change in route due to possible obstacles to the path due to structural failures during earthquake (i.e., electric power lines and bridges) could drastically increase evacuation time.
- The particular conditions of the evacuation route, the volume of pedestrians and its interaction with other generators of high volume of pedestrian traffic, the interaction of pedestrian movement with vehicular traffic (i.e., at intersections), geometric, environmental and human factors, and other characteristics are not explicitly factored in.

These observations lead to the recommendation than further study is necessary to refine the estimate of the total time required to evacuate schools in the event of tsunamis.

The reader can obtain more details of the first cycle of the research accessing the following link, where the full 388 pp report and a poster can be found: http://prcrepository.org:8080/xmlui/handle/20.500.12475/1166

FURTHER STUDY

The findings of the first year of the research lead to define a second, longer, ongoing research process. The research team is composed by a PhD student, an undergraduate student, three PUPR faculty members, and three researchers from Volpe National Transportation Systems Center, as a cooperative agreement between the center and PUPR.

- The focus of the ongoing research is:
- To expand the analysis performed in the first cycle. Private schools hazard analysis has already been developed and presented in this publication.
- Establish an evacuation timeline that considers all the stages of the evacuation process, including the initial time required to drop, cover, and hold when the earthquake is felt, the reaction time afterwards, the movement from the classroom to the school patio, the preparation time in the patio to move to the exterior, and the movement from the school patio to the external assembly point.
- Study all the factors that affect people reaction, pedestrian dynamics, and evacuation processes (i.e., human, environmental, geometric, social, among others).
- Study pedestrian dynamics simulation models, and simulation software.
- Obtain evacuation drills information to calibrate and validate simulation models.

The main objective is to develop a methodology that allows a better estimate of the evacuation time required for schools (and other facilities) in events of tsunamis, thus providing a tool that allows to better decide when vertical evacuation is required, contributing to the development of more safe and resilient communities.

Other factors that could be added in further studies are the evacuation time required by people with disabilities, the effect of flood depths in the area where the schools are located, the training of people on the evacuation routes, and the training they have to act based on the intensity they felt from the earthquake, without waiting for the tsunami alarm to go off (which could take several minutes).

We consider that a comprehensive (holistic) approach to schools' rehabilitation is highly recommended. An approach that: (a) Focus on the safety and the resilience of the community. (b) Is not limited to evaluate one hazard condition, but considers multihazard situations (earthquakes, tsunamis, hurricanes, floods, landslides, liquefaction). (c) Is not limited to the building itself, but considers the evacuation process, the evacuation routes, and people preparedness. We expect that the first cycle and this new stage of the research effectively contribute to have reliable data that contributes to this holistic approach and the safety and resilience of schools.

Finally, is important to mention that, if required, the vertical evacuation and shelters structures should be designed according to the latest recommendations (ATC 2019a and ASCE 2017 procedures). ASCE/SEI 7-16 (ASCE 2017) does not have tsunami design parameters already established for Puerto Rico. This is an area of recommended further study and development that requires serious attention from the research and professional community.

ACKNOWLEDGEMETS

The first cycle of the study was supported by the PUPR Undergraduate Research Program for Honor Students (PUPR URP-HS), part of the Grant Title V STEM Grant "Bridges to STEM Success" of the US Department of Education. Current stage of the research is being supported by PUPR Graduate School Assistantships and Awards Program, and PUPR Promoting Postbaccalaureate Opportunities for Hispanic Americans (PPOHA) Program. Authors would like to thank VOLPE center personnel for their availability and enthusiasm to collaborate. Special thanks to the Puerto Rico Seismic Network, for their excellent work defining the tsunami evacuation zones, and for providing reliable, accessible, geolocated data that could be used in hazard and vulnerability studies.

REFERENCES

American Society of Civil Engineers ASCE, (2017). Minimum design loads and associated criteria for buildings and other structures: ASCE/SEI 7-16.

Applied Technology Council ATC, (2019a). Guidelines for Design of Structures for Vertical Evacuation from Tsunamis: FEMA P-646. FEMA National Earthquake Hazards Reduction Program (U.S.), & NOAA National Tsunami Hazard Mitigation Program (U.S.). https://www.fema.gov/media-library-data/1570817928423 55b4d3ff4789e707be5dadef163f6078/FEMAP646_ThirdEdition_508.pdf

Applied Technology Council ATC, (2019b). Post-disaster Building Safety Evaluation Guidance: FEMA P-2055. Federal Emergency Management Agency. National Oceanic and Atmospheric Administration.https://www.fema.gov/sites/default/files/2020-07/fema_p-2055_post-disaster_buildingsafety_evaluation_2019.pdf

Artisan Global LLC. (n.d.). QuakeFeed App. Retrieved April 18, 2022, from https://www.quakefeed.com/

Bernal, J.; Hughes, K. S.; Morales Velez, A. C.; Pando, M.; Perez, J. C.; Rodriguez, L. A. (2020). "Geotechnical Reconnaissance of the January 7, 2020, M6.4 Southwest Puerto Rico Earthquake and Associated Seismic Sequence", A report of the NSF Sponsored Geotechnical Extreme Event Reconnaissance Association.

Biblioteca Nacional de Puerto Rico (1918), Recopilación de Fotografías del Terremoto y el Maremoto de 1918 en el Puerto Rico Ilustrado, recuperado del Archivo Digital Nacional de Puerto Rico, https://archivonacional.com/PL/1/1/21542

Caribbean Business En Español - CBEE, (2021). CIAPR advierte sobre deficiencias en subastas para reparar planteles escolares, 27 de Julio de 2021. https://cb.pr/ciapr-advierte-sobre-deficiencias-en-subastas-para-reparar-planteles-escolares/?cn-reloaded=1

Chen, S.-E., Lin, S., Cheng, C.-T., Bhowmik, S., Tang, W., Baez-Rivera, Y., & Martinez, R. (2022). "Two-Story Residential Structure Damages after the 2020 Puerto Rico Earthquake", *ASCE Journal of Performance of Constructed Facilities*, 36, (2).

Comisión Estatal de Elecciones de Puerto Rico CEEPR. (2020). Centros de Votación. https://ceepur.org/Elecciones/docs/centrosvotacion.pdf.

Departamento de Educación de Puerto Rico DEPR. (2019a). Busca tu Escuela - 2018-2019, https://buscatuescuela.dde.pr/.

Departamento de Educación de Puerto Rico DEPR. (2019b). Plan Operacional para Emergencias e Incidentes Catastróficos (2018-2019). https://issuu.com/june-rivera/docs/dept._educacion_final

Disdier-Flores, O. M., & Cruz-Soto, L. J. (2019). Anuario Estadístico del Sistema Educativo (2016th ed.). Instituto de Estadísticas del Gobierno de Puerto Rico. Retrieved October 10, 2020, from https://estadisticas.pr/files/Publicaciones/Anuario%20Estadistico%20del%20Sistema%20Educativo%202015-2016.pdf

Instituto de Estadísticas de Puerto Rico. (n.d.). Anuario Estadístico del Sistema Educativo. Retrieved October 10, 2020 from https://estadisticas.pr/index.php/en/inventario-de-estadisticas/perfil-de-escuelas-publicas-y-privadas

Esri. (n.d.). ArcGIS Online. Hosted layers. Retrieved November 20, 2020, from https://doc.arcgis.com/en/arcgis-online/manage-data/hosted-web-layers.htm

Esri. (n.d.). ArcGIS Online. Web maps. Retrieved November 20, 2020, from https://doc.arcgis.com/en/arcgis-online/reference/what-is-web-map.htm

Jones, J.M., Ng, P., & Wood, N.J. (2014). The pedestrian evacuation analyst: Geographic information systems software for modeling hazard evacuation potential. In U.S. Department of the Interior & U.S. Geological Survey, Collection and delineation of spatial data (pp. 1-25). U.S. Geological Survey. https://doi.org/10.3133/tm11C9.

Knoper, L.; Clark, M.; Medwedeff, W.; Townsend, K.; Gong, W.; Zekkos, D.; Kirschbaum, D. (2020). "Preliminary Map of 1/7/2020 Puerto Rico Co-Seismic Landslides". http://www.learningfromearthquakes.org/2020-01-07-puerto-rico/11-resources/57-preliminary-map-of-1-7-2020-puerto-rico-co-seismic-landslides

LaForge, R. and McCann, W. R. (2017). "Address-Level Effects in Aguadilla, Puerto Rico, from the 1918 Mw 7.3 Earthquake and Tsunami", *Seismological Research Letters*, Volume 88, Number 5.

Mercado, A., McCann, W., (1998). "Numerical Simulation of the 1918 Puerto Rico Tsunami", *Natural Hazards*, 18, 57–76. https://doi.org/10.1023/A:1008091910209

Miranda, Eduardo; Acosta Vera, Andres; Aponte, Luis; Archbold, Jorge; Cortes, Maria; Du, Ao; Gunay, Selim; Hassan, Wael; Heresi, Pablo; Lamela, Ana; Messina, Armando; Miranda, Sebastian; Padgett, Jamie; Poulos, Alan; Scagliotti, Giulia; Tsai, Alicia; Kijewski-Correa, Tracy; Robertson, Ian; Mosalam, Khalid; Prevatt, David; Roueche, David (2020). "StEER - 07 Jan. 2020 Puerto Rico Mw6.4 Earthquake: Preliminary Virtual Reconnaissance Report (PVRR)." DesignSafe-CI. https://doi.org/10.17603/ds2-xfhz-fz88.

National Institute of Building Sciences NIBS, (2010). Earthquake-resistant design concepts: An introduction to the NEHRP Recommended seismic provisions for new buildings and other structures: FEMA P-749. Washington, D.C: Building Seismic Safety Council.

National Oceanic and Atmospheric Administration NOAA, (2019, August 14). Tsunami inundation. NWS JetStream. Retrieved April 18, 2022, from https://www.weather.gov/jetstream/tsu_inundation

National Oceanic and Atmospheric Administration NOAA. (2010). Puerto Rico Hypothetical Tsunami. Science on a Sphere. Retrieved January 12, 2022, https://sos.noaa.gov/datasets/puerto-rico-hypothetical-tsunami/

NotiCel. (2020). “El 95% de las escuelas públicas no están bajo el Código de Construcción vigente”, NotiCel. https://www.noticel.com/top-stories/educacion/ahora/20200107/el-95-de-las-escuelas-publicas-no-estan-bajo-el-codigo-de-construccion-vig/

Pacheco-Crosetti, G. E. (2020). “Fundamentals of Earthquakes and Seismic Hazards”, Mega Viernes Civil 2020 Conference, Institute of Civil Engineers IIC, College of Engineers and Land Surveyors of Puerto Rico CIAPR, San Juan, PR, July 18, 2020.

Plotaroute.com. (n.d.). Route Planner for walking, running, cycling. Retrieved September 20, 2020, from https://www.plotaroute.com/routeplanner

Public School Review. (n.d.). Profiles of USA Public Schools. Retrieved September 20, 2020, from https://www.publicschoolreview.com/

Puerto Rico Seismic Network PRSN, (n.d. a). 1918 Earthquake, Retrieved November 12, 2020, http://www.prsn.uprm.edu/English/information/quake1918.php, https://redsismica.uprm.edu/english/tsunami/evacuation_maps.php

Puerto Rico Seismic Network PRSN, (n.d. b). Puerto Rico Evacuation Maps, Retrieved November 12, 2020, from https://redsismica.uprm.edu/english/tsunami/evacuation_maps.php

Puerto Rico Seismic Network PRSN, (n.d. c). Puerto Rico Tsunami Program Map Tool PRTPMT, Retrieved November 12, 2020, from https://prddst.uprm.edu/apps/prtmp/

Puerto Rico Seismic Network PRSN, (n.d. d). Puerto Rico Tsunami Program, Retrieved November 12, 2020, from https://redsismica.uprm.edu/english/tsunami/

Reid, H. F.; Taber, S. (1919). “Los Terremotos de Puerto Rico de 1918, con Descripción de Terremotos Anteriores”, Informe de la Comisión Encargada de la Investigación Sobre Terremotos, Negociado de Materiales, Imprenta y Transporte, San Juan, Puerto Rico.

UNESCO. (2020). “Preparing for Community Tsunami Evacuations: From inundation to evacuation maps, response plans and exercises”, UNESCO, Manuals and Guides, 82 (Suppl. 1), https://reliefweb.int/sites/reliefweb.int/files/resources/373019eng.pdf

United States Congress, (1919). “The Porto Rico Earthquake of 1918”, 66th Congress 1st Session, November 19, 1919.

U.S. Department of Homeland Security. (2020). “Homeland Infrastructure Foundation-Level Data (HIFLD)”, Public Schools, https://hifld-geoplatform.opendata.arcgis.com/datasets/public-schools?geometry=-67.882%2C17.736%2C-64.213%2C18.649). Copyright 2017 by U.S. Department of Homeland Security.

United States Geological Service USGS, (n.d.). “Earthquake Hazards”, https://www.usgs.gov/programs/earthquake-hazards/earthquakes

United States Geological Service USGS, (2020a). “2020 Puerto Rico Earthquakes”, https://www.usgs.gov/special-topics/2020-puerto-rico-earthquakes

United States Geological Service USGS, (2020b). “M 6.4 - 13 km SSE of Maria Antonia, Puerto Rico”, https://earthquake.usgs.gov/earthquakes/eventpage/us70006vll/executive#d

AUTHORS BIOSKETCH

G. Pacheco-Crosetti

Licensed professional engineer in Puerto Rico. He obtained a PhD Degree from the University of Puerto Rico at Mayagüez (UPRM); major: Structures, minor: Geomechanics, a Graduate Specialist Degree (Master of Engineering) in Theory and Practice of the Finite Element Method from UNED, Spain; a Master of Science Degree from the University of Puerto Rico at Mayagüez; major: Structures, minor: Geomechanics and a Professional Diploma in Civil Engineering from the University of Córdoba, Argentina; major: Transportation. He is a tenured full professor in the Department of Civil and Environmental Engineering and Land Surveying of the Polytechnic University of Puerto Rico (PUPR); Director of the Transportation Infrastructure Research Center; Coordinator of the Professional Development Program in Transportation Infrastructure Inspection PDPTII PUPR/ACI-Herzog; Co-Coordinator of the Undergraduate Research Program for Honor and Outstanding Students URP-HOS, and the Co-Coordinator of the ACE FE and CE/PE licensee exams review seminars offered at PUPR. Also, he is past president of the American Society of Civil Engineers (ASCE) Puerto Rico Section, and a current member of the Earthquake Commission of the College of Engineers and Land Surveyors of Puerto Rico (CIAPR). He has successfully mentored over 70 students in applied undergraduate and graduate research projects, many of them related to inspection and evaluation of infrastructure, its performance and resilience.

O. Collazos-Ordóñez

Tenured full professor in the Department of Civil and Environmental and Land Surveying at the Polytechnic University of Puerto Rico, where she teaches geotechnical classes at the graduate and undergraduate level. She obtained a PhD Degree from the University of Missouri-Columbia (UMC); major: Geotechnical; minor: Structures, a Master Degree from the University of Puerto Rico at Mayagüez (UPRM); major: Structures; minor Geotechnical and a Degree in Civil Engineering from the University of Cauca-Colombia. Also, she has been a mentor at the graduate and undergraduate level on many research topics related mainly to slope stability, soil improvement, and the evaluation of permeability in pavements.

AUTHORS BIOSKETCH (CONT.)

V. Torres-Rodríguez

Senior student at *Polytechnic University of Puerto Rico – PUPR*, enrolled in the Civil Engineering Program. Her interest in research started early during her High School studies and continued to develop at the university level, working on the research project entitled "Vulnerability of Schools in Puerto Rico to Tsunami Events", developed in cooperation with classmate Joel A. Cohen Vázquez in the *2020-2021 Undergraduate Research Program for Honor Students – URPHS*. This project led to her current research involvement, in the study of factors that affect the pedestrian evacuation time of schools during tsunami events and that is being developed in collaboration with PhD student Elisa Marrero Rodríguez, as part of a cooperative agreement between PUPR and Volpe National Transportation Systems Center, under the supervision of professors Gustavo Pacheco-Crosetti, and Miriam Pabón-González.

J. Cohen-Vázquez

Undergraduate student at the Polytechnic University of Puerto Rico and is in his fifth year in the Civil Engineering Program. He was a member of the "ASCE Concrete Canoe" team (2019-2020). He worked in the environmental laboratory of the university as an assistant to the laboratory technician. He participated in the "Undergraduate Research Program for Honor Students 2020-2021" investigating the Vulnerability of Schools in Puerto Rico to Tsunami Events. Currently, he is participating in a collaborative agreement with Rutgers University aimed to investigate the Impact of Coastal Erosion in Puerto Rico. He hopes to impact the community through research projects and internships.

LESSONS LEARNED FROM THE VIRGINIA REFLECTIVE CRACKING STUDY UNDER ACCELERATED PAVEMENT TESTING[1]

Freddie Salado Martínez[2], Gerardo W. Flintsch[3]

ABSTRACT: Road administrators encounter situations where they must make decisions regarding the maintenance and rehabilitation of a road network without knowing the outcome of those decisions until years later. The Heavy Vehicle Simulator has been widely used as an accelerated testing tool to study pavement performance in a shorter period and under more controlled conditions than in the field. The Virginia Department of Transportation, in conjunction with the Virginia Tech Transportation Institute and the Virginia Transportation Research Council, has initiated a research project to study the behavior and performance of different pavement materials and structures under accelerated load through a Heavy Vehicle Simulator. Six pavement sections with different structures were built and instrumented with strain gauges, load cells, temperature gauges, and linear vertical displacement transducers. Two lanes were dedicated to study reflection cracking. They included a concrete pavement with joints 9.5 mm (3/8 inch) wide to reflect cracks in the surface. These lanes were covered with two 1.5-inch (38.1-mm) layers of a control SMA mix asphalt and a similar mix modified with a synthetic fiber. This article presents the results of this reflection cracking study. The article describes the characterization of the asphalt mixtures used, the pavement structure, the construction design, the Heavy Vehicle Simulator used and the installed instrumentation. The paper also presents some of the lessons learned, experimental changes, and study results in terms of cracking and rutting performance.

Keywords: accelerated pavement testing, heavy vehicle simulator, reflective cracking, synthetic fiber

LECCIONES APRENDIDAS DEL ESTUDIO EN VIRGINIA DE REFLEXIÓN DE GRIETAS POR MEDIO DE PRUEBAS ACELERADAS AL PAVIMENTO

RESUMEN: Los administradores de carreteras se encuentran con situaciones en las que deben tomar decisiones sobre el mantenimiento y la rehabilitación de la red sin conocer el resultado de esas decisiones hasta años después. El Simulador de Vehículos Pesados (HVS) ha sido ampliamente utilizado como una herramienta de prueba acelerada (APT) para estudiar el desempeño del pavimento en un periodo más corto y bajo condiciones más controladas que en el campo. El Departamento de Transportación de Virginia (VDOT), en conjunto con *Virginia Tech Transportation Institute (VTTI) y el Virginia Transportation Research Council* (VTRC) ha iniciado un proyecto de investigación para estudiar el comportamiento y desempeño de diferentes materiales y estructuras de pavimento bajo carga acelerada a través de un Simulador de Vehículos Pesados. Seis secciones de pavimento con diferentes estructuras fueron construidas e instrumentadas con medidor de deformación, celdas de carga, medidores de temperatura y transductores de desplazamiento vertical lineal. Se dedicaron dos carriles para estudiar el agrietamiento por reflexión. Incluían un pavimento de hormigón con juntas de 9.5 mm (3/8 de pulgada) de ancho para reflejar las grietas en la superficie. Estos carriles se cubrieron con dos capas de 38.1 mm (1.5 pulgadas) de una mezcla asfáltica (SMA) como control y una mezcla similar modificada con una fibra sintética. Este artículo presenta los resultados de este estudio de agrietamiento por reflexión. El artículo describe la caracterización de las mezclas asfálticas utilizadas, la estructura del pavimento, el diseño de la construcción, el Simulador de Vehículos Pesados utilizado y la instrumentación instalada. El documento también presenta algunas de las lecciones aprendidas, los cambios experimentales y los resultados del estudio en términos de rendimiento de agrietamiento y ahuellamiento.

Palabras clave: estudio acelerado del pavimento, fibra sintética, reflexión de grietas, simulador de vehículos pesados

[1] Article received on April 17, 2022 and accepted for publication on May 27, 2022.
[2] Transportation Engineering Consultant, P.O. Box 3494 Carolina, PR 00984. Email: freddie.salado@gmail.com
[3] Director, Center for Sustainable Transportation Infrastructure, Virginia Tech Transportation Institute
Professor of Civil and Environmental Engineering, Virginia Polytechnic Institute and State University
3500 Transportation Research Plaza, Blacksburg, VA, 24061-0536. E-mail: gflintsch@vtti.vt.edu

INTRODUCTION

Background

One of the primary problems faced by road administrators is finding appropriate and affordable preservation and renewal treatments given the limited funding available to maintain those roads. In many cases, treatments are delayed, and roads have to be rehabilitated instead. The Virginia Department of Transportation (VDOT) is looking for innovative approaches for the preservation and renewal of the road network. In many cases, VDOT does not have enough information on the performance of some of the treatments that can be applied. Since testing performance using an experimental in-service section takes too long, decisions often rely only on laboratory testing and/or engineering judgment. To be able to estimate the performance of new solutions in a shorter time, VDOT has explored the use of accelerated pavement testing (APT).

Objective

The objective of this paper is to describe the first reflective cracking study of hot-mix asphalt (HMA) overlays over jointed Portland cement concrete pavements (PCCP) conducted at the Virginia APT facility. The paper describes the characterization of the asphalt mixes, the pavement structure, construction layout, the Heavy Vehicle Simulator (HVS) used, and the instrumentation installed. The paper also presents some of the lessons learned, experimental changes, and the results of the study in terms of cracking and rutting performance.

Reflective Cracking

When an HMA overlay is placed over a jointed rigid pavement or severe cracks, distress known as reflective cracking may occur. Figure 1 shows the different reflective cracking mechanisms that can occur due to the traffic load and environmental causes. One of the causes of reflective cracking is related to horizontal movements due to the changes in temperature that are concentrated at joints and cracks in the existing PCCP. Another possible cause is the slab curling when the temperature decreases significantly, which will cause the HMA overlay to become stiffer. Lastly, reflective cracking can occur due to vertical deflection at the joints, or the existing cracks caused by the traffic loading (Lytton et al., 2010).

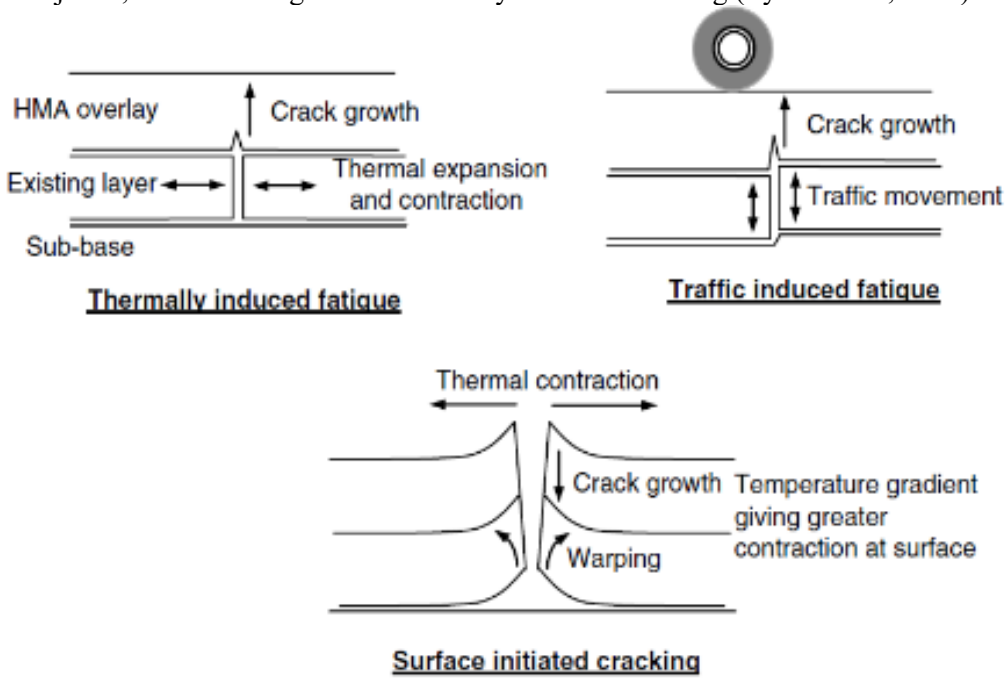

Figure 1: Reflective cracking mechanism (Lytton et al., 2010).

Von Quintus et al. (2009) studied techniques that can mitigate reflective cracking and concluded that methods such as pavement rubblization have the potential to delay the development of reflective cracking in overlays. They also found that it can be delayed through cold milling and placement of a new asphalt overlay or by increasing the thickness. Other strategies used to minimize or prevent reflective cracking are galvanized steel netting, geogrid, geonet, glass grid, paving fabric, geocomposite, stress-absorbing membrane interlayer (SAMI), rubblization, NovaChip, Strata®, saw and seal, different types of overlays or patches, leveling courses, heater scarification, and hot in-place recycling.

The Nevada Department of Transportation (DOT) monitored 33 projects in which they applied cold in-place recycling (CIR) overlays, reinforced fabric, stress-relief course, and mill/overlay. Results showed that CIR projects with roads subjected to an average annual daily traffic (AADT) of less than 6,000 developed reflective cracking as the main distress 1 to 2 years after construction. The reinforced fabric used on six roads with AADT between 1,000 and 10,000 had reflective cracking after being in service for 1 to 3 years. Results from the 1-inch stress-relief course used on five roads with an AADT between 1,900 and 40,000 showed that two projects presented reflective cracking 5 years after placing the stress-relief course. Lastly, mill and overlay used for roads with an AADT between 1,700 and 40,000 had reflective cracking 1 to 5 years after construction (Loria et al., 2008).

The Mississippi DOT evaluated the use of asphalt rubber interlayer systems for delaying the propagation of reflective cracking and found that the system in combination with an asphalt overlay of 38.1 mm (1.5-inches) can delay reflective cracking for 5 years (Amini, 2005).

A study conducted by Alabama DOT showed that asphalt rubber stress-absorbing interlayers delayed reflective cracking. The study used a 50.8 mm (2-inch) asphalt rubber layer placed below a 76.2 mm (3-inch) HMA overlay and monitored the section for 9 years to estimate the percentage of cracking on the surface. Results demonstrated the effect of asphalt rubber on cracking resistance. During the first 3 years there was no cracking on either pavement structure; however, after the third-year cracking started showing on both types of surfaces. After 9 years, 80% of the control section without the asphalt rubber had cracking and the experimental section with the asphalt rubber interlayer had cracking in 25% of the pavement section (Way, 1990).

Texas DOT (Chowdhury et al., 2009) evaluated the use of geosynthetics to delay reflective cracking. The researchers chose three locations in Texas with mild, moderate, and cool climates. The cool temperature section had a 50.8 mm (2-inch) overlay followed by the geosynthetic, 19.1 mm (0.75 inches) of leveling course, 63.5 mm (2.5 inches) of HMA, a 304.8 mm (12-inch) flexible base, and the subgrade. The moderate temperature section included a composite pavement with a jointed concrete base of 152.4 mm (6 inches) below a 44.5 mm to 50.8 mm (1.75- to 2-inch) HMA overlay and geosynthetic. The mild climate location had a 50.8 mm (2-inch) HMA surface with geosynthetic on a 355.6 mm (14-inch) flexible base 2% lime stabilized and a 304.8 mm (12-inch) subgrade 3% lime stabilized. The researchers monitored the sections over 5 to 6 years and found that at the end of the period the mild temperature sections had a maximum crack length of 381 mm (15 inches) versus 1.117 m (44 inches) for the control section without geogrid. The composite pavement located in the moderate temperature area developed a maximum crack length of 15.646 m (616 inches), versus 23.012 mm (906 inches) for the control section. Lastly, the cool temperature sections had a maximum crack length of 16.713 m (658 inches), versus 19.862 m (782 inches) for the section without a petrogrid. A common observation among the three areas of study was that cracks started showing up after 3 to 4 years depending on the thickness of the HMA overlay. Table 1 summarizes the results of the studies reviewed.

Table 1: Summary of Mitigation Techniques

ID	Location	Treatment	Performance (Reflective Cracking Delayed)
1	Nevada	Cold in Place Recycling Overlay	1–2 years
2		Reinforced Fabric	1–3 years
3		Stress-relief Course	5 years
4		Mill and Overlay	1–5 years
5	Mississippi	Asphalt Rubber Interlayer System + 38.1 mm (1.5-inch) Asphalt Overlay	5 years
6	Alabama	50.8 mm (2-inch) Stress-absorbing Interlayers (Rubber) + 38.1 mm (1.5-inch) Asphalt Overlay	3 years
7	Texas	Geosynthetics + HMA Overlay	3–4 years

Accelerated Pavement Testing

APT, in general terms, is defined as the controlled application of loading to a pavement structure using a wheel of known weight and pressure that is applied to the structure for a specific period. The loading simulates the traffic loading that the pavement will receive through its life, under controlled temperature, and sometimes moisture, conditions. The APT operation often involves measuring pavement response and testing conditions. Data such as load applications, subgrade and pavement material properties, temperature, drainage conditions, and/or the actual condition of the pavement structure help assess the pavement's performance under the APT and estimate its performance under real traffic.

PREVIOUS APT REFLECTIVE CRACKING STUDIES

A review of the literature showed that there have only been a few APT studies focus on reflective cracking on PCCP overlays. The main results of these studies are presented following.

National Center for Asphalt Technology

The National Center for Asphalt Technology (NCAT) began in 2015 a research study on its Test Track to validate asphalt mixes cracking tests by comparing performance results from the test track with the laboratory test. The sections included in the study were: (1) N1-control (20% RAP), (2) N2-control, higher density, (3) N5-control, low density, low asphalt content, (4) N8-control, 5% RAS, (5) S5-35% RAP, PG 58-28, (6) control, HiMA binder and (7) S13-gap graded, asphalt rubber. The surface layers of 1.5-inches were constructed over a HiMA layer with 17% RAP. Results showed that after 10 million ESALs cracking reached 21.5% of lane area in N1, 6.2% in section N2, 5.0% in N5, 16.9% in N8, and 0% in S5, S6, and S13.

Florida DOT

APT studies have improved throughout the years to target specific areas of pavement performance. Cracking has been one of the major concerns of the Florida DOT (Greene et al., 2012). The agency conducted a reflective cracking study to evaluate the effectiveness of SAMI. According to their report, SAMI is the primary reflective cracking mitigation technique used in the state. The tested section consisted of a 12.7 mm (0.5-inch) asphalt rubber membrane interlayer (ARMI) layer installed in one lane between a 228.6 mm (9-inch) slab with a joint spacing of 3.65 to 4.87 m (12 to 16 ft) and a 38.1 mm (1.5-inch) HMA overlay designed as a 12.5-mm (0.49-inch) Superpave mix with 5.1% of PG 76-22 asphalt binder. The second lane had a control section with the same pavement structure but without the ARMI layer. Within two weeks, reflection cracking appeared on all the joints of the section without ARMI, and approximately 25% of the joints had cracks in the section with ARMI. Analyzed cores showed that the cracks started from the surface, which according to the

author, was due to excessive tensile stress caused by the curling of the concrete. Linear vertical displacement transducer (LVDT) measurements showed that the average maximum daily horizontal and vertical movements were 0.29 and 0.07 mm (0.01 and 0.002-inch), respectively.

French Institute of Science and Technology for Transport (IFSTTAR)

The French national institute IFSTTAR, previously known as Laboratoire Central des Ponts et Chaussées, conducted APT using their two facilities, "Fatigue des chaussées en Béton Armé Continu" (FABAC), applying a load of 14.5 kips with a twin wheel (Perez et al., 2007). Each FABAC had four twin wheels in a chain that applied a load on a circular 30.5 m (100-ft) long and 2.04 m (6.7-ft) wide test track. Testing was conducted on a composite pavement with 78.7 mm (3.1-inch) thick concrete slabs. Eight joints were included in the testing. A surface layer composed of 60.9 mm (2.4 inches) of standard HMA had four joints (test temperature: 12.2 °C [54 °F]). A surface layer made of a 20.3 mm (0.8-inch) sand bituminous mixed layer and a 38.1 mm (1.5-inch) regular HMA layer was placed over two joints (test temperature: 16.1 °C [61 °F]). Finally, 10.2 mm (0.4 inches) of a bituminous layer with a metallic grid and 50.8 mm (2 inches) of regular HMA layer was placed above the last two joints (test temperature: 7.2 °C [45 °F]). Reflective cracking started to appear after 450,000 cycles for every mix except the standard bituminous, which reached 500,000 cycles.

Summary of APT Reflective Cracking Studies

The results of the four studies discussed in the previous sections are summarized in Table 2.

Table 2: Summary of Reflective Cracking Testing with HVS

Location	Lanes	Surface Thickness (in)	PCC Thickness (in)	Load (Kips)	Cracking
NCAT	N1	1.5-control (20% RAP)	-	18	21.5% - 10M ESALs
	N2	1.5-control higher density	-	18	6.2% - 10M ESALs
	N3	1.5-control, low density, low AC	-	18	5.0% - 10M ESALs
	N8	1.5-control + 5% RAS	-	18	16.9% - 10M ESALs
	S5	1.5-35% RAP, PG 58-28	-	18	0% - 10M ESALs
	S6	1.5-control, HiMA binder	-	18	0% - 10M ESALs
	S13	1.5-gap graded, asphalt rubber	-	18	0% - 10M ESALs
Florida	1	1.5-HMA + 0.5-Interlayer	9	9	2 weeks 25% of the joints
	2	1.5-HMA	9	9	2 weeks on every joint
France	1	2.4-standard bituminous	3.1	14.5	450K cycles
	2	0.8-sand bituminous + 1.5-regular bituminous	3.1	14.5	No cracks
	3	0.4-bituminous + Metallic Grid + 2-regular bituminous	3.1	14.5	450K cycles

VIRGINIA APT PROGRAM

The first set of experiments at the Virginia APT program included three studies. The first study evaluated two sections with 127 mm (5-inches) of a cold central plant recycling base with different surface thicknesses. The second study compared asphalt mixes designed with different compacting energies; one of them was designed using a lower number of gyrations (50) than the typical level (65). The third study, which covered the last two sections, compared two different premium asphalt mixes on a jointed PCCP and measured the effectiveness of the overlay in delaying reflective cracking.

Equipment Used, Pavement Section Construction, and Instrumentation

Heavy Vehicle Simulator

The HVS used for the loading application was the model Mark VI designed and built by Dynatest Consulting, Inc. (Figure 2). The Mark VI has a standard test wheel speed of 20 ± 3.2 km/h (12.4 ± 2 mph) for loads that range from 30 kN (6.744 lb) to 100 kN (22,500 lb). It has the capability of testing bidirectionally, achieving 24,000 passes in 24 hours, or unidirectionally with 12,000 passes in 24 hours (Figure 3; Cooke, 2011).

Figure 2: HVS MK VI testing on Lane 4, Cell A.

Figure 3: Dual tire load application.

Construction Layout

The APT program included the construction of an 18.3 m by 91.4 m (60 ft. by 300 ft.) pavement test section located at VTTI's facility. Figure 4 shows the sections included in the initial APT study and the HVS located on Lane 1, Section A. The pavement testbed was equally divided into six lanes with a width of 3.0 m (10 ft.) each. The third experiment of the first set focused on reflective cracking, was situated on Lanes 5 and 6.

Figure 4: Dimensions of pavement test sections.

Before lane construction, the area was excavated to provide a uniform foundation. The bottom of the excavation was covered with three layers of 152.4 mm (6-inch) Class I backfill material aggregate base 21-B with geogrids placed between each layer as shown in

Figure 5. These reinforced layers simulated a rigid foundation. The rest of the subgrade consisted of a soil with a California Bearing Ratio (CBR) of 7.5.

For the reflective cracking study, Lanes 5 and 6 were constructed with a base layer of 203.2 mm (8-inch) PCCP with an approximately 4,000-psi compressive strength at 28 days with 9.5 mm (3/8-inch) wide joints spaced at 3.0 m (10 ft) to create the cracks on the surface. Each lane was designed with the same 12.5 Nominal Maximum Aggregate Size (NMAS) stone matrix asphalt (SMA) mix, with the difference that one lane had a modified mix with synthetic fibers. There were two control sections built with two 38.1 mm (1.5-inch) layers of an SMA surface mix and two sections with two layers of the same SMA mix modified with 1 lb of the Forta-Fi synthetic fiber for each ton of asphalt mix. For the second phase of the study, one of the layers was milled, leaving a surface layer of 38.1 mm (1.5 inches).

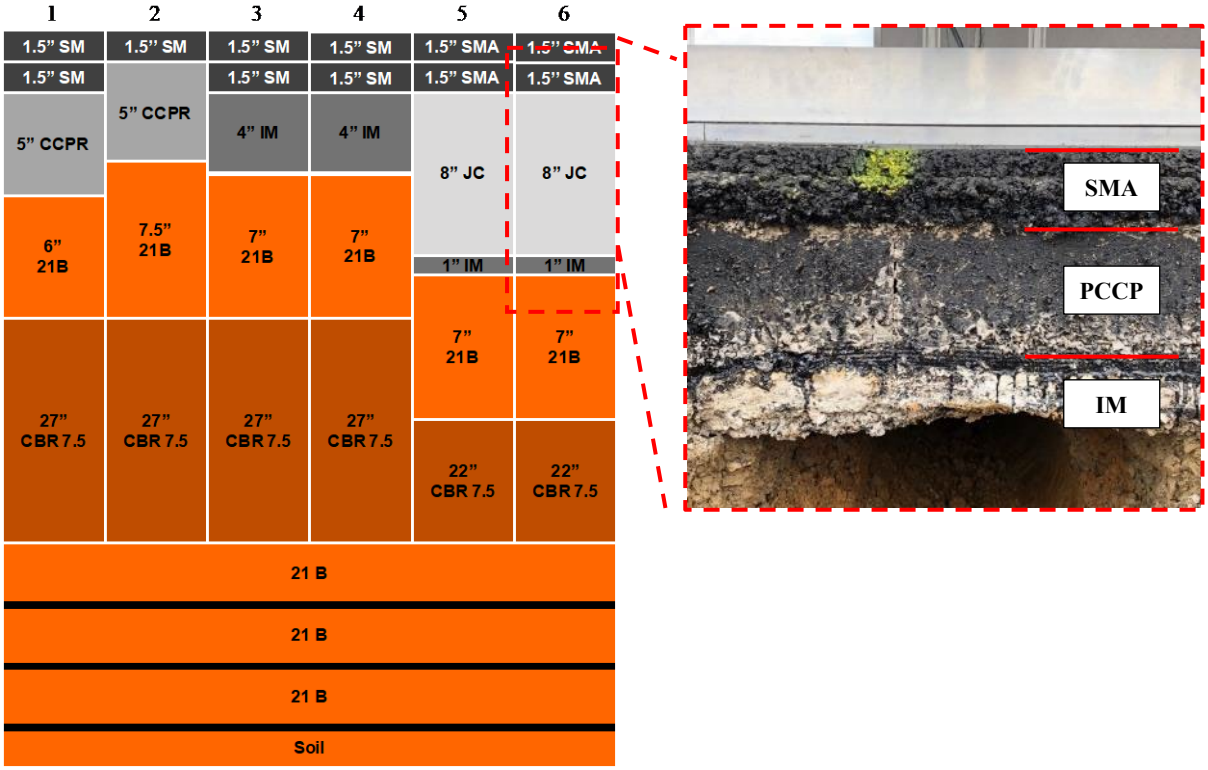

Figure 5: Pavement structure of tested sections (not to scale).

Instrumentation

Sensors were chosen from different manufacturers based on their reliability, accuracy, and compatibility.

Figure 6(a), (b), and (c) show the devices that were used for the test sections instrumented from subgrade to top layer with strain gauges, load cells, thermocouples, and LVDTs. The sensors were embedded under the wheel path to catch the critical responses from the pavement structure throughout its life cycle. Before the installation of the instruments, each one was calibrated and tested following the manufacturer's specifications.

(a) (b) (c)

Figure 6: (a) load cells, (b) strain gauge, (c) foil gauge.

A National Instruments PXIe-1075 data acquisition system was used in the experiment, along with the software LabVIEW, to collect signals from the embedded sensors. The cables of the sensors in the same pavement section were gathered and connected to the data acquisition system, which was accommodated in a conditioned stainless-steel cabinet.

Inside the HVS chamber, there is one camera to monitor the dual tire in case it stops working, if the load is not being applied correctly, or for times when maintenance is being conducted with a technician inside the chamber. Another camera monitored the initiation and propagation of the reflective cracking in Lanes 5 and 6.

Testing Conditions

Figure 7 shows a top view of the arrangement of the joints for the sections found in each lane. Although each section contains seven joints, only four were subjected to loading due to the length of the HVS, which does not cover the entire length of the section.

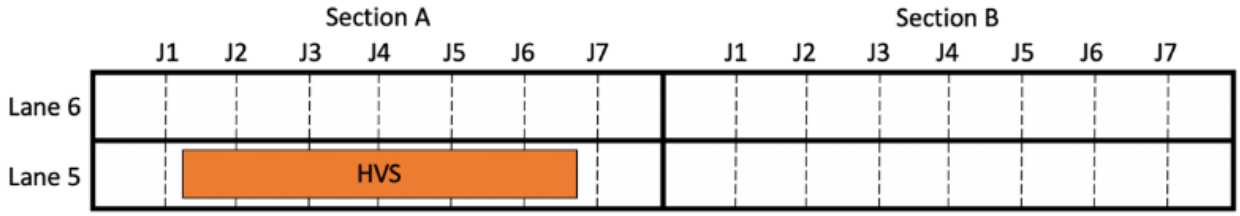

Figure 7: Arrangement of joints per section.

Each section had four samples to monitor the initiation and propagation of the cracks located at Joints 3, 4, 5, and 6. Each section was monitored and inspected daily to estimate the number of cycles needed for the crack to reach the surface. In addition to the visual inspection, the data acquired from the LVDTs were analyzed weekly to verify any changes in the measured vertical and horizontal movements of Joints 3 and 4.

All the tests were conducted at a constant speed of 4 mph. Due to the unknown response of the pavement sections for the reflective cracking study, during Phase I of the experiment, Lane 5, Section A started with a constant loading of 4.5 kips, which was incremented by 1.5 kips until reaching 15 kips.

Material Characterization

The study included a control SMA mix designed with an NMAS of 12.5 mm, of which 12% was composed of a limestone filler, 63% quartzite #7, 10% quartzite #8, and 15% recycled asphalt pavement (RAP). The mixes had 6.7% PG 64E-22 asphalt binder modified with 0.30% of the additive cellulose fiber and 0.50% of the antistripping Ad-here HP Plus. The experimental mix was a modified mix with synthetic fiber that had the same gradation and asphalt binder as the control mix with the difference that it was designed with 1 lb of Forta-Fi Fiber for each ton of asphalt.

These pavement sections tested with the HVS serve as a field study for comparison with the results obtained from a laboratory test by Salado et al. (2020), who evaluated the fracture resistance of asphalt mixes and determine the fracture resistance of these SMA mixes. They conducted the Indirect Tension Asphalt Cracking test to determine the Cracking Test Index, the Semi-Circular Bend test modified by the Louisiana Transportation Research Center to determine the critical strain energy release rate, the Semi-Circular Bend test modified by Illinois to estimate the Flexibility Index, and the Texas Overlay Test to estimate the crack propagation rate.

Phase I: Initial Experiment

The original plan included testing in the middle of each section using a typical wander pattern and increasing loading.

Wander

The load applied in the first phase used a normal distribution with higher application in the middle of the section and lesser on the sides, represented by the red bars in Figure 8. The red line with dashes represents the area where the unidirectional load was applied as a normal distribution. The green shaded area represents the coverage area of the HVS, which includes Joints 2 through 6, with Joints 3 through 6 being the samples under study.

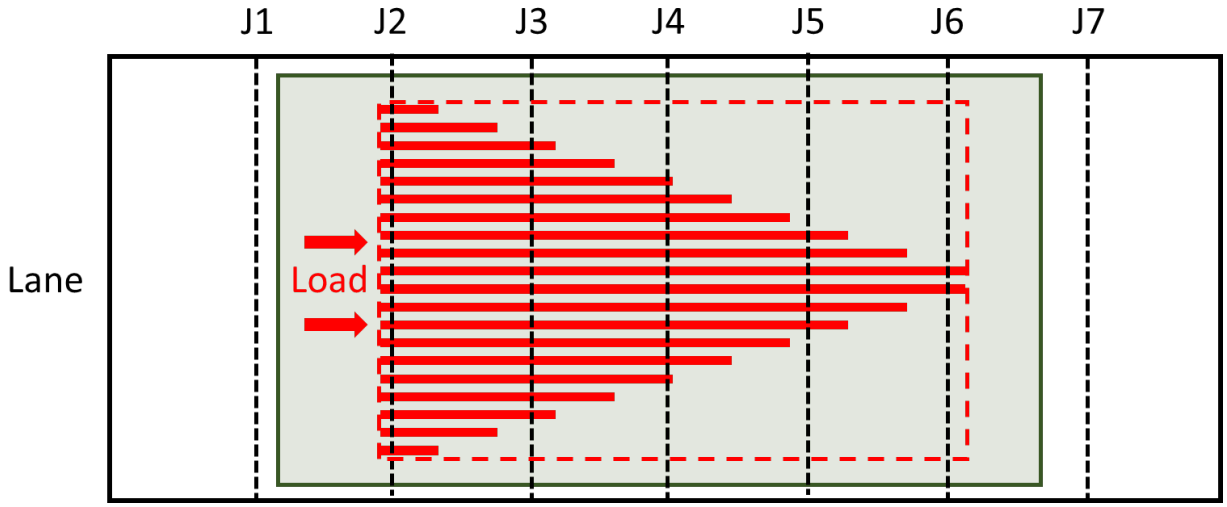

Figure 8: Distribution of load application.

The load was applied starting at 4.5 kips and incremented by 1.5 kips until reaching 15 kips. The wander had a transversal coverage of 1.5 m (5 ft.) wide, as shown in Figure 8. The testing started on Lane 5, Section B for 8 months, then was relocated covering the edges of sections A on Lane 5 and 6.

Instrumentation

Instruments for the reflective cracking study in Lane 5 and 6 only included LVDTs and strain gauges located at the joints. Vertical LVDTs were used to register the lateral and vertical changes of the slabs due to the load application.

Figure 9(a) shows the location of the LVDTs installed on each side of Joints 3 and 4. The LVDTs were installed on the edge of each slab between the joint, as shown in

Figure 9(b).

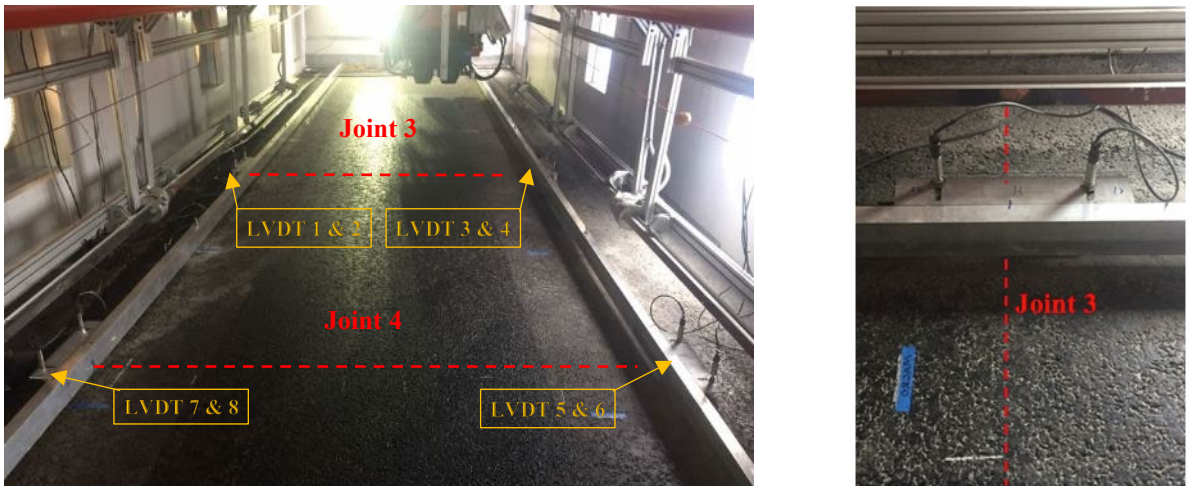

Figure 9: (a) LVDTs located in Joints 3 and 4; (b) LVDT installed at Joint 3.

Figure 10(a) shows an example of the vertical displacement measured by the LVDT located in the slab of Joint 4. The plot presents the peak displacements of more than 2 mm for a period of 200 s measured every time the wheel passed on the joint at approximately every 20 s.

Figure 10(b) shows the horizontal displacement during the same period of 200 s with a maximum displacement of 0.032 mm (.001-inch).

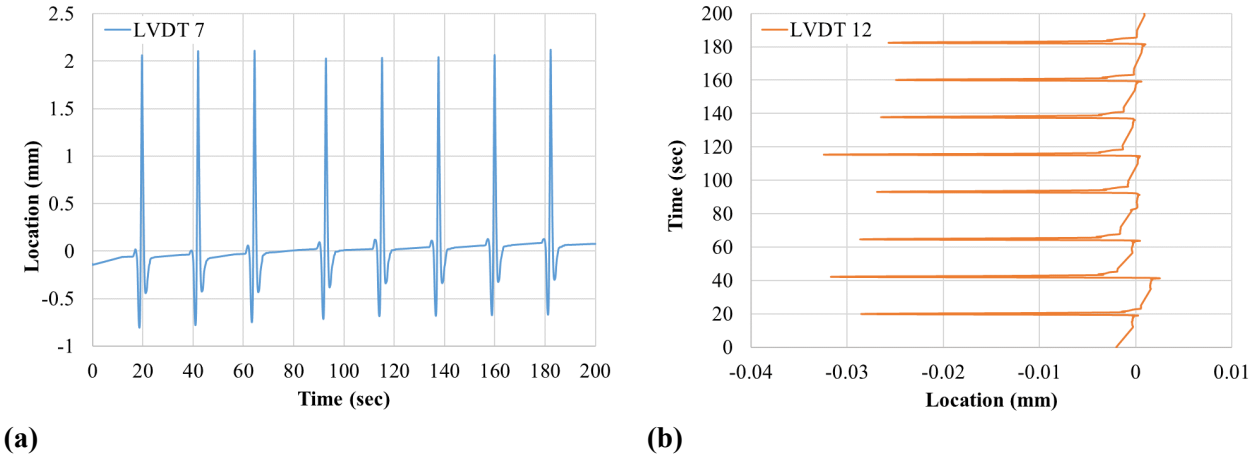

Figure 10: (a) Vertical and horizontal displacement measured by LVDT 7 and (b) LVDT 12.

Crack Recognition

Using the NI1778 camera, pictures were taken once a week to monitor the crack initiation and propagation on the surface at Joints 3, 4, 5, and 6. Figure 11 shows three images attached from Joint 5, taken from the top in December 2017 when the experiment started. The image has a coverage area of 1.4 m (4.5 ft.) wide and 0.5 m (1.8 ft.) in height.

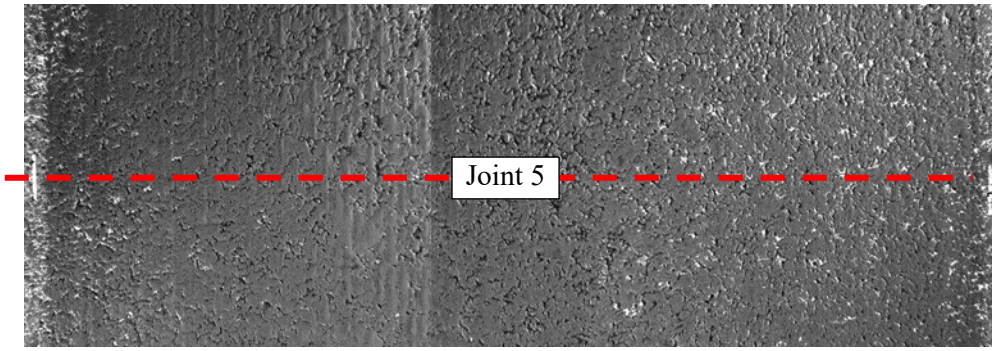

Figure 11: Top view image of SMA overlay at Joint 5.

Phase II: Experimental Changes

During the first 6 months of APT, there were no cracks reflected from the joints of the pavement section located in Lane 5 with the control SMA mix. Therefore, several modifications were made to the pavement structure and loading to increase the movement at the joints and allow the cracks to reach the surface faster. Table 3 shows the itinerary of major changes to the experiment. Due to the unknown response from the pavement, the study started in December 2017 with a small load of 4.5 kips. The load was increased by 1.5 kips every two weeks until March 2018 and was kept at 15 kips until the end of the experiment.

Table 3: Itinerary of Changes to HVS Experiment

	Dec 2017	Jan 2018	Feb 2018	Mar 2018	April 2018	May 2018	June 2018	July 2018	Aug 2018	Oct 2019
HVS Started (lane 5 cell B)										
Load increased										
Load Direction: Unidirectional to Bidirectional										
Subbase Drilling: Joints 4 and 5										
Cold Milling: 38.1 mm (1.5-inches)										
HVS Relocation: Edges of lanes 5 and 6										
Load Direction: Bidirectional										
HVS Stopped										

Load Direction

At the beginning of the pavement testing, loads were applied in only one direction. The first major modification to the experiment was to change the HVS from unidirectional to bidirectional travel. At 4 mph

the daily number of passes increased from 3,500 to 6,500, which represented an increment of approximately 30,000 ESALs per day.

Subbase Drilling

It was decided to drill horizontally the subbase below Joints 4 and 5 to allow movement at the joints. Each hole had an approximate diameter of 406.4 mm (16-inches).

Figure 12 shows the change made to the pavement structure with the two holes drilled below Joints 4 and 5. After running for almost 16,200 passes (138,428 ESALs) there were no transversal cracks on the surface. However, the LVDT registered a maximum vertical movement of the slabs located at Joint 5 of almost 1 mm (0.04-inch).

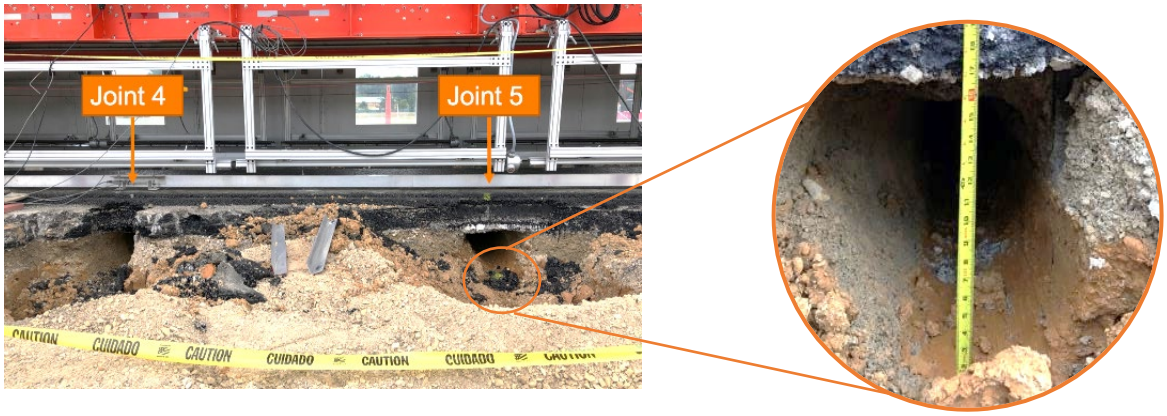

(a) **(b)**

Figure 12: (a) Subbase drilling below Joints 4 and 5 with (b) an average diameter of 406.4 mm (16 inches).

Cold Milling

A third modification to the experiment was the cold milling of the surface. The original pavement section had two 38.1 mm (1.5-inch) layers, but it was decided to remove the top 38.1 mm (1.5-inch) layer.

HVS Relocation and Revised Wander

After the cold milling, the HVS was relocated between Lanes 5 (control) and 6 (synthetic fibers) to test both lanes at the same time. The wander was applied on the edge of both lanes, following a narrower normal distribution with a much smaller standard deviation, as shown in Figure 13.

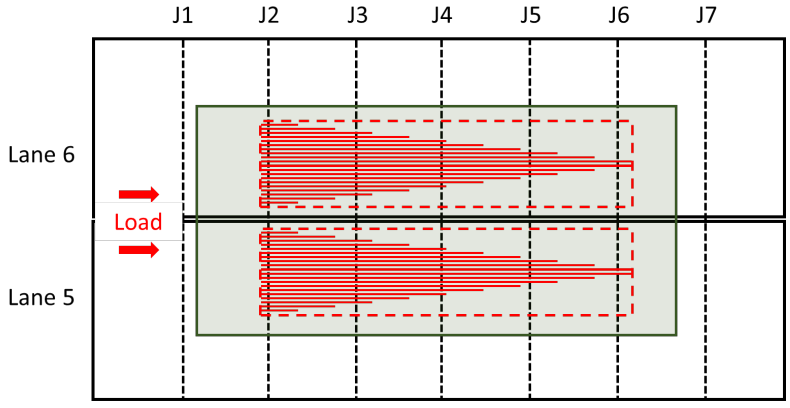

Figure 13: Load application distribution between Lanes 5 and 6.

PERFORMANCE RESULTS: SURFACE CRACKING AND RUTTING

Although the purpose of the research was to study cracking initiation and propagation from the joints to the surface, daily measurements of the surface profile were taken to estimate the permanent deformation or rut depth of the surface layer due to the load applied.

Reflective Cracking Propagation

After the HVS was relocated between Lanes 5 and 6, the experiment continued running until October 2019. During Phase I, the experiment in Lane 5 applied a load equal to 2,775,000 ESALs. A crack was first seen on Joint 5, during Phase II, after 291,716 passes (1,170,000 ESALS) during the inspection conducted on September 5, 2019.

Figure 14(a) shows a top view of Lane 5 (left side) and Lane 6 (right side) with the longitudinal joint that separates the lanes. The crack started from the left side of Lane 5, as shown in

Figure 14(b), and continued propagating to Lane 6.

Figure 14(c) shows the crack propagated on Lane 6, which was first seen during the inspection on October 16, 2019. Compared to the crack on Lane 5, it appeared on the surface of Lane 6 approximately after an additional 373,321 passes, which corresponds to an additional 697,000 ESALs, (cracking at 1,867,000 ESALs).

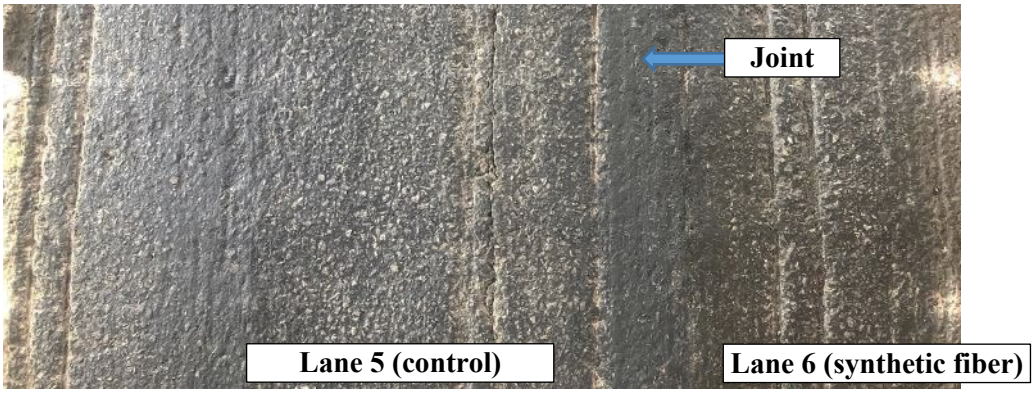

(a)

(b)

(c)

Figure 14: (a) Top view of Lane 5 and 6. (b) Crack on Lane 5. (c) Crack on Lane 6.

Surface Profile: Rutting

Daily measurements of the profile helped to monitor the rut depth of the pavement surface. Measured rut depth was compared to the measurements taken before the experiment started to determine the increment in depth.

Figure 15 shows the rut depth versus ESAL plot for the data acquired while the HVS was on call B of Lane 5 and after it was relocated between Lanes 5 and 6.

The first line, "Phase I: Lane 5," shows the results obtained during the first cycle of the study before it went through the experimental changes mentioned above (e.g., subbase drilling, load direction). The maximum rut depth measured by the sensors from the HVS was negligible, 0.2 mm.

During Phase II, in which the HVS was relocated between Lanes 5 and 6, maximum depths of 3.6 mm and 4.3 mm (0.14-inch and 0.16-inch) were measured for Lane 5 and 6, respectively. The nonuniform increasing trend reflects the accumulated rubber from the tire, asphalt binder, and uneven surface due to the cold milling performed and the accuracy of the method used to determine the rutting.

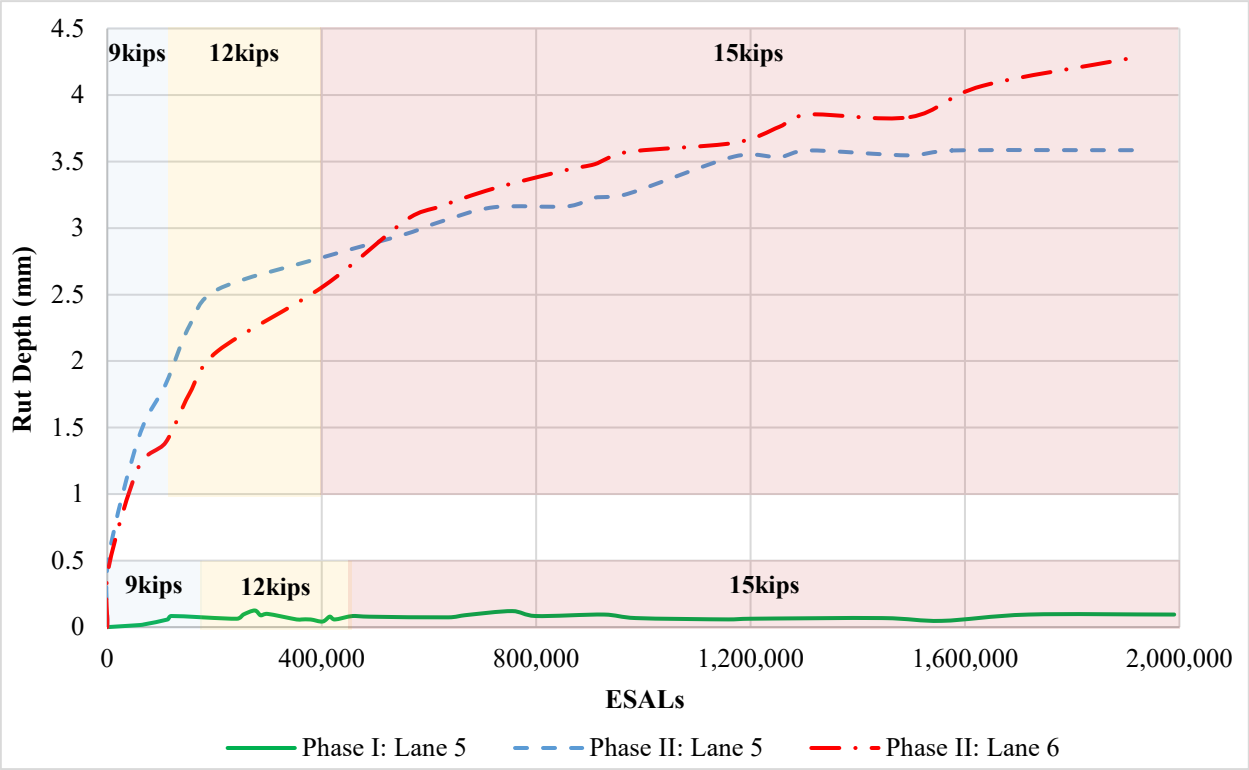

Figure 15: Rut depth vs. ESAL plot for Lane 5 during Phase I and Lanes 5-6 during Phase II.

LESSONS LEARNED

The following are some of the key lessons that were learned during the construction, instrumentation, and testing of the pavement sections:

- Numerical processing and analysis of the data collected by the HVS system should be supplemented by visual inspection of the pavement deterioration. The camera was not able to detect the initiation of the crack, probably due to the rubber deposit on the surface.
- Laboratory testing should be done to characterize the core samples taken at each tested section and/or plant mixed samples collected before placement and compaction.

- Profile readings should be taken every 24 hours to measure depth changes.
- After rainfall, the surface of the test section should be dried to avoid possible errors on the measured profile.
- The overall section was built too strong. Future tests should limit the overlay thickness to 38.1 to 50 mm (1.5 to 2-inch) and artificial voids should be built below some of the joints to simulate erosion due to pumping the generate movement at the joints.

CONCLUSIONS

Testing conducted using the HVS model Mark VI on the two SMA overlays showed that the modified mix with Forta-Fi synthetic fiber had better performance compared to the control mix. The crack started at approximately 1,170,000 and 1,867,000 ESALs on the control mix the mix modified with synthetic fibers, respectively. This suggests that the addition of fibers increased the time to develop the first crack by approximately 697,000 ESALs, which represents an increase of more than 50% with respect to the control mix. Rutting measurements were less than 5 mm on both sections suggesting good performance of both mixes.

The experiment also showed that it is hard to realistically replicate the conditions experienced by asphalt overlays over deteriorated concrete joints within the APT facility. The design of the original experiment did not allow enough movement at the joints to produce reflective cracking. It was necessary to create artificial voids below the surface, reduce the overlay thickness, and load the slabs close to the edge to produce the reflecting cracking over the joints

REFERENCES

Amini, F. (2005). "Potential Applications of Paving Fabrics to Reduce Reflective Cracking, Jackson State University", Prepared for Mississippi Department of Transportation, FHWA/MS-DOT-RD-05-174.

Chowdhury, A., Button, J.W., and Lytton, R.L. (2009). "Tests of HMA Overlays Using Geosynthetics to Reduce Reflection Cracking", FHWA/TX-10/0-1777-3.

Cooke, B. *HVS MK VI I- VDOT User's Manual*, Virginia Department of Transportation, Virginia, 2015.

Greene, J., Kim, S., Chun, S. & Choubane, B. (2012). "Effect of Asphalt Rubber Membrane Interlayer (ARMI) on Instability Rutting and Reflection Cracking of Asphalt Mixture", Retrieved 2017 from http://www.fdot.gov/materials/administration/resources/library/publications/researchreports/pavement /12-552.pdf

Loria, L., Sebaaly, P., and Hajj, E. (2008). "Long-Term Performance of Reflective Cracking Mitigation Techniques in Nevada", *Transportation Research Record: Journal of the Transportation Research Board*, 2044(-1): p. 86-95

Perez, S., Balay, J., Tamagny, P., & Petit, C. (2007). "Accelerated pavement testing and modeling of reflective cracking in pavements", Science Direct, 1526-1537

Salado, F., Flintsch, G., Diefenderfer, B. & Marcobal, J. (2020). "Laboratory Assessment of Fracture Resistance of Modified Mixtures with Forta-Fi Synthetic Fibers".

Von Quintus, H. L., Mallela, J., & Weiss, W. (2009). "Techniques for Mitigation of Reflective Cracks", Final Report AAPTP 05-04, Auburn: Airfield Asphalt Pavement Technology Program.

Way, G.B. (1990). "Flagstaff I-40 Asphalt Rubber Overlay Project Nine Years of Success", Transportation Research Board.

West, R., Timm, D., Powell, B., Heitzman, M., Tran, N., Rodezno, C., Watson, D., Leiva, F., Vargas, A. (2019). "Phase VI (2015-2017) NCAT Test Track Findings. No. NCAT Report 18-04", National Center for Asphalt Technology, Auburn University.

AUTHORS BIOSCKETCH

F. Salado

Civil engineer with over 10 years of experience in asphalt mix design, construction, evaluation, and road maintenance. While pursuing his doctoral degree, worked at the Virginia Tech Transportation Institute where he gained experience in pavement structure construction, pavement macrotexture, improvement of skid resistance for crash reduction, accelerated pavement testing to evaluate pavements performance, mixture design, and other pavement-related topics. His main area of expertise is the design and evaluation of asphalt mixes modified with rubber, synthetic fibers, reclaimed asphalt pavement, cellulose fiber, additives, and other recycled materials. Currently works for the Federal Transit Administration, San Juan office as a program manager and project oversight of formula grants, Emergency Relief Program, and Triennial Reviews for several municipalities and transit agencies in Puerto Rico.

G. Flintsch

Director of the Center for Sustainable & Resilient Infrastructure at VTTI and the Dan Pletta Professor in Virginia Tech's College of Engineering. Since the mid-1980s, he has worked in the areas of asset management, pavement engineering, and sustainability. His main areas of technical experience are pavement design, construction, evaluation and management, and infrastructure management. He has taught classes and workshops on pavement and infrastructure design, evaluation, and management in eleven countries and has more than 150 publications. Dr. Flintsch has also served as a consultant to several national and international organizations and has recently been inducted as a member of the National Academy of Engineering of Uruguay (NAE).

TRAFFIC CRASH INJURIES OCCURRENCE VARIETIES ACROSS BARCELONA DISTRICTS[1]

Ahmad Aiash[2], **Francesc Robusté**[3]

ABSTRACT: Barcelona (Spain) had a total population of 1,636,762 in 2019 that are distributed on 10 districts across the city. These districts have different characteristics in size and population density. As a result, this can lead to different traffic crashes injuries occurrences and numbers in these areas. Therefore, this study is attempting to determine the conditional probabilities for each district in order to identify the district that has highest number of injuries compared to other areas. A Bayesian network approach is utilized to analyze the dataset and identify the high-risk district alongside analyzing the varieties of traffic crashes during four-year intervals. The results have shown that the district that has the highest population, highest usage of private transport mode, and highest density of passenger cars per km^2 (compared to all other districts), has the highest risk of having all types of injuries resulting from traffic crashes. For the temporal factor represented by the four years interval, traffic crashes occurrences varied from district to district based on the level of injury.

Keywords: Barcelona, districts, injuries, traffic crashes, Bayesian network

RESUMEN: Barcelona (España) tenía una población total de 1.636.762 en 2019 que se distribuyen en 10 distritos de la ciudad. Estos distritos tienen diferentes características en tamaño y densidad de población. Como resultado, esto puede conducir a diferentes ocurrencias y números de lesiones por choques de tránsito en estas áreas. Por lo tanto, este estudio intenta determinar las probabilidades condicionales de cada distrito para identificar el distrito que tiene el mayor número de lesiones en comparación con otras áreas. Se utiliza un enfoque de red bayesiana para analizar el conjunto de datos e identificar el distrito de alto riesgo junto con el análisis de las variedades de choques de tráfico durante intervalos de cuatro años. Los resultados han demostrado que el distrito que tiene la mayor población, el mayor uso del vehículo privado, y la mayor densidad de vehículos por km^2 (en comparación con todos los demás distritos), tiene el mayor riesgo de sufrir todo tipo de lesiones derivadas de choques de tráfico. Para el factor temporal representado por el intervalo de cuatro años, las ocurrencias de choques de tránsito variaron de un distrito a otro según el nivel de lesión.

Palabras claves: Barcelona, distritos, lesiones, choques de tráfico, red Bayesiana

INTRODUCTION

European countries have a plan that is updated from time to time in order to achieve less traffic crashes injuries with more focusing on fatalities and severe injuries. Fig. 1 portrays the change of road fatalities in some European countries by comparing the data between 2010 and 2019 based on a *14th Road Safety Performance Index Report (2020)*. The negative percentages in the figure are referring to a decrease in road fatalities in the designated countries and vice versa. The report showed that the reduction difference for the total number of road deaths in EU27 between 2019 and 2010 is 7,023 deaths. Greece has the highest decreasing percentage with -44.4%, while Malta had the highest increasing percentage of 6.7%. For Spain, the percentage of road fatalities was 30.4% reduced by comparing the two years 2010 and 2019. However, the medium-term target was halving the number of deaths, but as shown, the progress of lessening the number in some countries is stagnated.

[1] Article received on April 29, 2022 and accepted for publication on May 17, 2022.
[2] Doctoral Candidate, Civil Engineering School, UPC – BarcelonaTech, Jordi Girona, 1-3, 08034, Barcelona, Spain.
Email: ahmad.aiash@upc.edu
[3] Professor, Civil Engineering School, UPC – BarcelonaTech, Jordi Girona, 1-3, 08034, Barcelona, Spain.
Email: f.robuste@upc.edu

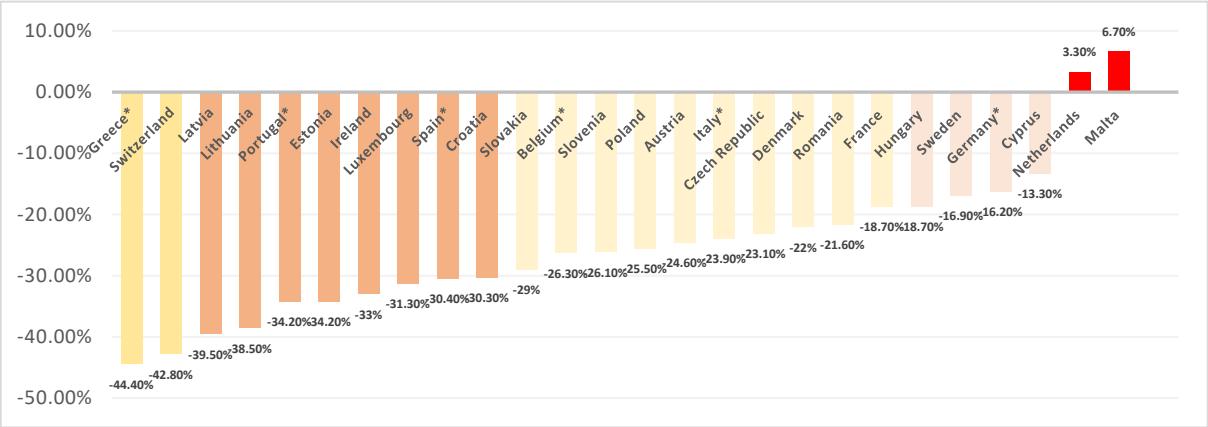

Figure 1: Relative change in road deaths 2010-2019 in Europe
(Provisional data for 2019 for some indicated countries based on the provided report).

Therefore, many studies have attempted to examine traffic crashes from different perspectives to thoroughly detect and mitigate the risk factors that may impact the level of injury resulted from traffic crashes. In Barcelona, Spain, a recently published study (Aiash & Robusté, 2021a) has examined several risk factors. This study applied two models: a binary *probit* model and *chi-square* automatic interaction (CHAID) tree. The total traffic crashes that are examined are 47,153 crashes with including five potential risk factors. The findings showed that elderly and males injured-prone were more likely to have severe or fatal injuries compared to other categories. For the user type, pedestrians and drivers have shown similar trend in having severe of fatal injuries. For the temporal factors, weekends, afternoon, and night timing all are considered as a risk timing due to the likelihood of having severe or fatal injuries compared to other timings. Another recently published study (Aiash & Robusté, 2021b) have conducted an analysis for two other factors that can contribute traffic injuries. These two factors are both temporal factors including the working hours timing period and the season of the year. A Bayesian network is employed for this reason to conduct the analysis process and identify their potential impact of traffic injuries. The results showed that both summer season and working hours timing period were more likely to have higher number of reported injuries.

Bayesian network is one of the utilized approach models to analyze and predict traffic crash data. A study (Alkheder *et al*., 2020) has employed several data mining techniques to predict and detect the risk factors and their consequential impact. The study found that Bayesian network was accurately predicted the crash data better than CHAID tree and linear support vector machine. The results showed that males drivers, front seat passengers, and elderly drivers were all at higher risk of having severe or fatal injuries compare to other groups. The importance of using the seat belt in case of traffic crash was also asserted. The types of crashes and road classifications were found to have an impact on injuries resulted from traffic crashes. A side from the accurate prediction that Bayesian network can provide, a study (Zhao & Deng, 2015) has deployed the Bayesian network to make inference on crash types at urban intersections. The findings revealed that bicycle and electric bikes were more likely to be involved in frontal collision at urban intersections crashes than small cars and heavy vehicles, whereas, heavy vehicle was more likely to be involved in side collision compared to light vehicles.

Space-temporal factors can have a potential impact on traffic crash injuries. Several research studies are conducted to examine this impact. A study (Wang *et al*., 2013) have employed a Bayesian network approach to analyze the spatiotemporal effect of traffic congestion. Fatal and severe injuries were found to be more associated with the increase in traffic congestion. Another research (Jia *et al*., 2018) found that residential density and bank and hospitals point of interests have an impact on traffic crashes. Consistently, mixed use development, urban residential, single-family residential, multi-family residential, business and, office district all are found to have strong correlations with traffic analysis zones level crashes (Pulugurtha *et al*., 2013).

METHODOLOGY

Barcelona districts

Barcelona has a total population of 1,636,762 inhabitants in 2019 that are distributed on 10 districts across Barcelona. These districts are *Ciutat Vella, Eixample, Sants-Montjuïc, Les Corts, Sarrià-Sant Gervasi, Gràcia, Horta-Guinardó, Nou Barris, Sant Andreu,* and *Sant Martí,* as shown in Fig. 2. Fig. 3 is depicting the road network across Barcelona city with red lines based on (Ajuntament de Barcelona, 2022). Each of these districts is assigned to a different number based on the database source. Table 1 is presenting the detailed population in each district. The highest number of population and density per ha is found in *Eixample,* while the lowest population and density per ha is found in *Les Corts* and *Sarrià-Sant Gervasi,* respectively. This data is gathered from the City Hall of Barcelona database (Ajuntament de Barcelona*, 2019a).*

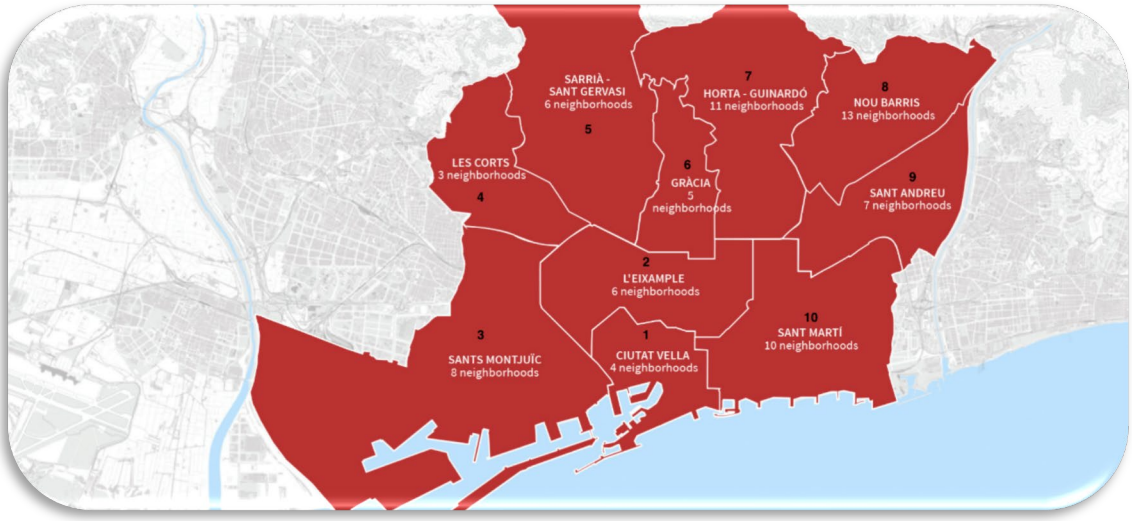

Figure 2: Barcelona districts' location and boundaries.
https://www.barcelona.cat/en/living-in-bcn/living-neighbourhood

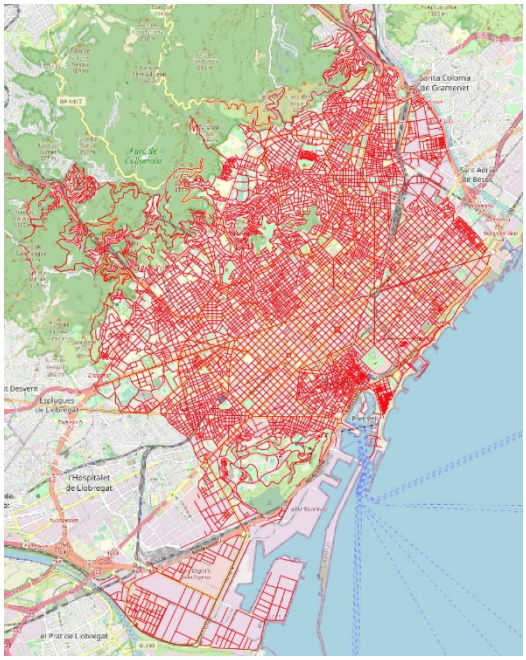

Figure 3: Road network in Barcelona city.

Table 1: Barcelona Districts population and size.

District	Population	Size in (ha)	Density (inhabitants/ha)
1. Ciutat Vella	103,429	412.1	251
2. Eixample	**265,910**	746.4	**356**
3. Sants-Montjuïc	184,091	2,267.6	81
4. Les Corts	81,974	601.1	136
5. Sarrià-Sant Gervasi	149,260	1,991.6	75
6. Gràcia	121,798	422.4	288
7. Horta-Guinardó	171,495	1,191.9	144
8. Nou Barris	170,669	805.1	212
9. Sant Andreu	149,821	658.9	227
10. Sant Martí	238,315	1,038.6	229

A recently published Statistical Yearbook of the City of Barcelona (Ajuntament de Barcelona, 2021) has included the indicators and vehicle stats across the different districts of Barcelona. Table 2 is presenting passenger car distributions across Barcelona districts. It can be noticed that *Eixample* has the highest number of passenger cars with having the highest density of passenger cars per $\mathbf{km^2}$. Table 3 is showing the number of registered vehicles in Barcelona districts in 2020. Similar to previously noticed statistics, *Eixample* has the highest number of all types of registered vehicles except for registered mopeds and trucks. Consistently, table 4 is presenting the usage of different modes of transport in Barcelona districts in 2020. It can be also noticed that *Eixample* has the highest usage of both on foot and bicycle mode of transport and private transport mode, while Sant Marti has the highest usage of public transport compared to other districts.

Table 2: Density Indicators of passenger cars in 2020.

District	Passenger car	Surface ($\mathbf{km^2}$)	Passenger car / $\mathbf{km^2}$
Ciutat Vella	17,679	4.2	4,204
Eixample	**77,912**	**7.5**	**10,438**
Sants-Montjuïc	49,494	22.9	2,163
Les Carts	31,393	6.0	5,223
Sarria-Sant Gervasi	59,474	19.9	2,986
Gracia	33,709	4.2	7,980
Horta-Guinardó	49,751	11.9	4,174
Nou Barris	45,792	8.1	5,684
Sant Andreu	44,922	6.6	6,815
Sant Martí	68,992	10.4	6,610

Table 3: Vehicles registered by typology and district in 2020.

District	Passenger cars	Motorcycles	Mopeds	Vans	Trucks	Other vehicles
Ciutat Vella	624	554	1,135	92	33	27
Eixample	**3,227**	**2,194**	1,171	**236**	52	**190**
Sants-Montjuic	1,962	1,054	310	184	**53**	112
Les Carts	1,369	700	36	33	12	11
Sarria-Sant Gervasi	2,363	1,846	101	75	22	60
Gracia	1,278	1,002	103	53	10	17
Horta-Guinard6	1,887	1,307	104	126	27	26
Nou Barris	1,645	826	78	114	25	34
Sant Andreu	2,018	822	56	142	25	34
Sant Marti	2,652	1,358	**2,583**	200	29	58

Table 4: Transport type usage by district in 2020.

District	Total	By foot & Bicycle	Private transport	Public transport
Ciutat Vella	333,300	253,308	25,329	54,662
Eixample	**802,039**	**544,185**	**147,750**	110,104
Sants-Montjuïc	500,419	294,860	97,666	107,894
Les Corts	264,350	176,951	53,956	33,444
Sarria-Sant Gervasi	455,135	259,254	136,183	59,699
Gracia	380,898	250,154	68,424	62,320
Horta-Guinardó	490,973	271,132	108,942	110,899
Nou Barris	526,307	294,752	108,715	122,840
Sant Andreu	460,405	289,878	88,952	81,574
Sant Martí	713,044	435,258	137,993	**139,793**

Bayesian network

In this study, a Bayesian network is employed to analyze the utilized data that is gathered from *The City Hall of Barcelona* (Barcelona's City Hall Open Data Service, 2019b). Tree Augmented Naïve Bayes technique is used through the IBM Watson Studio platform that is developed based on *Bayesian Network Classifiers* (Friedman *et al*., 1997). Two predictors are analyzed including all districts of Barcelona and a range of years that extended from 2016 to 2019. The dependent variable is the level of injury which consists of slight injury and severe or fatal injury. The total number of utilized crashes in this study is 47,081. The undefined areas or values are eliminated from the final utilized data. The conditional probabilities are determined as shown in the following equation and similar to a previously mentioned and conducted study (Aiash & Robusté, 2021b). More details about the applied model can be found at IBM report (2016):

$$Pr\left(Y_i|X_1 = x_1^j, X_2 = x_2^j, \dots, X_n = x_n^j\right) = \frac{Pr(Y_i)\left(X_1 = x_1^j, X_2 = x_2^j, \dots, X_n = x_n^j|Y_i\right)}{Pr\left(X_1 = x_1^j, X_2 = x_2^j, \dots, X_n = x_n^j\right)} \quad (1)$$

$$\propto Pr\ (Y_i) \prod_{k=1}^{n} Pr\left(X_k = x_k^j | \pi_k^j, Y_i\right)$$

d is the data set. the case that is classified to which it belongs to i^{th} target category is d_j. The target Y_i is level of injury including two categories: slight injury and severe or fatal injury. The independent variable is x. The number of independent variables which is two in this study is n. As a result, $d_j = \left(x_1^j, x_2^j, \dots, x_n^j\right)$. Non-redundant parameters number is K. The parent set of the independent variables alongside the dependent variable is π_k, it maybe empty for Tree Augmented Naïve Bayes. The conditional probability is $Pr\left(X_k = x_k^j \middle| \pi_k^j, Y_i\right)$ related to the developed two nodes.

RESULTS AND DISCUSSIONS

Figure 4 is showing the structure of the applied TAN model. It consists of three nodes starting with the injury level which is the dependent variable followed by district and year nodes. District node is including the ten different aforementioned districts in Barcelona, while the year node is including 4 years which they are 2016, 2017, 2018, and 2019. Based on the applied model, district as an independent variable is more important than year variable in predicting the utilized data. The prediction accuracy for the applied model is found to be for the training and testing is 98.01% and 98%, respectively.

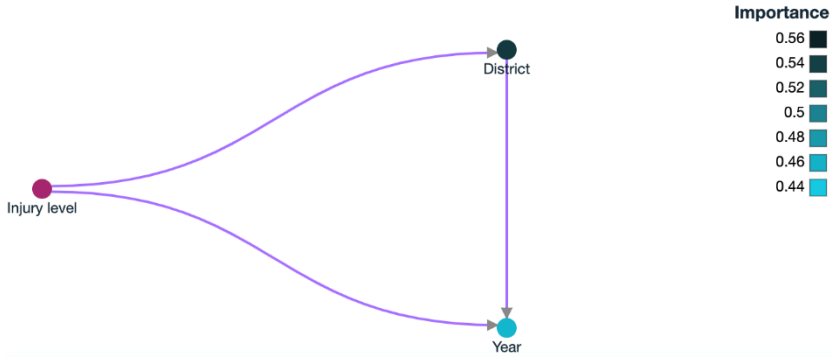

Figure 4: Structure of the applied TAN model.

Table 5 and Table 6 are showing the determined conditional probabilities for both nodes of the independent variables. Table 5 is presenting the probabilities for the districts. As shown, *Eixample* has the highest probabilities compared to all other districts which indicate that both slight, severe, and fatal injuries are more likely to happen in this district. *Sant Martí* is following *Eixample* in having the highest probabilities, followed by *Sants-Montjuïc* and *Sarrià-Sant Gervasi.* It is worth mentioning that the differences between the last mentioned three districts is slightly low and training and testing sample should be considered as these results are representing 70 % of the utilized dataset, while the testing set represents 30%.

Table 5: Calculated conditional probabilities for districts.

Parents	Probability										
Injury level	Ciutat Vella	Eixample	Gràcia	Sants-Montjuïc	Sarrià-Sant Gervasi	Horta-Guinardó	Les Corts	Sant Martí	Sant Andreu	Nou Barris	Total
Slight Injuries	0.051	**0.304**	0.046	0.111	0.107	0.07	0.073	0.125	0.062	0.051	32,482
Severe or fatal injuries	0.048	**0.273**	0.026	0.102	0.108	0.064	0.092	0.145	0.067	0.076	660

Table 6 is depicting the calculated conditional probabilities for different years with having two parents based on the applied model which they are the district and the dependent variable which is the level of injury. For *Ciutat Vella* as a parent node, all types of injuries have higher probabilities in 2018 compared to all other years. While for ***Eixample*****,** slight injuries are higher in 2016, and severe or fatal injuries are higher in 2018 compared to other years. *Gràcia* has the highest probabilities in 2017 for all types of injuries. Slight injuries are higher in 2019 while severe and fatal injuries are higher in 2016 in *Sants-Montjuïc* district. *Sarrià-Sant Gervasi* has higher number of slight injuries in 2018, however, severe or fatal injuries are found to be high at three different years 2016, 2017 and 2018. For *Horta-Guinardó*, 2016 has the highest number of slight injuries and 2019 has the highest number of severe or fatal injuries. *Les Corts* has the highest number of slight injuries in 2016 and the highest number of severe or fatal injuries in 2017. In 2019, the highest number slight injuries is identified in *Sant Martí,* while in 2017, the highest number of severe or fatal injuries is identified at the same district. For *Sant Andreu,* 2019 has the highest probabilities for all types of injuries. *Nou Barris* has its highest number of slight injuries during 2018 and its highest number of severe or fatal injuries during 2016.

Table 6: Calculated conditional probabilities for years.

Parents		Probability				
District	Injury level	2016	2017	2018	2019	Total
Ciutat Vella	Slight Injuries	0.225	0.253	**0.259**	0.262	1,655
Ciutat Vella	Severe or fatal injuries	0.25	0.188	**0.344**	0.219	32
Eixample	Slight Injuries	**0.262**	0.239	0.245	0.254	9,862
Eixample	Severe or fatal injuries	0.233	0.222	**0.306**	0.239	180
Gràcia	Slight Injuries	0.249	**0.257**	0.250	0.244	1,487
Gràcia	Severe or fatal injuries	0.118	**0.471**	0.118	0.294	17
Sants-Montjuïc	Slight Injuries	0.258	0.238	0.242	**0.262**	3,591

Sants-Montjuïc	Severe or fatal injuries	**0.328**	0.239	0.224	0.209	67
Sarrià-Sant Gervasi	Slight Injuries	0.241	0.246	**0.267**	0.247	3,479
Sarrià-Sant Gervasi	Severe or fatal injuries	**0.254**	**0.254**	**0.254**	0.239	71
Horta-Guinardó	Slight Injuries	**0.273**	0.240	0.256	0.231	2,283
Horta-Guinardó	Severe or fatal injuries	0.167	0.214	0.262	**0.357**	42
Les Corts	Slight Injuries	**0.256**	0.252	0.253	0.238	2,386
Les Corts	Severe or fatal injuries	0.295	**0.328**	0.197	0.180	61
Sant Martí	Slight Injuries	0.255	0.255	0.232	**0.258**	4,076
Sant Martí	Severe or fatal injuries	0.167	**0.365**	0.302	0.167	96
Sant Andreu	Slight Injuries	0.254	0.224	0.260	**0.262**	2,005
Sant Andreu	Severe or fatal injuries	0.205	0.182	0.250	**0.364**	44
Nou Barris	Slight Injuries	0.252	0.258	**0.262**	0.229	1,658
Nou Barris	Severe or fatal injuries	**0.360**	0.220	0.220	0.200	50

CONCLUSIONS

Traffic crashes intensity or occurrence can vary greatly from region to region or from district to district. Therefore, this spatial influence on traffic crashes can also impact the level of injury and its types. In Barcelona, 10 different districts with different populations and size that are distributed across the city. Consequently, this study is attempting to classify these districts according to traffic crashes and their resulted injuries whether it is a slight injury, severe, or fatal injury. A Bayesian network represented by TAN technique is employed in order to analyze the utilized data that consists of 47,081 traffic crashes that resulted into different level of injuries during four years interval including 2016, 2017, 2018, and 2019.

The results have shown that *Eixample* has the highest probabilities of having all types of injuries compared to all other districts. This could be a result of a combination of factors that can lead to this status. One of these factors is, the fact that, *Eixample* has the highest density per hectare and population compared to all other districts; street traffic is also high on the grid streets designed by Civil Engineer Ildefons Cerdà. Additionaly, *Eixample* has the highest figures related to owned passenger cars, motorcycles and vans, highest usage of private transport mode, and the highest density of passenger cars per $\mathbf{km^2}$compared to all other districts. For the temporal factor represented by years, the number of injuries vary significantly from district to district during different years as there is no one single year that has the highest number of injuries for all districts. For the future work, an extensive analysis can be carried out related to traffic crashes in *Eixample* in order to identify risk factors. These risk factors can include spatiotemporal factors, average daily traffic, person characteristics who was involved in the crash, type of the crash, and the transport mode that led to the crash.

REFERENCES

Aiash, A., & Robusté, F. (2021a). Traffic accident severity analysis in Barcelona using a binary probit and CHAID tree. International Journal of Injury Control and Safety Promotion, 29(2), 256-264. https://doi.org/10.1080/17457300.2021.1998136

Aiash, A., & Robusté, F. (2021). Working hours and traffic accident injuries: Case study in Barcelona. Transportation Research Procedia, 58, 678-682.

Ajuntament de Barcelona. (2019a). Barcelona's City Hall Open Data Service. Retrieved from https://opendataajuntament.barcelona.cat/data/en/dataset?q=accident&sort=fecha_publicacion+desc

Ajuntament de Barcelona. (2019b). Estadística i Difusió de Dades. Retrieved from https://ajuntament.barcelona.cat/estadistica/castella/Territori/sup/a2019/S0202.htm

Ajuntament de Barcelona (2021). Anuari Estadístic de la Ciutat de Barcelona 2021. Oficina Municipal de Dades, Barcelona.

Ajuntament de Barcelona. (2022). Barcelona's City Hall Open Data Service. Retrieved from https://opendata-ajuntament.barcelona.cat/data/en/dataset/mapa-graf-viari-carrers-wms

AlKheder, S., AlRukaibi, F., & Aiash, A. (2020). Risk analysis of traffic accidents' severities: An application of three data mining models. ISA Transactions, 106, 213-220. https://doi.org/10.1016/j.isatra.2020.06.018

Carson, J., Adminaité-Fodor, D., & Jost, G. (2020). 14th Road Safety Performance Index Report. Brussels: ETSC.

Friedman, N., Geiger, D., & Goldszmidt, M. (1997). Bayesian Network Classifiers. Machine Learning, 29, 131–163. https://doi.org/10.1023/A:1007465528199

IBM. (2016). IBM SPSS Modeler 18.0 Algorithms Guide. IBM Corporation.

Jia, R., Khadka, A., & Kim, I. (2018). Traffic crash analysis with point-of-interest spatial clustering. Accident Analysis & Prevention, 121, 223-230. https://doi.org/10.1016/j.aap.2018.09.018

Pulugurtha, S., Duddu, V., & Kotagiri, Y. (2013). Traffic analysis zone level crash estimation models based on land use characteristics. Accident Analysis & Prevention, 50, 678-687. https://doi.org/10.1016/j.aap.2012.06.016

Wang, C., Quddus, M., & Ison, S. (2013). A spatio-temporal analysis of the impact of congestion on traffic safety on major roads in the UK. Transportmetrica A: Transport Science, 9(2), 124-148. https://doi.org/10.1080/18128602.2010.538871

Zhao, J., & Deng, W. (2015). The use of Bayesian network in analysis of urban intersection crashes in China. Transport, 30, 411-420. https://doi.org/10.3846/16484142.2013.816365

AUTHORS BIOSCKETCH

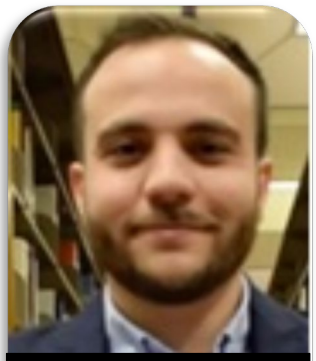

A. Aisah

Doctoral candidate at BarcelonaTech, Department of Civil and Environmental Engineering and at Doctoral Training Network – EIT, European Institute of Innovation and Technology, Urban Mobility. He obtained his Master Degree in Civil Engineering at Transportation at Kuwait University.

F. Robusté

Professor of Transportation at BarcelonaTech, Department of Civil and Environmental Engineering. He is Civil Engineer and obtained his Doctoral Degree; MEng in Transportation, Master Degree in Operations Research at University of California at Berkeley. Coordinator of the research group Barcelona Innovative Transportation (BIT). He has been President of the Spanish Transportation Engineering Association, Director of the Civil Engineering School in Barcelona, and Director of the Abertis Chair on Transportation Infrastructure Management.

2022 Transportation Research Board (TRB) Events. La organización TRB anuncia una serie de sus próximos adiestramientos en línea para todo el año. Para más información sobre los próximos adiestramientos y registro favor dirigirse al siguiente enlace https://www.nationalacademies.org/trb/events.

Making the Case for Sustainable Infrastructure Online Course. La Sociedad Americana de Ingenieros Civiles (ASCE) anuncia curso en línea cuyos tópicos tratan sobre Geotecnia, Costas, Océanos, Puertos, entre otros. El curso describirá formas avanzadas e innovadoras de utilizar el pensamiento sostenible al diseñar infraestructura resistente antes las condiciones ambientales cambiantes. Auspiciado por la Educación Continua de la ASCE y se llevará a cabo del 6 de junio al 15 de julio de 2022. Para más información sobre el curso en línea y registro favor dirigirse al siguiente enlace https://mylearning.asce.org/diweb/catalog/item/eid/.

2022 National Conference on Earthquake (NCEE). El Instituto de Investigación de Ingeniería Sísmica anuncia su doceava conferencia y reunión anual a realizarse en Salt Lake City, Utah del 27 junio al 1 de julio de 2022. Para más información sobre la conferencia favor dirigirse al siguiente enlace https://www.eeri.org.

20th LACCEI International Multi-Conference for Engineering, Education and Technology. El Consorcio Latinoamericano y del Caribe de Instituciones de Ingeniería (LACCEI) anuncia su Vigésima Conferencia Internacional con el lema *"Education, Research and Leadership in Post-pandemic Engineering: Resilient, Inclusive and Sustainable Actions"* que se llevará a cabo de manera híbrida los días 18 al 22 de julio de 2022: Boca Ratón, USA. Para más información sobre la conferencia favor dirigirse al siguiente enlace https://laccei.org/blog/laccei2022/program-at-glance/.

2022 ITE International Annual Meeting and Exhibition. El Instituto de Ingenieros en Transportación (ITE) anuncia su reunión anual con el tema *"Investing in Our Future"* a realizarse del 31 de julio al 3 de agosto de 2022 en el Sheraton, New Orleans, LA, USA. Para información y registro favor dirigirse al siguiente enlace https://www.iteannualmeeting.org/

5ta Conferencia Internacional de Infraestructura de Transporte. La Sociedad Internacional de Mantenimiento y Rehabilitación de Infraestructuras del Transporte (iSMARTi) y el Instituto de la Construcción y Gerencia (ICG) anuncian la 5ta Conferencia Internacional de Infraestructura de Transporte que se llevará a cabo los días 10 al 13 de agosto de 2022 en el Sheraton Lima Hotal & Convention Center, Lima Perú. Para más información sobre sobre la conferencia y registro favor dirigirse al siguiente enlace https://icg.construction/.

International Coalition for Sustainable Infrastructure (ICSI) Summit. La Institución de Ingenieros Civiles (ICE) anuncia su Cumbre Virtual que considerará formas de impulsar el cambio transformador necesario para brindar una infraestructura resiliente y sostenible para nuestro planeta tierra. La Cumbre se llevará a cabo el 28 de junio de 2022. Para más información sobre la Cumbre favor dirigirse al siguiente enlace https://www.ice.org.uk/events/latest-events/icsi-summit/.

World Conference on Cimate Change & Sustainability. *The People Events*, organizadora de eventos, anuncia la Conferencia Mundial sobre el Cambio Climático y Sostenibilidad con el tema *"Avance de los Esfuerzos Globales sobre Transparencia Climática"*. Es una conferencia educativa internacional para profesionales de las ciencias climáticas, ambientales y atmosféricas que ofrecerá un foro interdisciplinario para la discusión del impacto del cambio climático y el calentamiento global. La Conferencia se llevará a cabo los días 1 al 3 de septiembre de 2022 en Frankfurt, Germany. Para más información sobre la conferencia favor dirigirse al siguiente enlace https://climateweek.thepeopleevents.com/.

NORMAS PARA PUBLICACIÓN DE ARTÍCULOS TÉCNICOS

Las siguientes son las normas básicas a las que se deben ajustar los autores al enviar sus artículos en la revisión final:

1. Los artículos deben estar escritos en español, inglés o portugués.
2. Los artículos deben ser escritos en letra Times New Roman, tamaño 11.
3. El título del artículo debe proveerse en español (o portugués) y en inglés.
4. El artículo debe tener un resumen de no más de 250 palabras, el cual debe estar escrito en español (o portugués) y en inglés.
5. Se debe adjuntar un máximo de cinco Palabras *claves*, las cuales deben estar escritas en español (o portugués) e inglés, en orden alfabético en cada idioma, y en minúsculas.
6. Las diferentes secciones y subsecciones del artículo no deben estar enumeradas.
7. El nombre de las secciones debe ir todo mayúscula, en negrilla y tamaño 11.
8. El nombre de las subsecciones debe ir en mayúscula y minúsculas, en negrilla y tamaño 11.
9. La indentación de la primera línea de párrafos debe ir a 0.2".
10. Las figuras y fotografías no deben presentarse en colores claros.
11. El nombre de las tablas debe estar ubicado en la parte superior, en negrilla y escrito de la siguiente manera: **Tabla #: Nombre de la tabla.** Sólo la primera letra de la primera palabra va en mayúscula.
12. El nombre de las figuras debe estar ubicado en la parte inferior, en negrilla y escrito de la siguiente manera: **Figura #: Nombre de la figura.** Sólo la primera letra de la primera palabra va en mayúscula.
13. Las tablas deben estar hechas con Word.
14. En el texto, al referirse a una figura o a una tabla, la primera letra debe ser escrita en mayúscula: la Figura, la Tabla.
15. Las ecuaciones deben ser escritas con el editor de ecuaciones de Word, o con *MathType*. Deben ser escritas en letra Times New Roman y en un tamaño de *Font* 10. Las ecuaciones deben estar numeradas entre paréntesis y justificadas a la derecha.
16. En el texto, al hacer referencia a una ecuación, el número debe estar en paréntesis y debe escribirse la palabra completa en minúscula: ecuación (#).
17. Las palabras o frases en inglés deben escribirse entre comillas dobles (por ejemplo, ensayo "down-hole").
18. Las referencias deben ser indentadas 0.5 pulgadas (12.7 mm) a partir de la segunda línea y escritas de la siguiente manera:
    - En el caso de un libro, el nombre debe estar en itálica:
      Chopra, A. K. (2006). *Dynamics of Structures, Theory and Applications to Earthquake Engineering*, 3rd edition, Prentice Hall, New Jersey.
    - Publicación en una revista técnica ("journal"). Se debe incluir el volumen, número y las páginas del artículo. El título debe estar entre comillas y el nombre de la revista en *itálica*. Solo la primera letra del título debe estar en mayúscula. La forma correcta de escribir este tipo de referencia es:
      Liang, R.Y. y Choy, F. (1992). "Theoretical study of crack – induced eigen frequency changes on beam structures", *Journal of Engineering Mechanics*, Vol. 118, No. 2, pp. 384-396.
    - Para los reportes técnicos, tesis o disertaciones se debe adoptar el siguiente formato:
      Schultz, A. (1986). "An experimental and analytical study of the earthquake response of R/C frames with yielding columns", Ph.D. dissertation, Department of Civil Engineering, University of Illinois at Urbana-Champaign, Illinois.
      Bergman, D.M. y Goel, S.C. (1987). "Evaluation of Cyclic Testing of Steel-Plate Devices for Added Damping Dissipators", Report UMCE 87-10, Civil Engineering Department, University of Michigan, Ann Arbor, Michigan.

19. Todas las referencias en la lista deben citarse al menos una vez en el texto principal del artículo.
20. Incluir la dirección postal completa y la dirección electrónica, al menos del autor que servirá de contacto.
21. Al referirse en el texto a un trabajo en la lista de referencia, debe citarse el mismo como: (Apellido, año), (Apellido 1 y Apellido 2, año), o (Apellido *et al.,* año), dependiendo si hay uno, dos o más autores.
22. En el caso de que dos o más referencias vayan seguidas deben colocarse en el mismo paréntesis separadas por punto y coma: (Apellido, año; Apellido 1 y Apellido 2, año).
23. No se deben usar abreviaturas en las referencias.

Aquellos autores interesados en recibir un archivo electrónico con un artículo típico preparado en el formato de la Revista deben escribir a ridnaic.editor@uprm.edu.

INFORMACIÓN PARA SUBSCRIPTORES

La Revista Internacional de Desastres Naturales, Accidentes e Infraestructura Civil es una publicación científica y técnica que comenzó a publicarse a partir de mediados del año 2001, bajo el auspicio del Departamento de Ingeniería Civil y Agrimensura del Recinto Universitario de Mayagüez de la Universidad de Puerto Rico. Inicialmente se están publicando dos números de la revista por año y se espera que el número de volúmenes por año aumente en los próximos años. La revista está disponible en la Internet en: https://www.scipedia.com/sj/ridnaic; https://www.uprm.edu/ridnaic/publications/.

Dirección Postal de la revista:
Revista Internacional de Desastres Naturales, Accidentes e Infraestructura Civil, Departamento de Ingeniería Civil y Agrimensura, UPR-Recinto Universitario de Mayagüez, Mayagüez, PR 00681-9000.
Teléfono: (1-787) 832-4040, Exts.3815, 3393.
Dirección de correo electrónico: ridnaic.editor@uprm.edu

ALCANCE TEMÁTICO

El alcance de esta publicación comprende los sistemas de ingeniería que dan apoyo y sirven para el diseño de la infraestructura civil, y a los desastres naturales y accidentes de origen humano que pueden afectar esa infraestructura. La revista publica contribuciones que se refieran a la conjunción de más de una de las áreas temáticas definidas en el título, o a una de ellas. El término infraestructura civil se usa aquí para designar al conjunto de instalaciones físicas que permiten movilizar o almacenar bienes, materias primas, agua, residuos, energía, información o personas. En general, se incluyen aquí puentes, puertos, canales, aeropuertos, ferrocarriles, sistemas de tránsito urbano, carreteras, líneas de comunicación y energía, tuberías, represas, plantas de tratamiento de aguas, tanques, silos, etc. El énfasis en desastres naturales está en el estudio de acciones de huracanes, tornados, terremotos, inundaciones, sequías, fuego, deslizamientos, maremotos. Asimismo, la revista publica temas relacionados con accidentes y eventos producidos por causas humanas, incluyendo fallas por diseño o construcción, colisiones, explosiones, entre otras.

INFORMACIÓN PARA AUTORES

La revista está abierta a contribuciones de profesionales e investigadores de cualquier nacionalidad y lugar de trabajo. Los idiomas de preferencia para la publicación de artículos son español, inglés o portugués. Para mantener la calidad de las contribuciones que publique la revista, los artículos se someten a un proceso de revisión por pares. Los manuscritos deben someterse utilizando MS Word, en letra tipo Times New Roman. No se admitirán contribuciones que utilicen otros procesadores de texto. Si bien la transferencia al formato oficial de la revista es responsabilidad de los Editores, el esfuerzo de los autores para enviar su trabajo siguiendo el formato de la revista es apreciado, en especial en lo que respecta a las Referencias y a su cita. Las instrucciones para los autores son muy similares a las que se utilizan en las publicaciones periódicas de la "American Society of Civil Engineers" (ASCE), con la diferencia que la revista usa el formato de una columna. Aquellos autores interesados en consultar un ejemplar anterior disponible deben escribir a ridnaic.editor@uprm.edu.

La Revista Internacional de Desastres Naturales, Accidentes e Infraestructura Civil (RIDNAIC) es publicada por el Departamento de Ingeniería Civil y Agrimensura del Recinto Universitario de Mayagüez de la Universidad de Puerto Rico.

Arte diseñado por Irmalí